DETERMINATION OF WIND UPLIFT FORCES USING DATABASE-ASSISTED DESIGN (DAD) APPROACH FOR LIGHT FRAMED WOOD STRUCTURES

By

AKWASI FRIMPONG MENSAH

A THESIS PRESENTED TO THE GRADUATE SCHOOL
OF THE UNIVERSITY OF FLORIDA IN PARTIAL FULFILLMENT
OF THE REQUIREMENTS FOR THE DEGREE OF
MASTER OF SCIENCE

UNIVERSITY OF FLORIDA

2010

To my parents Mr. & Mrs. P. K. Mensah

ACKNOWLEDGMENTS

The completion of this research and report would not have been successful without the support and encouragement of a number of persons. I want to first thank the Almighty God through Jesus Christ for being my Lord and sufficiency.

I also wish to express my sincere gratitude to my thesis committee chair, Dr. David O. Prevatt for his continual support, time and guidance in this endeavor. I am grateful to my committee members: Dr. Kurtis R. Gurley and Dr. Forrest Masters, and Dr. Gary Consolazio, who have each contributed immensely to the success of this research. I am also grateful to the faculty and staff of the Civil and Coastal Engineering Department for their tutorage and assistance during my stay in University of Florida. I am again appreciative of the financial support provided by National Science Foundation (NSF) through grant #080023 "Performance Based Wind Engineering (PBWE): Interaction of Hurricanes with Residential Structures".

To my parents, Mr. and Mrs. P. K. Mensah, I am indebted to you for all the love, encouragement, care and support you have given me. God richly bless you. I also wish to thank all the friends I met in Gainesville. Of mention especially are Patrick Bekoe and Joyce Dankyi whose presence in this chapter of my live cannot be overemphasized. My deep appreciation also goes to my entire family and friends for their timely encouragements.

Lastly, I wish to express my profound gratitude to all my office colleagues and the hurricane group of University of Florida especially Peter L. Datin, Jason Smith and Scott Bolton for their assistance and contributions.

TABLE OF CONTENTS

page

APPENDIX

LIST OF TABLES

LIST OF FIGURES

Abstract of Thesis Presented to the Graduate School
of the University of Florida in Partial Fulfillment of the
Requirements for the Degree of Master of Science

DETERMINATION OF WIND UPLIFT FORCES USING DATABASE-ASSISTED DESIGN (DAD) APPROACH FOR LIGHT FRAMED WOOD STRUCTURES

By

Akwasi Frimpong Mensah

August 2010

Chair: David Prevatt
Major: Civil Engineering

During major hurricanes, damages to light framed wood structures (LFWS) represented the largest proportion of monetary losses. The absence of wind load transfer mechanism in wood structures was identified as a major cause of their structural failures. Wind load paths in LFS are not well understood.

This study aims to develop a better approach for determining wind design loads on LFWS. The study was part of an on-going National Science Foundation (NSF) funded project titled, "Performance Based Wind Engineering: Interaction of Hurricane Forces with Residential Structures", which has a primary objective of investigating the relationship between spatially varying wind loads and structural load paths on LFWS.

This study was accomplished in two phases. In Phase 1, a Database-Assisted Design (DAD) methodology was used to combine time histories of wind tunnel pressure coefficients with experimentally determined influence functions for a wood framed structure. From this analysis, structural reactions at roof-to-wall and wall-to-foundation connections were developed. Peak reactions were compared to wind design loads based on ASCE-7 (2005) provisions for main wind force resisting systems (MWFRS) and components and cladding (C&C). Whereas,

peak reactions estimated, using DAD methodology, were higher than maximum reactions obtained using the MWFRS provisions, they were lower than C&C based maximum reactions.

In Phase 2 of the project, an experimental study was conducted to validate the DAD methodology. A1/3-scale LWFS instrumented, with surface pressure transducers and load cells, was the immersed in wind flow. Structural reactions were developed from measured roof pressures using the DAD methodology. A comparison of developed reactions with directly measured reactions showed a good agreement between their mean and peak values.

CHAPTER 1
INTRODUCTION

Background and Motivation

Wind flow over low-rise buildings is characterized by patterns of flow separation and reattachment which creates spatially and temporally varying pressure fields on building surfaces. Generally, peak wind suction forces occur on the leeward walls and at roof edge areas while positive pressure are created on the windward walls and interior roof areas. Such forces in recent hurricanes caused substantial damage to wood-framed residential structures.

Hurricane damage to light framed wood structures (LFWS) are by far the largest contributor to the monetary losses associated with hurricane disaster (Rosowsky et al. 2003). Post-hurricane investigations report widespread structural damage to wood structures due to loss of roof sheathing, and failure of load transfer at joints and mechanical connections (FEMA 2005; van de Lindt et al. 2007). Clearly, there is a lack of understanding of structural load paths in wood structures.

Wind design of light framed wood residential structures is problematic because of their complex geometric shapes. Current wind design provisions lack codified pressure values for typical residential buildings. i.e. pressure coefficients are only provided only for simple shaped building. Moreover, high variability in material properties of wood introduces greater uncertainty in wind resistance estimates. Selection of materials and connections for LFWS has been mainly based on prescriptive building guidelines which increase their susceptibility to wind damages.

In the United States, wind load design provisions are included in the ASCE 7 (2005), which codifies information on wind flow characteristics (obtained from meteorological data) and aerodynamic pressures (developed on scaled models in boundary layer wind tunnels). Pressure coefficients and climatological data, which are used by structural engineers for wind load

designs, are presented in reductive figures and tables suitable for hand calculations. However, a research conducted by Simiu & Stathopoulos (1997) suggests that such design standards can produce risk inconsistent results. Simiu & Stathopoulos (1997) asserted that the current code provides insufficient information for designers to realistically account for the spatial and temporal variation of wind load effects.

To address these codification deficiencies, a new wind analysis approach, in which utilizes large aerodynamic and climatological databases are used to define wind design loads, was proposed by Simiu & Stathopoulos (1997). This analysis methodology, called database assisted design (DAD) was used by Simiu et al. (2003) to estimate internal forces in a steel portal framed building. They used wind tunnel databases of surface pressure time-histories and analytically derived influence functions to determine bending moments at knee and ridge joints of the portal frames. When the DAD results were compared with ASCE 7 design values, they concluded that the ASCE provisions produced risk inconsistent designs and errors in excess of 50 % in peak load estimations.

With the availability of powerful computations and proven usefulness of the DAD methodology, its application has been extended to light-framed wood structures. The hypothesis of this research is that, the DAD methodology will provide better accuracy in predicting wind load effects on LFWS than using the current codes. The validation of this hypothesis would lead to a better understanding of structural load paths on LFWS and improved engineering design models for LFWS.

Objective

The specific objectives of this investigation are to:

1. Apply the DAD methodology to predict structural reactions in a LFWS system.

2. Validate the DAD approach by experimentally determining structural loads on a 1/3 wood building model.

Scope of Work

Wind tunnel data developed on a 1/50 scale house model were analyzed to generate spatial distributions of wind pressure coefficients on the roof of a gable roof building. The DAD methodology was used to combine the pressure time histories and experimentally-derived influence coefficients for vertical reactions on a third scale wood-structure. The data was analyzed to determine peak values of roof-to-wall and wall-to-foundation connection loads for LFWS. Results of the analysis were compared to wind design loads based on the ASCE 7-05 standard.

In phase two of this study, the validity of the DAD approach was evaluated experimentally by subjecting the third-scale house to fluctuating wind forces while simultaneously measuring surface pressures and structural reactions. The DAD methodology was applied by utilizing the measured pressure distributions and the influence coefficients to determine reaction loads at roof-to-wall connections. The results and directly measured structural loads were compared.

Organization of Report

Literature reviews of relevant topics to this project are presented in Chapter 2. The chapter discusses wind load effects on low-rise buildings, the current provisions for wind load designs and the concept and development of the DAD approach. Finally, a review of previous experimental studies in which structural responses and wind pressures were simultaneously monitored on LFWS is presented.

In Chapter 3, the wind tunnel study, which produced the aerodynamic pressure data utilized in this project, is introduced. Analysis of wind tunnel derived pressures to generate a pressure coefficient database for this study is described. Extreme value analysis based on the

Lieblien BLUE (best linear unbiased estimators) estimation procedure to obtain the expected peak pressure distributions is explained also in Chapter 3. Lastly, area-averages of pressure coefficients from wind tunnel analysis are compared to ASCE 7-05 external pressure coefficients for components and cladding.

The DAD-based procedure for evaluating wind load reactions is described in Chapter 4. Chapter 4 also contains an overview of experimental derivation of structural influence functions for this study as well as experimental results. Analysis of results to estimate peak reactions is discussed in this chapter. Peak reactions based on the DAD approach are compared to results based on ASCE 7-05.

In Chapter 5, the TFI Cobra Probe, which is used in the experimental study, is introduced. Tests undertaken to validate and understand the operations of this equipment are reported as well. Finally, characterization of the wind field for the experimental study is also described.

In Chapter 6, the 1/3-scale model house experiment is described. The chapter contains descriptions of materials and equipments used in the tests, such as the 1/3 scale house, UF wind generator and load and pressure sensors. The test arrangement and procedures are also described. Finally, analysis of experimental results and correlation of structural loads derived from pressure measurements and directly measured structural loads are reported in this chapter.

A summary of the entire project is contained in Chapter 7. The usefulness of this research is also discussed in this chapter. Lastly, recommendations for future work are presented.

CHAPTER 2
LITERATURE REVIEW

Wind Flow over Low-Rise Buildings

Wind loading on a building depends upon the flow pattern around the building, which, in turn, depends on building geometry, dimensions, surroundings, upstream terrain and wind flow characteristics.

Wind flow over a low-rise building is characterized by separation and reattachment pattern (shown in figure 2-1) which together with its velocity fluctuations generate a spatially and temporally varying pressure field on the surface (Ginger et al. 2000). Ginger and Letchford (1993) observed that large fluctuating suction pressures are generated in flow separation regions close to the leading edges of the roof of low rise buildings. They explained that the flow mechanisms that generate these pressures are the 2D separation bubble for flow perpendicular to the edge discontinuity and the 3D conical vortex for flow at oblique angles to the edge discontinuity and that the largest suction pressures are generated close to the leading corner for a wind orientation of approximately 30°.

Ginger et al. (2000) determined wind loads on the roof of a typical low-rise house for approach wind directions of 0^o to 90^o by carrying out a wind tunnel model study at a 1/50 geometric scale. They observed that the second truss from the windward gable end was subjected to the largest wind load

Stathopoulos et al. (2000) conducted and presented a wind tunnel study which provided detailed extreme local and area-averaged pressure coefficients for low-building roofs exposed to open-country upstream terrains. They observed that when the wind flow is normal to the ridgeline of a gable roof building, quasi-flat roofs in the range of 0^o-30^o create a similar flow pattern of separation, entrainment, and reattachment; a high suction prevails, especially at the

windward edges and corners. They noted however that, if the roof angle is greater than 30^o, wind flow generally strikes on the windward roof prior to separating from the windward edge or ridge which induces a positive pressure region on part of the windward slope and a negative region on the leeward slope. They concluded that these flow patterns and pressure distributions may vary with the wind direction, but remain comparable in respective roof slope ranges.

Current Design Provisions of ASCE 7 for Wind Loads on Low-Rise Buildings

Background on ASCE 7 Wind Load Provisions

The provisions of ASCE 7-05 for wind loads on low buildings are largely based on wind tunnel study works conducted in the late 1970s at the boundary wind tunnel in the University of Western Ontario (UWO)(Davenport et al. 1978; Stathopoulos 1979). Researchers at UWO used an approach that consisted essentially of permitting the building model to rotate in the wind tunnel through a full 360^o in increments of 45^o while simultaneously monitoring the loading conditions on each surfaces. Both open and suburban exposure conditions were considered. Wind pressure coefficients which represent "pseudo" loading conditions, that when applied to a building, envelope the desired structural actions (bending moment, shear, thrust), and the maximum induced force components to be resisted for all possible directions and exposures were developed from the studies (see C6.5.11 (ASCE/SEI. 2005)).

The current edition of the ASCE 7 standard (2005) has refined pressure and force coefficients to reflect the latest boundary-layer wind tunnel and full-scale research findings. This research has been however only limited to gable-roof buildings, and a rational method of applying the coefficients to hip roofs based on experience, intuition and judgment has been developed and presented in ASCE 7-05.

Three methods are provided in the ASCE 7 standard for determining wind design loads. These are the "simplified method" (method 1), the analytical procedure (method 2) and a wind tunnel procedure (method 3).

Analytical Procedure for Wind Design Loads on a Low-Rise Building

The main wind-force resisting system (MWFRS) of a building consists of a structural frame or an assemblage of structural elements such as roof trusses, cross-bracing, shear walls and roof diaphragms that work together to transfer wind load action on the entire structure to the ground (ASCE/SEI. 2005). MWFRS provides support and stability for the overall structure and generally receives wind loading from more than one surface. ASCE 7-05 defines components and cladding as elements of the building envelope that do not qualify as part of the MWFRS. Cladding receives wind loads directly. Components receive wind loads directly or from cladding and transfer the load to the MWFRS. Members which are categorized as components and cladding included fasteners, purlins, girts, studs, roof ducking, and roof trusses.

In the determination of design wind loads on all buildings, a velocity pressure, q_z, is evaluated at a height z above the ground using the equation below:

$$q_z = 0.00256 K_z K_{zt} K_d V^2 I \ (lb/ft^2) \qquad (2\text{-}1)$$

where K_z is velocity pressure exposure coefficient, obtained from table 6-3 of ASCE 7-05, which modifies the design wind speed to account for terrain exposure condition and the height *z*; K_{zt} is a topographic factor which accounts the wind speed-up (topographic) effect; K_d is the wind directionality factor, which is 0.85 for buildings to account for reduced probability of maximum winds coming from any direction and the reduced probability of the maximum pressure coefficient occurring for any wind direction; *V* is the basic wind speed determined from figure 6-1 in ASCE 7-05 and its value is a nominal 3-second gust wind speed in miles per hour at 33 ft

above ground for an open exposure; and I is importance factor of the building determined from table 6-1 in ASCE 7-05 which is used to adjust the level of reliability of building or structure to be consistent with the building classifications indicated in the standard.

Design wind pressures, for both MWFRS and components and cladding, are determined as the product of the velocity pressure and the sum of internal and external pressure coefficients. The internal pressure coefficients, GC_{pi} are provided in figure 6-5 of ASCE 7-05 in terms of the building enclosure classification (i.e. open, partially enclosed or enclosed building). The external pressure coefficients are given separately for MWFRS and components and cladding for different scenarios but generally in terms of pressure zones. Pressure zones specified in the ASCE standard for both MWRS and Components and Cladding are in terms of a dimension denoted by a (Simiu and Miyata 2006). The dimension a is 10% of the least horizontal building dimension or 0.4 h (h=mean roof height), whichever is smaller, but not less than 4% of the least horizontal building dimension or 3ft.

Design wind pressures on the MWFRS of low-buildings are determined by the equation below:

$$p = q_h\left[(GC_{pf}) - (GC_{pi})\right](lb/ft^2) \tag{2-2}$$

Where: q_h is velocity pressure evaluated at mean roof height using equation 2-1, GC_{pi} internal pressure coefficient (obtained from Figure 6-5 in ASCE 7-05) and GC_{pf} is an external pressure coefficient combined with a gust effect factor. Values for GC_{pf} are provided in figure 6-10 in ASCE 7-05 as a function of the building roof angles. Roof overhangs are to be designed for a positive pressure on the bottom surface of windward roof overhangs corresponding to C_p = 0.8 in combination with the pressures determined from Figure 6-10. For determining eternal pressure coefficients, eight loading patterns are to be considered to design the building for all wind

directions. The loading patterns have the walls and roofs zoned into several building surfaces which envelope wind load distributions on the building. Figure 2-2 shows typical load patterns in the ASCE 7-05 for wind design loads on a MWFRS of a building.

Design wind pressures on component and cladding of low-buildings are determined by the equation below:

$$p = q_h\left[(GC_p) - (GC_{pi})\right](lb/\ ft^2) \tag{2-3}$$

where GC_p are the external pressure coefficients and the other terms are as defined previously. Values of GC_p are selected from Figures 6-11 through 6-16 of the ASCE 7-05 based the type of roof and angle roofs. Figure 2-3 shows the typical pressure zones of a gable roof building and external pressure coefficient provision for roof angles between 7^o and 27^o. External pressure coefficients for deign of component and cladding are specified for the wall, roof and overhang as a function of effective wind area. The effective wind area is defined by the ASCE 7-05 as the span length multiplied by an effective width that need not be less than one-third the span length. It is worth noting that the resulting induced wind load is however applied over the actual tributary area to the component been designed.

Limitations of Current Design Provisions

Several investigations have over the years been conducted and results compared with ASCE 7-05 wind load provisions. Issues have been raised by researches on the standard provisions and this section discusses some of them.

Simiu et al. (2003) illustrated the practical effects of simplifications inherent in the ASCE 7-05 provisions by evaluating moments in steel portal frames of a building(shown in Figure 2-4) by using ASCE 7-05 standard provisions on one hand and the DAD procedure (discussed later in this chapter) based on wind tunnel database on the other. Table 2-1 shows values obtained. Simiu

et al. (2003) demonstrated that the use of the tables and plots in wind load design provisions can entail errors that can exceed 50% in the estimation of wind effects.

Furthermore, Whalen et al. (2002) assert that the accuracy in the definition of wind loads inherent in such tables and plots are lower than that inherent in current methods for stress computation. There is so much complexity with geometries and shapes of low-rise buildings and hence high accuracy in predicting design loads based on tables and plots cannot be achieved.

Wind directionality effects on low-rise buildings are accounted for in the ASCE 7 standard by a reduction factor of 0.85. Simiu et al. (2003) observed that this approach is inadequate as wind effect reductions due to directionality effects are less significant as the mean recurrence interval of the wind effects increase, rending the use of this factor potentially unsafe, particularly for MWFRS.

Design parameters such as building geometry, building orientation, proximity of adjacent structures and, the spatial and temporal variation of wind loads are not realistically and comprehensively accounted for when a designer uses the conventional standard provisions (Simiu and Stathopoulos 1997).

Recently, wind tunnel test data on generic low buildings were obtained at UWO to contribute to the National Institute of Standards and Technology (NIST) aerodynamic database (Ho et al. 2005b). St. Pierre et al. (2005) compared the NIST aerodynamic database to the historical data obtained by Stathopoulos in the late 1970s, from which the current ASCE 7 provisions were developed. They observed that for the exterior bay of the test building model, ASCE 7 generally underestimates the response coefficients significantly. For the interior bays, the ASCE 7 overestimates the response coefficients. They also observed that generally, there was 10-85% underestimation of peak response coefficients in the suburban terrain by ASCE 7.

Attempts by writers of the standard provisions on wind loads to reduce the limitations of earlier versions of the standard (example ASCE 7-05) resulted in bulky and complex provisions (Simiu and Stathopoulos 1997).

Database-Assisted Design (DAD) Methodology for a Low-Rise Building

Background of the DAD methodology

With the backdrop of the above mentioned limitations of the wind design load provisions, it was necessary to work on an alternative approach which offers the potential for significantly more risk-consistent, realistic, safer and economical design by using adequate aerodynamic databases and information. Owning to current information storage and computational capabilities, Simiu and Stathopoulos (1997) proposed a new generation of standard with provisions on wind loads that are no longer based on reductive and distorting tables and plots, but can be structured on knowledge-based systems drawing the requisite information from large databases.

Their postulation was that, wind loads evaluated via the new methodology would be functions of design parameters, which includes building geometry, building orientation, position with respect to and geometry of neighboring buildings, built-up terrain roughness, etc. They intimated that their proposal would allow the designer to target specific situations, rather than providing blanket coverage for a broad range of situations. They explained that this methodology would furthermore allow the designer to account for the specific linear or non-linear structural characteristics of the building or structure (eg. influence function).

Subsequently, Whalen et al. (1998) conducted a pilot project on the estimation of wind effects in low-rise building frames using this methodology. Whalen et al. (1998) used records of pressure time histories measured at large number of taps on a building surface at the UWO boundary layer wind tunnel. Time histories of bending moments in a frame were obtained by

summing up pressures time histories tributary to that frame multiplied by the respective tributary areas and frame influence coefficients. They compared results with results based on ASCE 7 standard provisions. Their comparison suggested that, significantly more risk-consistent, safer and economical designs could be achieved using this approach than using conventional standard provisions.

The approach of using electronic aerodynamic and climatological databases to define wind loads was coined “database-assisted design” (DAD) and was accepted by the ASCE 7-98 standard (Rigato et al. 2001) .

DAD Concept and Software Development

The first generation DAD application called WiLDE-LRS – Wind Load Design Environment for Low-rise Structures was developed by NIST (Whalen et al. 2000). WiLDE-LRS, a MATLAB®-based software, adopted interactive graphical user interfaces (GUI) to give a visual, user-friendly design environment. MATLAB scripts were used in the software to analyze the behavior of rigid portal frames and other components under high winds and to produce time histories of wind load effects in these structural members. The software had its origins in a prototype application called Frameloads, used to study wind effects on moment resisting frames in low-rise buildings designed by the Standard Metal Building Manufactures Association methodology. A latter version (2.7) of WiLDE-LRS (Whalen et al. 2002) greatly enhanced the GUIs that directly accepted input of influence coefficients accounting for frame properties. Post-processing was incorporated in this version to calculate realistic and robust statistical estimates of the peak load effect values based upon the entire time history.

Subsequently, the DAD approach has been extended to consider nonlinear static response of low buildings (Jang et al. 2002) and also to account for the probability distribution of the peaks of time histories of wind effects and of sampling errors in the estimation of that

distribution (Sadek and Simiu 2002; Sadek et al. 2004). A scheme to interpolate existing data in available database to other configurations in a reliable, accurate and simple way, without resorting to further wind tunnel experiments, has been incorporated in DAD applications (Kopp and Chen 2006).

In 2006, NIST released software packages developed using the MATLAB language to fully implement the DAD approach and all its improvements (Main and Fritz 2006). Two separate software packages are available through the internet at http://www.nist.gov/wind for rigid, gable-roofed buildings and for tall, flexible buildings.

Limitation to the Application of DAD Approach

To the best of author's knowledge:

1. Application of the DAD approach and its software has been limited to steel portal frame buildings.
2. Structural influence functions used by researches so far in DAD applications have been analytically derived using hand-calculations or 2-D models in structural analysis software
3. .The validity of the approach has not been demonstrated experimentally.

Design and Construction of Light Framed Wood Structures and their Performance to Wind Forces

Wood-frame construction forms the majority of residential and other low-rise structures. A number of these structures are located along hurricane-prone zones in the United States. This section discusses the construction methods prevalent in the wood-frame industry and their performance during hurricane events. The literature presented here is based on studies done by Rosowsky and Schiff (2003) and van de Lindt et al. (2007).

Construction Methods

Three construction methods have been identified by van de Lindt et al. (2007). These are the conventional, engineered and prescriptive. The conventional method consists of following

documents such as the International Residential Code outlining certain exceptions and limitations. Most wood constructions are based on conventional methods. For engineered construction, structures are specifically designed by a design professional to meet jurisdictional requirements. Interestingly, very few residential buildings are engineered. Prescriptive construction involves the use of basic material strength level and tabulated values obtained from construction manuals.

Rosowsky and Schiff (2003) referred to designs based on the conventional method as deemed-to-comply design, which is largely derived from traditional rules of thumb for building light-frame wood structures (LFWS). They observed that most of the rules focused on building structures to safely resist gravity loads, ignoring geographic considerations. Until recently, most buildings, including those located in high-wind environments, were constructed using conventional methods which did not meet wind-resistant design requirements. This caused these structures to have the greatest vulnerability to extreme wind events.

Critical Components and Systems

According to Rosowsky and Schiff (2003), the three most important areas to consider in designing a wind-resistant wood-frame structure are:

1. **The building envelope**: This forms the first line of defense against wind and water intrusion. Traditionally, the building envelope is considered to be architecture in nature and therefore not designed by engineers. However, studies have shown that a direct correlation exists between the performance and damage (losses) sustained by wood-frame buildings. Structural engineers are becoming actively involved in the building envelope designs.

2. Attachment of roof and wall sheathing: this component is critical in keeping structures enclosed, preventing infiltration and providing critical links in the structural load path. Removal of roof sheathing is the second largest failure mode observed in post-hurricane investigation after removal of roof cover. Significant highlight has been given to the need to provide more and larger fasteners around roof edges to resist high wind uplift pressures.

3. Structural systems to transfer the applied loads to foundation: In most wood-frame construction, complicated load paths exist because of conventional framing techniques and irregular floor and roof plans in residential buildings.

Structural Failures of LFWS in Hurricane Events

Structural observation made by van de Lindt et al. (2007) during a reconnaissance trip after Hurricane Katrina are discussed as follows:

1. In many of the houses examined, there was absence of continuous load path for the transfer of wind loads from the roof down to the foundation.
2. Loss of roof sheathing at corners, which typically experience the highest uplift pressure during wind storms. In most of these cases, the current code minimum nail spacing requirements were not met.
3. Gable end wall losses as a result of loss of vinyl siding and failure of the foam sheathing.
4. The prevalent use of conventional construction in high wind regions.

Light framed wood structures (LFWS) have generally not performed well when subjected to high wind loads due to design/construction practices. Rosowsky and Schiff (2003) remarked that better understanding of the wind loading on buildings and behavior of wood-frame structures under sever wind events must be sought. This, they noted, will lead to improvements in both prescriptive and engineered design methodologies for new and retrofit construction.

Wind-Induced Pressures and Structural Responses on Light Wood Framed Structures

The final stage of this project is to validate the DAD methodology for its application to LFWS by simultaneously monitoring pressures and structural loads on a 1/3 scale house subjected to wind forces. This section presents experimental studies done by researchers whereby wind-loads and structural responses were simultaneously measured on full-scale buildings. These experiments are generally aimed at investigating whether observed structural responses correspond to predictions by numerical models.

Doudak et al. (2005) monitored a single story industrial shed building to determine its displacement response to wind and snow loads. He attempted to correlate the observed displacements with real-time estimates using SAP 2000 of these environmental loads. Wind speed and direction was measured as well as displacements on the building during the typical wind storm season. Doudak et al. (2005) however did not take pressure measurements on the house. Wind pressures for numerical simulations were estimated from archived pressure coefficients and the measured wind speeds. They achieved a quite reasonable agreement between measured and predicted displacements. Discrepancies ranged from as low as 6 % in most cases to as high as 90 % for all four incident wind directions.

In a follow-up to the experiment done by Doudak et al. (2005), Zisis and Stathopoulos (2009) undertook an experimental study whereby they monitored and collected full-scale pressure and force data on a light framed wood building. A total of 51 load cells were installed at roof-to-wall and wall-to-foundation interfaces of the building while ensuring that the stiffness of the building was unaltered. The building was also equipped with 27 pressure taps. All acquired data were analyzed and converted into dimensionless coefficients based on the following equations:

Pressure measurements

$$C_{p,mean/peak} = \frac{P_{mean/peak} - P_a}{1/2\rho U_{BH}^2} \tag{2-4}$$

Force measurements

$$C_{f,mean/peak} = \frac{R_{mean/peak}}{(1/2\rho U_{BH}^2)LW} \tag{2-5}$$

where ρ = air density; U_{BH} = wind speed at the building height; P_a = ambient atmospheric pressure; P = actual surface pressure; R = reaction at the load cell location; L = length of the building and W = width of the building.

Zisis and Stathopoulos (2009) also conducted wind tunnel experiments on a 1-200 scale model and obtained pressure data which were also converted into pressure coefficients. Force coefficients were also derived by area averaging the measured local pressure coefficients from the wind tunnel studies on the building. These pressure coefficients were input into a numerical (finite element analysis) model of the test building which computed reaction forces at each of the 27 foundation load cell locations. These forces were transformed into dimensionless coefficients.

They observed good a greement of pressure distribution comparison between the wind tunnel and full-scale data. They also concluded that the comparison between the full-scale load cell readings and the base reactions computed by the finite element analysis made in the form of force coefficients shows good agreement as far as mean values are concerned.

Zisis and Stathopoulos (2009) also conducted a 2-dimensional structural analysis of two main frames of the building. In the analysis, the individual roof pressures tap records (full scale) acting on each frame were used to evaluate the total expected vertical reaction due to wind pressure on each frame. They compared the estimated results to the actual total reactions measured by the respective load cells of each frame in terms of force coefficients. Their comparison as well as the layout of their test building is shown in Figure 2-5. Zisis and Stathopoulos (2009) found excellent agreement as far as the mean values were concerned. They also observed significantly more fluctuating signals with higher peak forces were obtained using the measured pressure coefficients on the building envelope in comparison with recorded signal by load cells placed in the building foundation. They explained that this observation may be

partly attributed to the dynamic load attenuation effect due to structural and material damping of the building components hence lower reactions measured than computed.

Both experimental studies discussed above exposed the test buildings to natural wind forces. Consequently, wind pressure data collected from the field was highly affected by fluctuations of wind directions during the test. Moreover, the structure does not experience winds that would cause the worst load effects or design level events.

Table 2-1. Comparison of bending moments (KNm) determined using ASCE 7-98 and DAD (Simiu et al. 2003)

Frame	6.1 m eave height						9.75 m eave height					
	Knee			Ridge			Knee			Ridge		
	ASCE	DAD	%	ASCE	DAD	%	ASCE	DAD	%	ASCE	DAD	%
Outer	339	330	3	118	136	-13	463)	631	-27	86	137	-37
1	520	401	30	180	168	7	724	723	0	134	179	-25
2	471	301	56	163	97	68	624	799	-22	115	150	-23
3	471	310	52	163	101	61	624	782	-20	115	145	-21
4	471	327	44	163	106	54	624	586	6	115	112	3

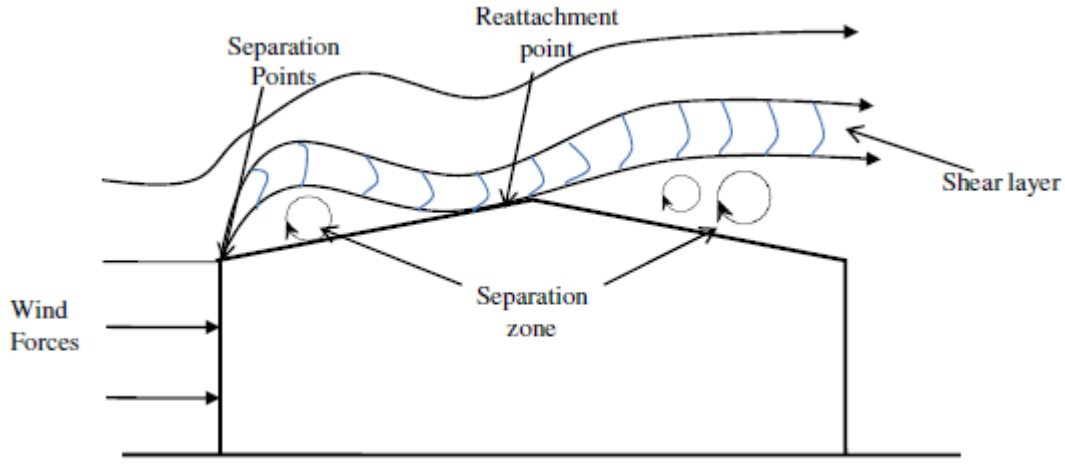

Figure 2-1. Separation and reattachment pattern of wind flow over a low-rise building (After Simiu & Miyata (2006))

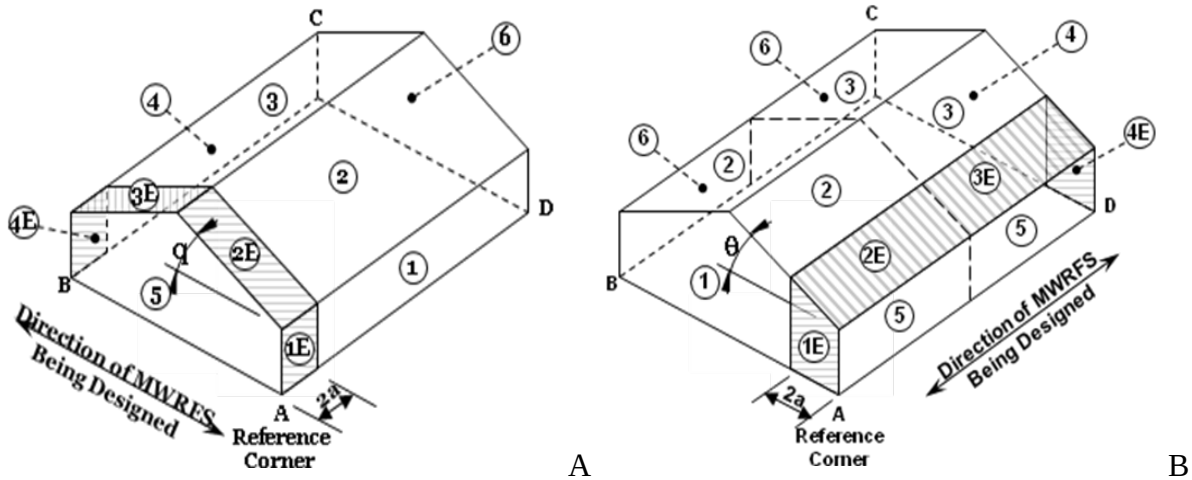

A B

Figure 2-2. Typical building surfaces for ASCE 7-05 MWFRS external pressure coefficients

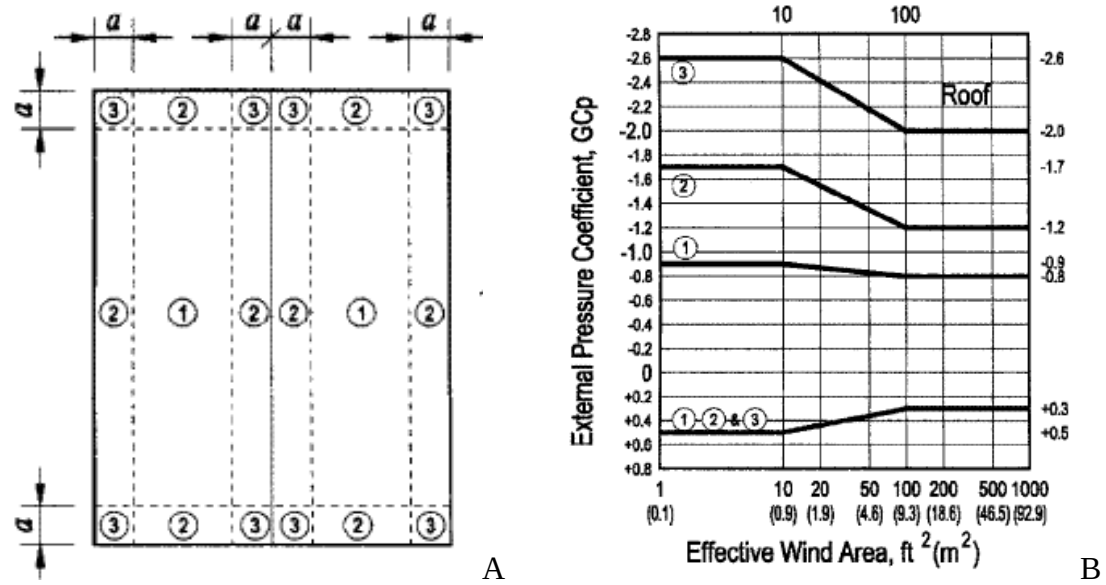

A B

Figure 2-3. ASCE 7-05 provision for determining external pressure coefficients for the design of components and cladding.

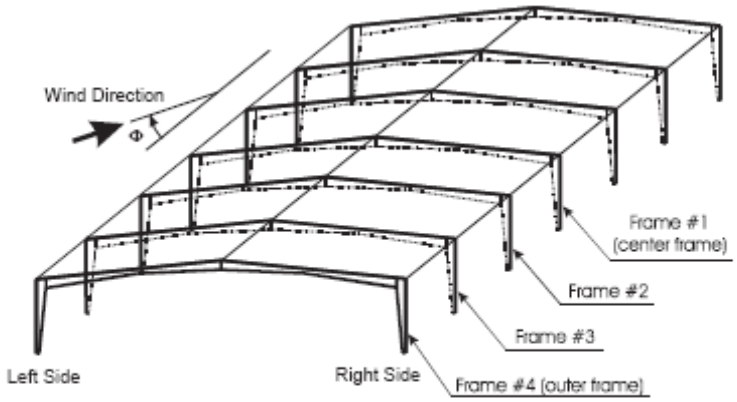

Figure 2-4. Isometric view of the steel portal frame structure (Simiu et al. 2003) (End frame not shown)

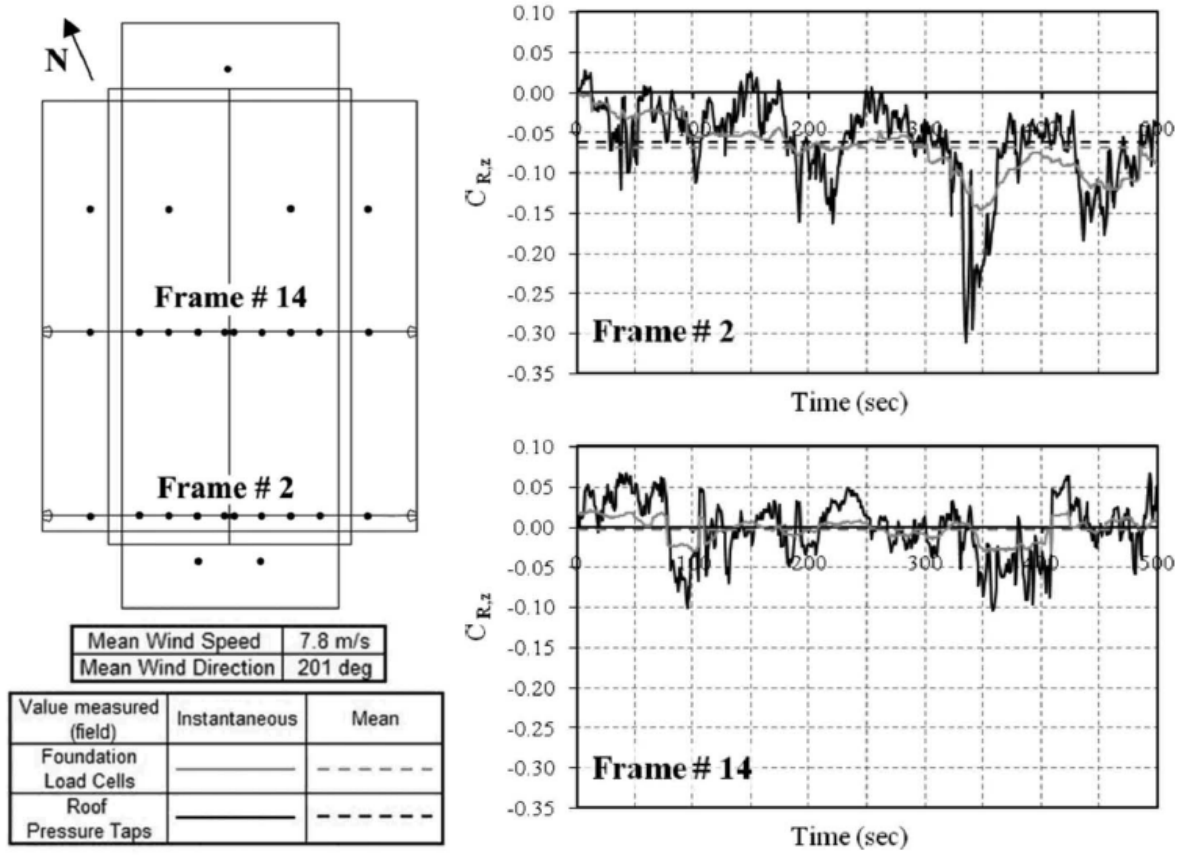

Figure 2-5. Comparison of vertical reaction records (in terms of force coefficients) measured by load cells and estimated based on envelope roof pressures (Zisis and Stathopoulos 2009)

CHAPTER 3
ANAYSIS OF WIND TUNNEL DATA TO GENERATE PRESSURE COEFFICIENTS

Wind Tunnel Data

For this study, pressure coefficients were derived from wind tunnel data developed by Datin and Prevatt (2007) on a 1:50 scale model house. The experiments were carried out in an atmospheric boundary layer wind tunnel at the Wind Load Test Facility (WLTF) at Clemson University. An overview of the experiment is discussed below.

House Model and Pressure Tap Layout

The tests were conducted on a 1/50 house model called Clemson standard model (CSM) 4-12 which is shown in Figure 3-1A. The house model has length of 14.4 in. and width of 7.2 in with a mean roof height of 3.4 in. CSM 4-12 has a gable roof with a slope of 18.4^{o} (4 in 12). The model was configured for a 60 ft X 30 ft full scale building with a mean roof height of14.3 ft.

The model has 387 pressure taps installed on its roof. The pressure taps are evenly spaced along the length of the roof at a nominal distance of 1 in except around the edges of the roof where they are densely grid at a nominal distance of 0.2 in. Figure 3-1B shows the pressure tap layout. These pressure taps were constructed with 0.063 outside diameter metal tubes glued to Plexi-glass sheets and which are connected to Scanivalve electronic pressure scanners by 12 in long vinyl tubes.

Wind Simulation and Pressure Measurements

A suburban exposure was simulated upstream of the wind tunnel (shown in figure 3-2). The velocity profile and turbulence intensity profile of the created exposure condition plotted against the log law profiles for suburban terrain are shown in Figure 3-3A. Figure 3-3B shows the longitudinal wind speed normalized power spectrum taken in the wind tunnel at equivalent full scale height of 10 m (33 ft) as well as von Karman spectrum.

Near simultaneous pressure time-histories were recorded using a scanivalve ZOC 33 system. Tests were repeated for five wind directions; 0^o, 45^o, 90^o, 135^o and 180^o, as defined in Figure 3-1B. Eight test repeats were done for each wind direction. Data was sampled at 300 Hz and recorded for 120 seconds for each test repeat. Table 3-1 summarizes the common test parameters used.

. These stored files were used as the raw wind tunnel data for this project. There were forty text files each containing 389 columns and 36000 rows.

Aerodynamic Data Processing

The raw data was low-pass filtered at 150 Hz prior to analyzing them. Pressure coefficients were developed from the raw data as follows:

- It was corrected for tubing response to remove any effects of tube length and size on the data
- Pressures were normalized by mean hourly pressure measured at 33 ft full scale height to obtain pressure coefficients.
- Pressure coefficients were re-referenced to 3-second gust mean velocity measured at the mean roof height of the building (14.2 ft)

Tubing Response Correction

The effect of the tubing system, used in the wind tunnel study, on the measured wind pressure data was eliminated using a tubing frequency response shown in Figure 3-4. This response was reported in Liu et al. (2009).

The raw pressure signal measured at each tap was first converted to the frequency domain using a Fast Fourier Transformation. This provided a frequency (power) spectrum of the pressure signal. The frequency spectrum was then divided by the frequency response to remove the distortion caused by the volume and length of the tube. The corrected spectrum was then converted to time domain using an Inverse Fast Fourier Transformation.

Determining Pressure Coefficients

Pressure coefficients were derived from the measured local pressure time series as follows:

$$C_{p,ref,i}(t,\theta) = \frac{P_i(t,\theta)}{\overline{P}_{ref}(\theta)} \tag{3-1}$$

where, $C_{p,ref,i}(t,\theta)$ is the pressure coefficient at Pressure Tap *i*, referenced to the dynamic pressure at reference height, at time *t* for wind angle θ; $P_i(t,\theta)$ is the measured wind pressure at tap *i* at time *t* for wind angle θ; $\overline{P}_{ref}(\theta)$ is the mean hourly reference dynamic pressure recorded by a Pitot tube at the reference height of full height of 33ft for wind angle θ. Pressure coefficients were referenced at that height because flow is uniform with low turbulence levels at that height. This ensures accurate speed control of the wind tunnel and accurate calibration of the pressure scanners (Ho et al. 2005a).

Re-referencing of Pressure Coefficients

It is widely accepted that aerodynamic data referenced to mean roof height dynamic pressure produce the least variability and therefore all low building pressure data sets, including those in the building codes, follow this convention (Ho et al. 2005a). It is intended that the wind tunnel results should be comparable to those in ASCE 7 and other aerodynamic database. For this reason, the wind pressure coefficients were normalized to a 3-second gust mean wind speed at the mean roof height (14.3 ft full-scale), $\overline{U}_{3sec,mrh}$. The wind pressure coefficients $Cp_{,ref,i}(t,\theta)$ were converted to the equivalent coefficient as follows.

$$C_{p,i}(t,\theta) = C_a \times C_{p,ref,i}(t,\theta) \tag{3-2}$$

where, $C_{p,i}(t,\theta)$ is the wind pressure coefficients at pressure tap *i*, referenced to a 3-second gust wind speed at the mean roof height, at time *t* for wind angle θ; and C_a is an adjustment factor

which is given by the squared ratio of the mean wind speed at reference height $\overline{U}_{ref}$ to the equivalent 3-second gust wind speed at mean roof height $\overline{U}_{3\,sec,mrh}$ (Shown in Equation 3-3).

$$C_a = \frac{\overline{U}_{ref}^2}{\overline{U}_{3\,sec,mrh}^2} \tag{3-3}$$

The mean hourly wind speeds at the reference height $\overline{U}_{ref}$ (13.03 m/s) and mean roof height U_{mrh} (6.54 m/s) were determined from the velocity profile for the wind tunnel testing. The ASCE 7-05 provides the Durst curve which relates the wind speed averaged over gust duration, t (in seconds), U_t to hourly mean speed, U_{3600}. However, the curved corresponds to open terrain conditions and an elevation, z = 10 m (Simiu and Scanlan 1996). As already stated, the wind tunnel data was developed for a suburban terrain condition and pressure coefficients are intended to be referenced to mean roof height of 14.3 ft (4.2 m). Hence, conversion of the mean hourly speed to 3-second gust was done using Equation 3-4 provided by Simiu & Scanlan (1996).

$$U_t(z) = U_{3600}(z)\left[1 + C(t)\frac{\sqrt{\beta}}{2.5\ln\left(z/z_o\right)}\right] \tag{3-4}$$

where, *C(t)* is the time averaging constant for a given time averaging interval β is the squared ratio of the friction velocity to the longitudinal turbulence fluctuations; z_o is the roughness length; *z* is the height at which the wind speed is to be evaluated. The calculation of 3-second gust wind speed at mean roof height, which was based on *C(3sec) =2.85;* z_o *= 0.22m, z = 4.2m (14.3ft)* and β *= 5.25,* is as follows:

$$\overline{U}_{3\,sec,mrh} = U_{mrh}\left[1 + C(3\,sec)\frac{\sqrt{\beta}}{2.5\ln\left(z/z_o\right)}\right] \tag{3-5}$$

$$\overline{U}_{3\,sec,mrh} = (6.54m/s)\left[1 + 2.85\frac{\sqrt{5.25}}{2.5\ln\left(\frac{4.2m}{0.22m}\right)}\right] = 12.33m/s \tag{3-6}$$

The resulting adjustment factor, C_a for re-referencing the pressure coefficients is 1.1168.

Wind Tunnel Results and Analysis

Wind Pressure Coefficients Time Histories

The resulting pressure coefficient time histories were converted to equivalent full-scale pressure coefficients using the reduced frequency relationship shown in Equation 3-7.

$$\left(\frac{fL}{V}\right)_m = \left(\frac{fL}{V}\right)_p \tag{3-7}$$

where f, L and V are respectively sampling frequency, characteristic dimension, and wind speed referenced at mean height over a specified duration. Subscripts m and p denote model (1:50 scale) and prototype (full scale) buildings respectively. Based on model frequency and 3-second gust wind speed at mean roof height of 300 Hz and 29 mph respectively, and 3-second gust full scale wind speed, at mean roof height of prototype for suburban terrain, of 80.27 mph, the prototype frequency is calculated as:

$$\frac{300Hz \times 1}{29mph} = \frac{f_p \times 50}{80.27mph} \qquad f_p = 17.46\ Hz \tag{3-8}$$

Using equality of non-dimensional time, the equivalent full-scale duration is given by:

$$T_p = \frac{f_p \times T_m}{f_m} \tag{3-9}$$

$$T_p = \frac{300Hz \times 120s}{17.46Hz} \qquad T_p = 34.36\,minutes \tag{3-10}$$

The equivalent full-scale time step for the time histories is:

$$t_p = \frac{1}{f_p} = \frac{1}{17.46\,Hz} = 0.0573s \tag{3-11}$$

Pressure coefficient time histories in duration of 34 minutes in full scale of the 387 pressure taps were generated for each sample of a wind direction. Calculation for determining the equivalent full-scale duration of the 120 seconds of test period is presented in the appendix. Figure 3-5 shows time series plots pressure coefficients at pressure taps 1 and 387 for wind direction 0^o.

Pressure coefficient time series, which are useful for analyzing dynamic responses of low-rise buildings; have been saved in a MATLAB data format, as shown in Figure 3-3. There are 40 binary files with filenames structured as "CSM4-12_Suburban_Cp_data_dir_XXX_Y.mat", where "CSM4-12" identifies that the "Clemson Standard Model" with a roof slope of 4-12 was used in the wind tunnel study; "XXX" denotes the wind direction; and "Y" denotes the sample number. Each file also contains information of full scale geometric properties of the building model tested, sampling frequency and period, time-step, locations of the pressure taps on model, data sample number, wind azimuth, etc.

Observed Statistical Values of Wind Pressure Coefficients

The sample mean, root mean square (RMS) and peak local pressure coefficients were computed for the eight samples of each wind azimuth. The statistical values of pressure coefficients, which are useful for the design of cladding and components such as roof fasteners, purlins and panes, have been evaluated for 34-minute equivalent full-scale aerodynamic pressure coefficient time histories. These values were also saved in the forty MATLAB files containing the pressure coefficient time histories. The mean and RMS pressure coefficient values were averaged values of the eight samples:

$$\overline{C_{p,i}}(\theta) = \frac{1}{8}\sum_{n=1}^{8}\overline{C_{p,i}}(n,\theta) \tag{3-12}$$

$$\overline{\overline{C_{p,i}}}(\theta) = \frac{1}{8}\sum_{n=1}^{8}\overline{\overline{C_{p,i}}}(n,\theta) \tag{3-13}$$

where, $\overline{C_{p,i}}(\theta)$ and $\overline{\overline{C_{p,i}}}(\theta)$ are respectively the mean and RMS pressure coefficients for at pressure tap *i*, for wind angle θ of the entire experiment; and $\overline{C_{p,i}}(n,\theta)$ and $\overline{\overline{C_{p,i}}}(n,\theta)$ are respectively the mean and RMS values of time series of the nth sample *i*, for wind angle θ. Contour plots of mean and RMS pressure coefficients measured for each direction are shown in Figures 3-7 and 3-8.

Extreme Value Analysis of Pressure Coefficients

Peak values estimated based on a probability distribution function are generally more statistically stable quantities than the observed peaks from individual samples (Ho et al. 2005a). The extreme negative and positive pressure coefficients measured from the eight samples of each wind direction were fitted to an Extreme Type 1 Value Distribution. The probability density function (PDF) and the cumulative distributive function (CDF) of the Extreme value Type 1 (also referred to as Gumbel distribution) are given by:

$$f(x) = \frac{1}{\beta}e^{(x-\mu)/\beta}e^{-(x-\mu)/\beta} \tag{3-14}$$

$$F(x) = e^{-(x-\mu)/\beta} \tag{3-15}$$

where, μ is the location parameter (mode); and β is the scale parameter (NIST 2003). The parameters were calculated using the Best Linear Unbiased Estimators (BLUE) (Lieblein 1974). There are three methods proposed by Lieblein (1974) based on sample sizes for the estimation of the location and scale parameters. Method o ne is for an analysis with sample size less than

sixteen. The second method should be used for a study with sample size larger than sixteen but generally smaller than about fifty. For an analysis with larger same size, method three is to be used. The first method is adopted in this study since the sample size is eight. Furthermore, for this analysis, the peak negative pressure coefficients were multiplied by negative one to make them positive since BLUE analysis was developed for maximum values of the Type I extreme Value distribution. The positive values were then sorted in the ascending order to place them in the following order:

$$x_1 \le x_2 \le ... \le x_8$$

The location parameter, μ and the scale parameter, β were then estimated as follows:

$$\mu = \sum_{n=1}^{8} a_i x_i \qquad\qquad \beta = \sum_{n=1}^{8} b_i x_i \tag{3-16}$$

where, x_i is the ith value of the ascending array of maximum values of the eight samples and a_i and b_i are given by Table 3-2.

The "best" expected (mean) peak pressure coefficient measured at each pressure tap in a given wind direction is given by:

$$\hat{C}_p = \mu + 0.5772\beta \tag{3-17}$$

Figures 3-9 and 3-10 show the spatial variations of the expected extreme pressure coefficients on the roof of the building for different wind directions. The roof corners and gable edges experience spatial variations at close distances and higher magnitude of suctions for all wind directions except for wind direction 90°. A nearly even distribution is observed away from roof edges and corners. A similar pattern is observed between the mean, RMS and extreme pressure coefficient distributions of wind azimuths 45° and 135° are at opposing angles. The same observation is made between the distributions of 0° and 180°. Appendix A provides mean,

RMS and extreme pressure coefficients of selected pressure taps for wind azimuths 0^o, $45^o$and 90^o.

Area-Averaged Pressure Coefficients

Area-averaged pressure coefficients have been derived from pressure coefficient time histories for regions of different size as follows:

$$C_F(j,t) = \sum_{i=1}^{N_j} (C_p(t,i) \times A_i) / \sum_{i=1}^{N_j} A_i \tag{3-18}$$

where $C_F(t)$ is a area-averaged wind pressure coefficient on region j at time t; $C_p(i,t)$ is the wind pressure coefficient at pressure tap i at time t; A_i is the tributary area of pressure tap i and N_j is the total number of pressure taps on region j.

The mean, RMS and extreme values of area-averaged pressure coefficients for the eight samples of each direction were determined. The average mean and RMS of were calculated as discussed above, while an extreme value analysis was done to determine the peak negative and positive area-averaged pressure coefficients. Figures 3-11 to 3-13 display the area-averaged pressure coefficients as a function of wind azimuth for corner, ridge corner, eave, ridge, interior, and gable edge, corner, ridge corner, eave, ridge, interior, and gable edge. These pressure coefficient values measured in the different regions on the surface of the building are compared to ASCE 7-05 external wind pressure coefficients for components and cladding provided in Figure 6-11C of the ASCE 7-05. Table 3-3 provides a summary of peak local pressure coefficients observed within each of the three zones defined in ASCE 7-05, the area averaged pressure coefficients and the C&C external pressure coefficients corresponding to the zones.

It is observed that, the peak local (tap) negative pressures (suctions) are generally higher in magnitude as compared to the ASCE 7-05 provisions for the design of components and cladding.

However, the peak area-averaged pressure coefficients measured for each zone fall within the provisions of ASCE 7 for the various zones. Also, it is observed that, the peak area averaged pressure coefficients for two wind directions (i.e. 0^o and 180^o; and 45^o and 135^o) are identical.

Table 3-1. Measurement configuration and parameters

Model scale	1:50
Sampling frequency	300 Hz
Sampling period	120 s
Test angles	000^0, 045^0, 090^0, 135^0 and 180^0
Upstream exposure	Suburban
3-second gust nominal wind tunnel speed at mean roof height	12.33 m/s

Table 3-2. Coefficients of BLUE for Type 1 Extreme-Value Distribution (Lieblein 1974)

i	1	2	3	4	5	6	7	8
a_i	0.274	0.190	0.150	0.121	0.097	0.076	0.056	0.036
b_i	-0.394	-0.06	0.011	0.059	0.087	0.103	0.108	0.102

Table 3-3. Comparison of wind tunnel and ASCE 7-05 peak pressure coefficients

Zones	Wind Tunnel		ASCE 7-05
	Local Peak	Area-averaged	C&C
1	-2.73	-0.81	-0.9
2	-4.06	-1.84	-1.7
3	-4.39	-2.77	-2.6

A

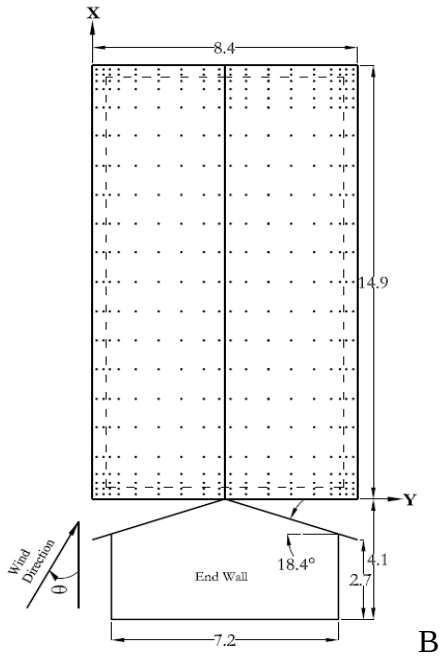

B

Figure 3-1. 1:50 Scale house model (CSM 4-12) used in the wind tunnel study

Figure 3-2. Test section arrangement for 1:50 suburban terrain

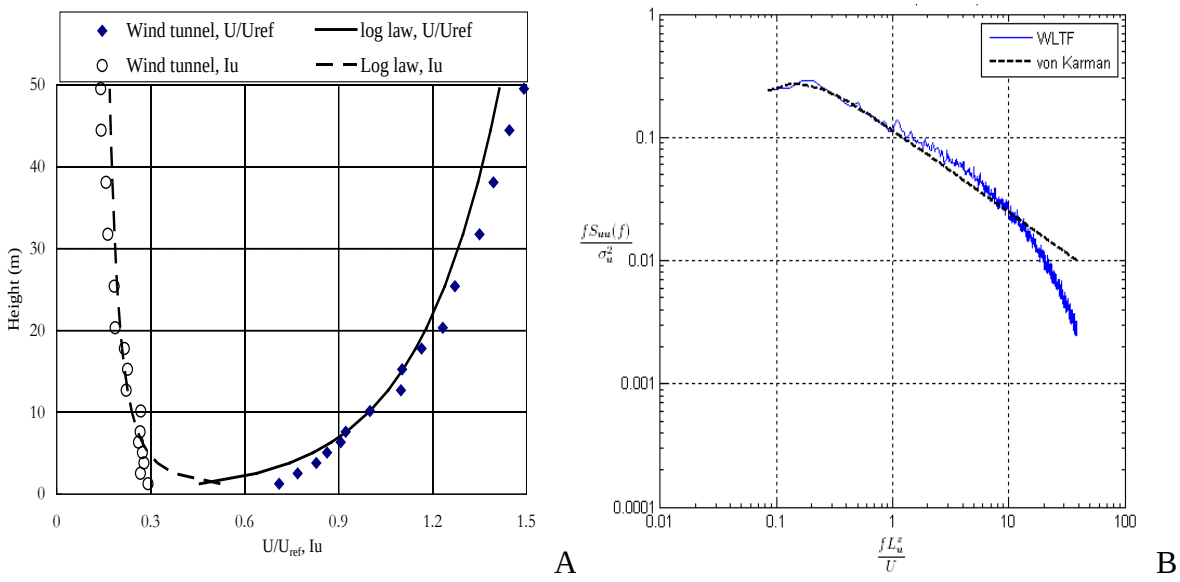

Figure 3-3. Wind flow characteristics for 1:50 suburban wind tunnel study. A) Mean wind speed and turbulence intensity profiles B) Longitudinal spectrum of wind speed at full scale height of 32.8 ft

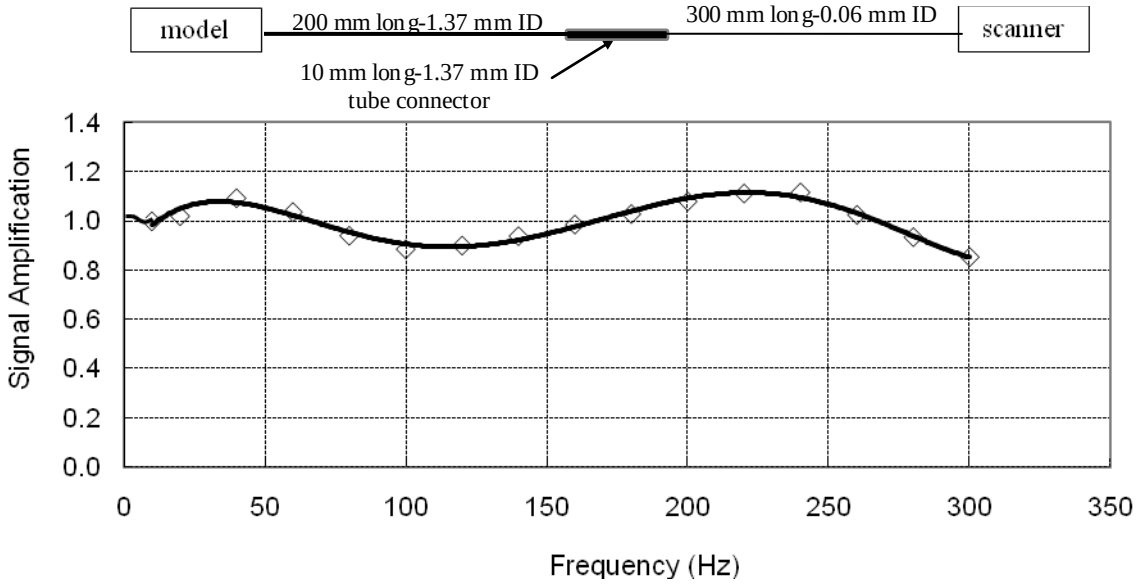

Figure 3-4. Frequency response characteristics of the pressure tubing system

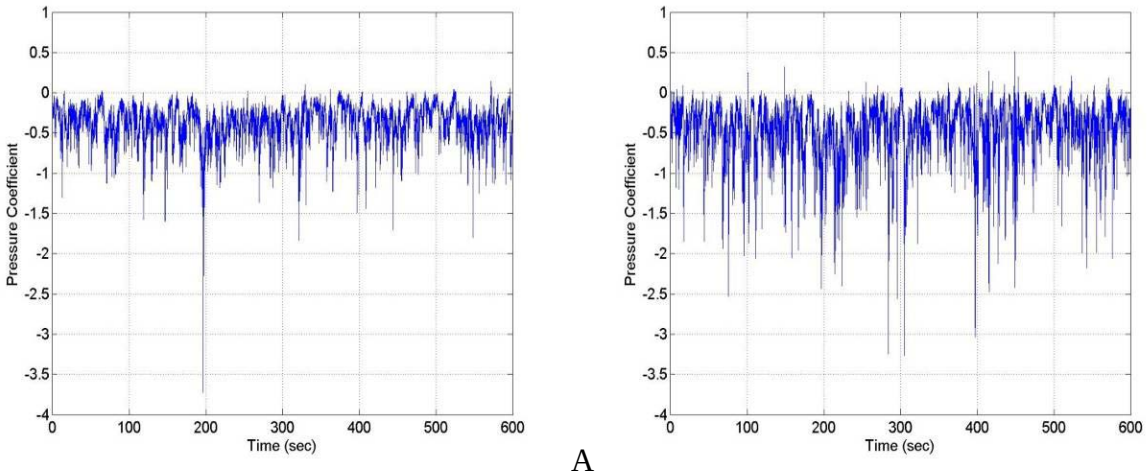

Figure 3-5. First 10 minutes time Series of wind pressure coefficient measured in direction 0^o at A) Tap 1 B) Tap 2

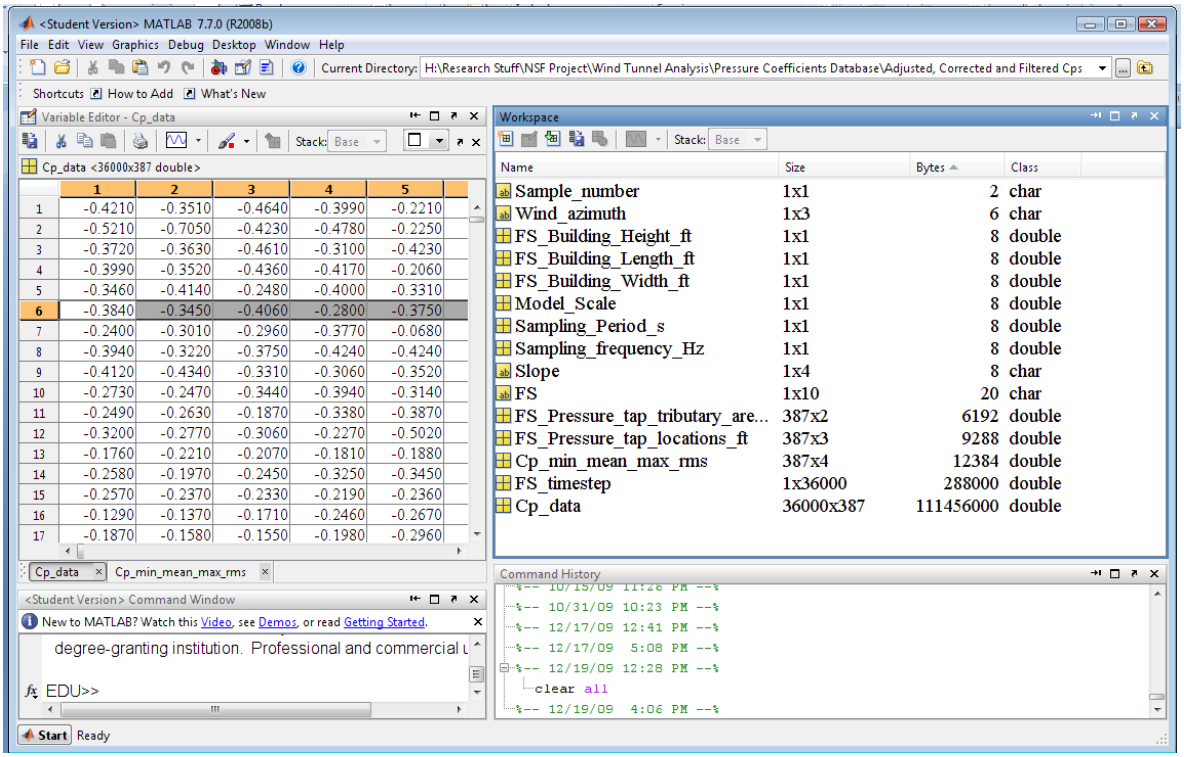

Figure 3-6. Format of MATLAB files of pressure coefficient data

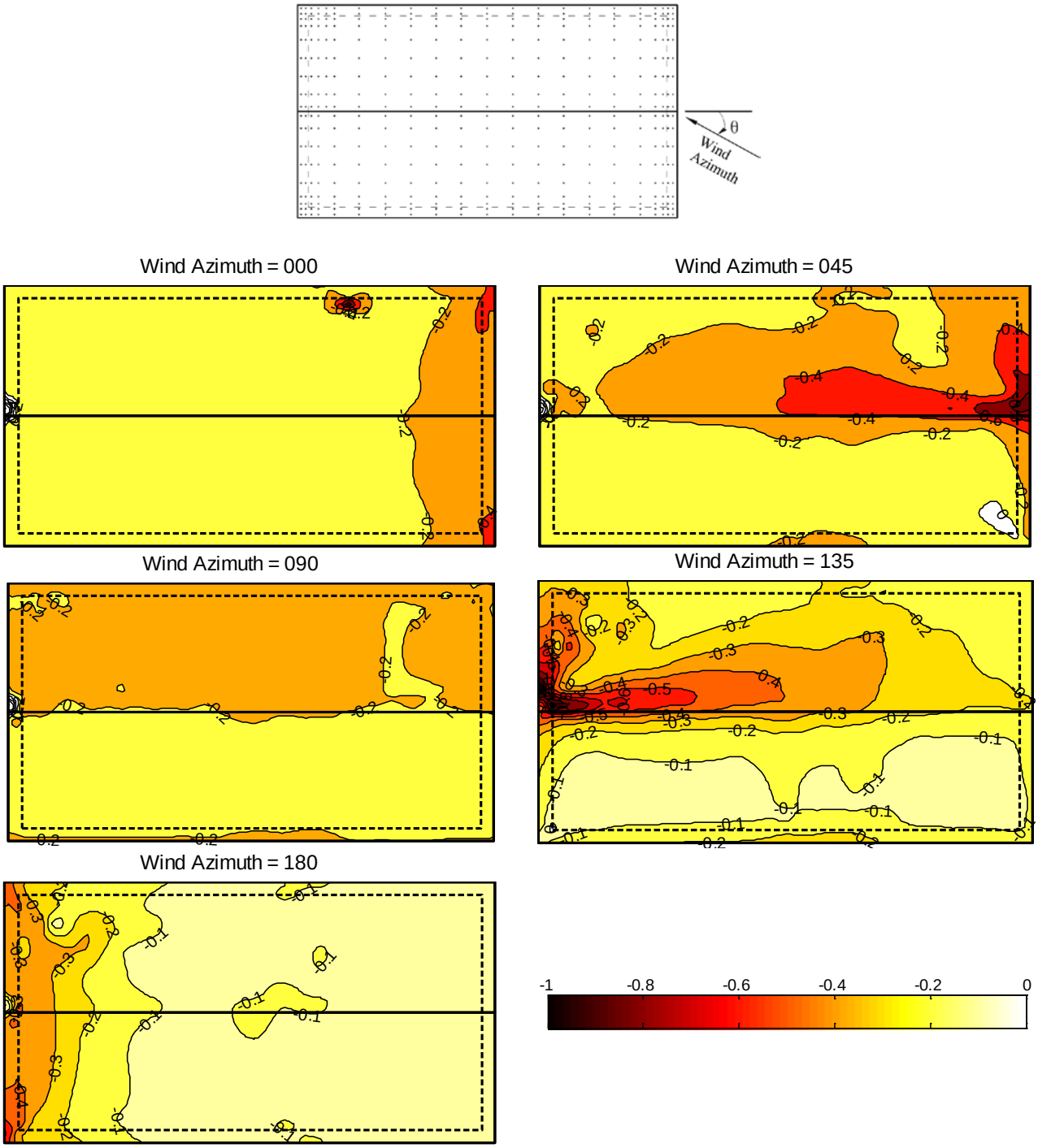

Figure 3-7. Spatial distributions of mean wind pressure coefficients

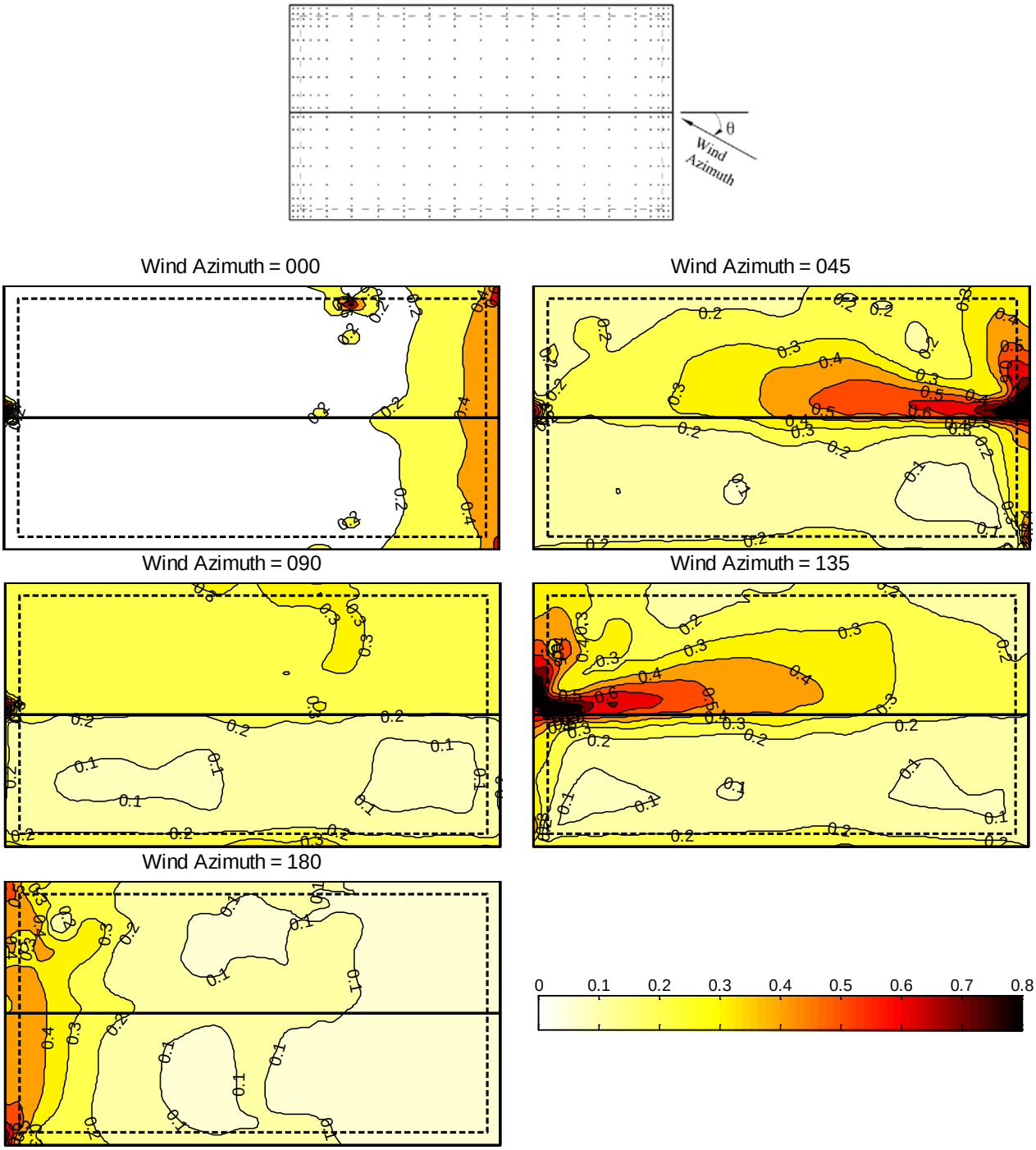

Figure 3-8. Spatial distributions of RMS of pressure coefficients

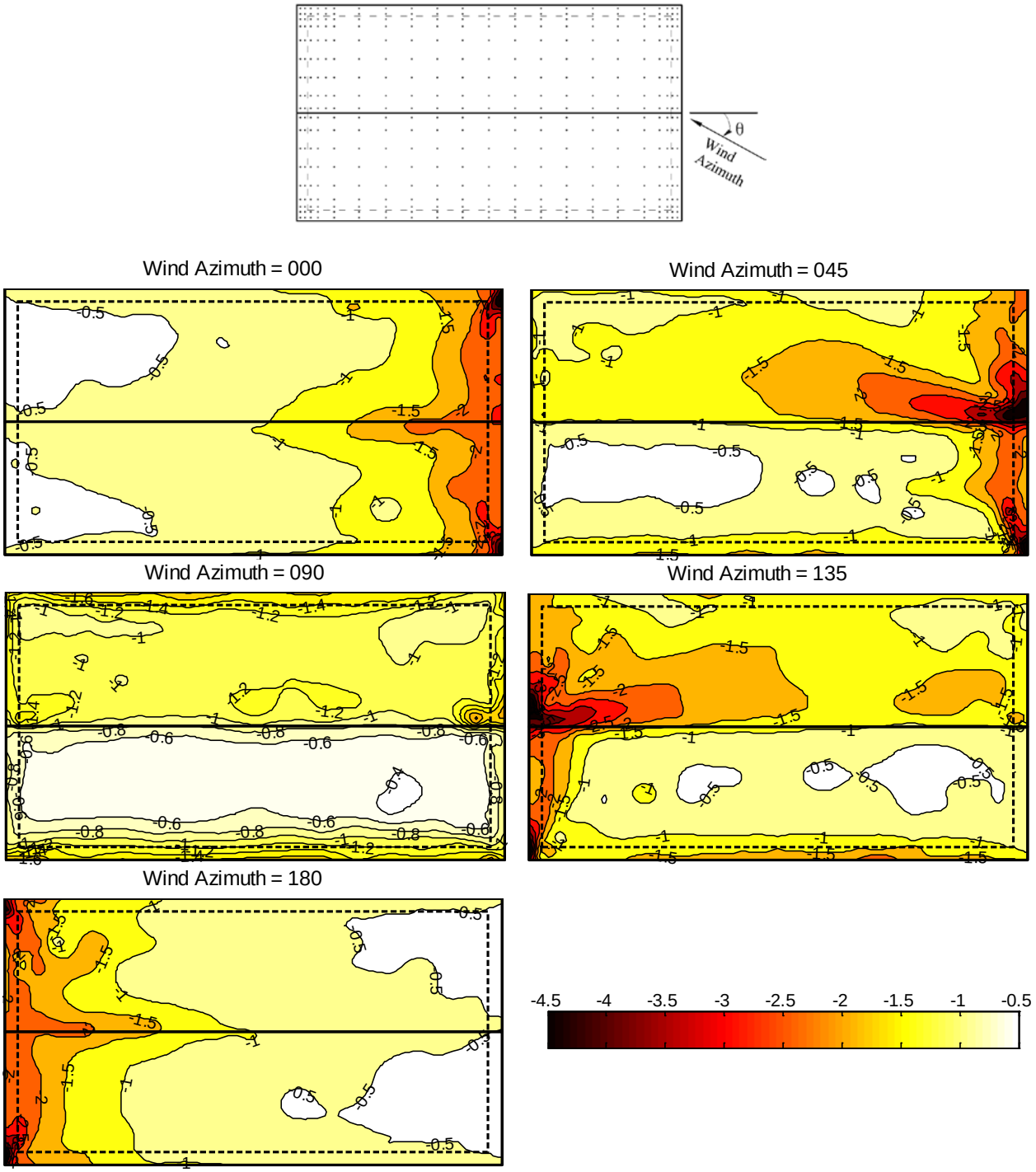

Figure 3-9. Spatial distributions of expected negative peak wind pressure coefficients

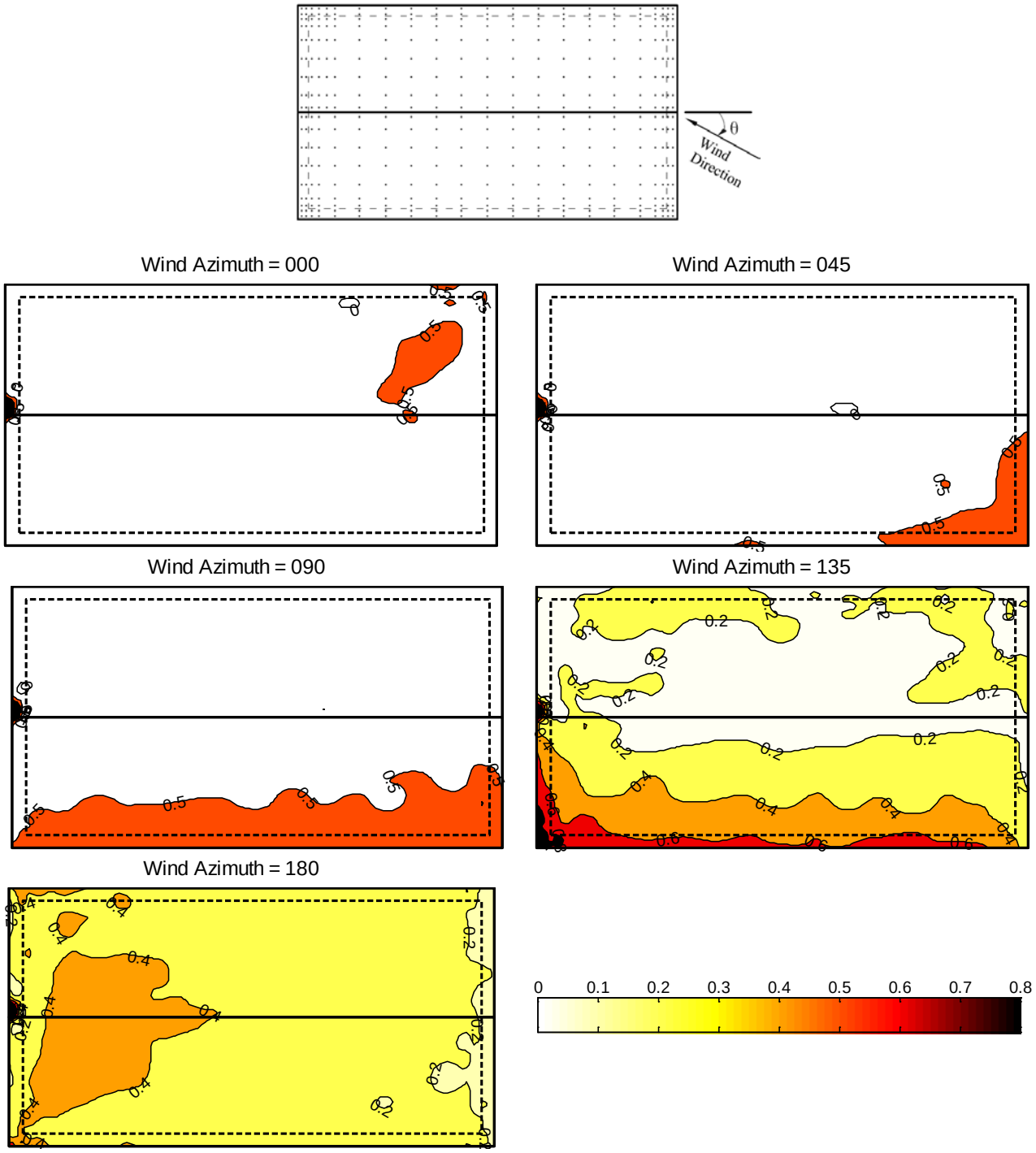

Figure 3-10. Spatial distributions of expected positive peak wind pressure coefficients

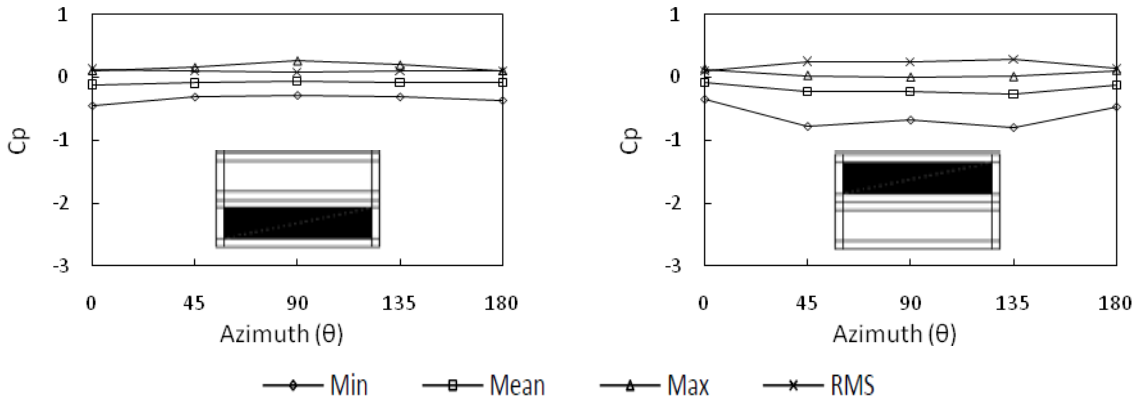

Figure 3-11. Area-averaged pressure coefficients for regions corresponding to zone 1 (Figure 6-11C in ASCE 7-05).

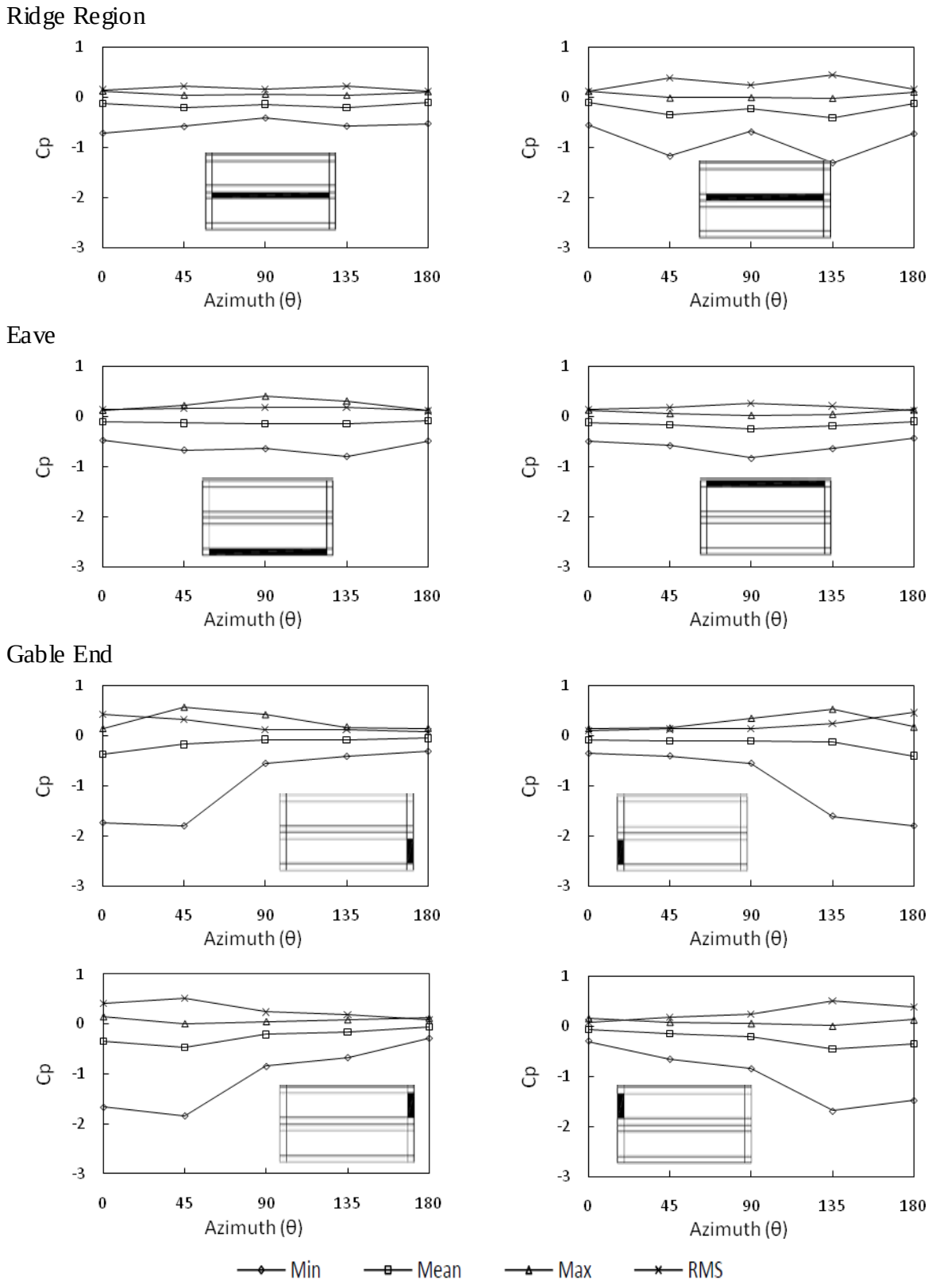

Figure 3-12. Area-averaged pressure coefficients for regions corresponding to zone 2 (Figure 6-11C in ASCE 7-05).

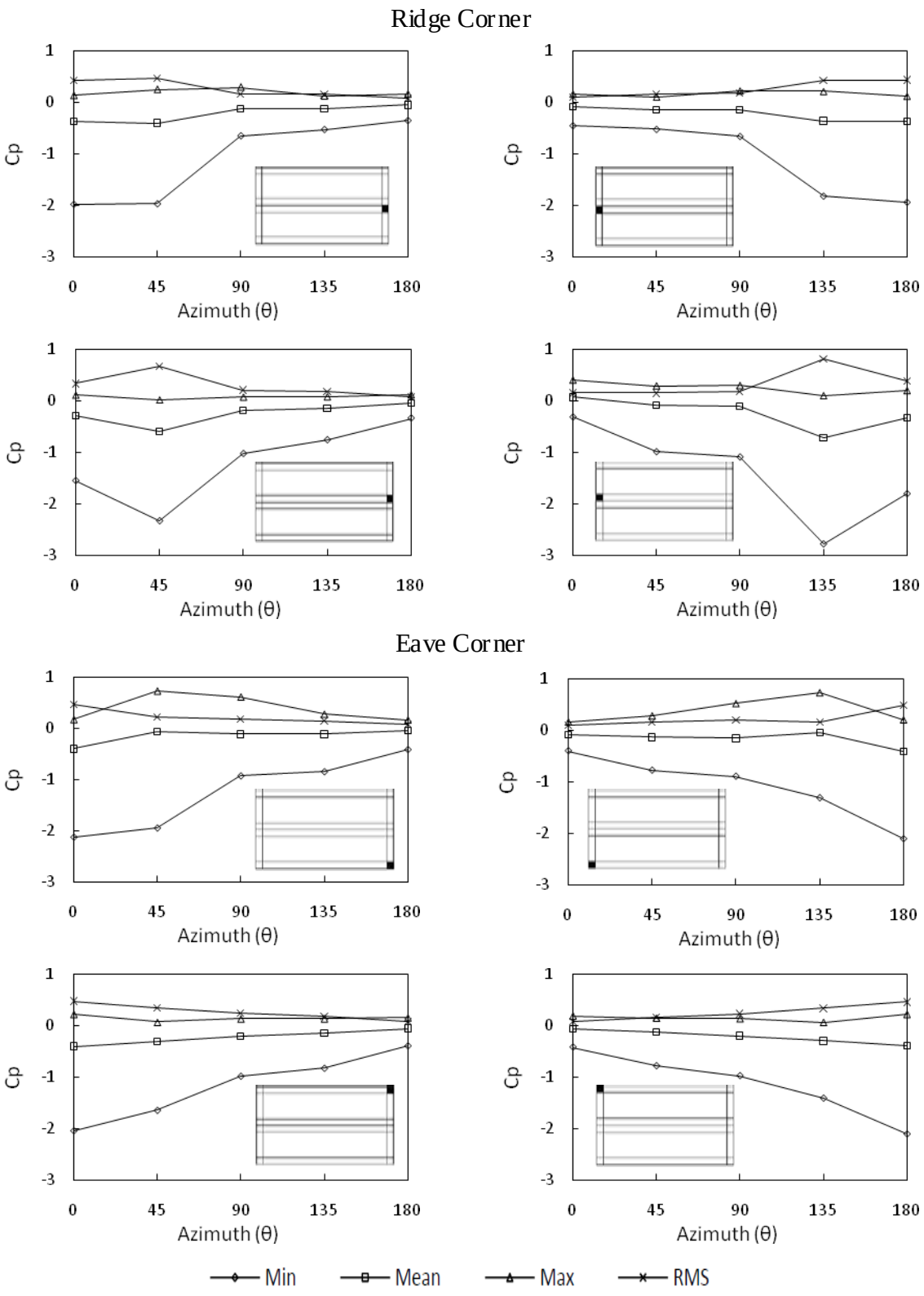

Figure 3-13. Area-averaged pressure coefficients for regions corresponding to zone 3 (Figure 6-11C in ASCE 7-05).

CHAPTER 4
APPLICATION OF DAD METHODOLGY

The database-assisted design (DAD) methodology utilizes wind-tunnel derived aerodynamic database of wind pressures in combination with structural influence functions to predict the wind load effects on a structural system.

In this chapter, pressure coefficient time histories developed in Chapter 3 are used with experimentally derived structural influences to estimate structural reactions at roof-to-wall and wall-to-foundation connections. This chapter opens with an overview of the structural influence functions which were determined by Datin et al.(2010). A detailed explanation of the application of the DAD approach in this study is provided. Finally, estimated structural reactions, analysis of results and their comparison with design wind loads based on ASCE 7-05 are presented.

Structural Influence Function

In structural analysis, the variation of shear, reaction, bending moment or deflection in a structure subjected to live load or moving load is generally best described using an influence line (Hibbeler 2006). An influence line therefore represents the variation of any structural response at a specific point in a member as a concentrated force moves over the member. Usually, the numerical values of a function for an influence line are determined using a dimensionless unit load. Subsequently the value of a response due to a force applied at any position can be obtained by multiplying the ordinate of the influence line at that position.

This concept of influence functions is also adopted in the use of the DAD methodology to predict wind-induced structural responses. For steel framed structures, influence functions used in DAD-based software provided by NIST(2008) are derived analytically from simple 2D model of a single frame. However, due to the high variability in wood properties, this study utilizes

influence functions determined experimentally on a 1/3-scale wood house model (shown in Figure 4-1A).

In the experiment, a point load was applied at grid points (shown in figure 4-1C) on the roof surface of the model house. The reactions induced by the point loads at 8 roof-to-wall and 9 wall-to-foundation connections were measured by load cells (locations shown in figure 4-1B). Influence coefficients at each load cell were determined by dividing the measured reactions by the load applied at the grid points. The resulting fraction (percentage) of the applied load provides a relative measure of forces transferred to the connections. Structural influence surfaces over of vertical reactions were generated for each load cell.

To justify the experimental procedure used, simple 2-D and 3-D models of the building roof system were analyzed in structural analysis software, 'Visual Analysis 4.0'. Truss members were modeled as simply supported beams and were pinned together. For the 3-D model, the roof sheathing was modeled as a plate element. In both cases, a unit load was applied at points on a truss of the system and an influence line was drawn for reaction at the truss support. Figure 4-3 shows a comparison of the results with the experimentally derived influence coefficients at grid points on a truss for a roof-to-wall connection of the truss. Influence function determined by 2D analytical model decreased linearly with distance between loading point and the support. However, while the 3D analytical model produced a close agreement with respect to the variation of influence function as compared to the experimental work, its influence coefficients differ from experimental results by as much as 30%.

Typical experimentally derived influence surfaces are shown in Figure 4-4.

Evaluating Vertical Reactions Based on DAD methodology

Velocity Pressure

Estimates of vertical reactions at the roof-to-wall and wall-to-foundation connections are based on wind speeds estimates without regard for direction as in the ASCE 7-05 provision. Velocity pressure, q_z *(psf)* was evaluated at the mean roof height of 14.3 ft as follows:

$$q_z = \frac{1}{2}\rho_{air} V_{14\,ft,sub}^2 \tag{4-1}$$

$$V_{14\,ft,sub} = \sqrt{K_z} V_{33\,ft,open} \tag{4-2}$$

where ρ_{air} is the density of air; K_z is an velocity pressure exposure coefficient whose square root transforms the 3-second wind speed in miles per hour at 33 ft above ground over open terrain, $V_{33ft,open}$ into 3-second gust wind speed at mean roof height over a suburban terrain, $V_{14ft,sub}$. K_z*=0.70* (Table 6-3 of ASCE 7-05) was used in the DAD approach in order to be consistent with the ASCE 7 procedure. Also the design wind speed, $V_{33ft,open}$*=130 mph* (figure 6-1 of ASCE 7-05 (2005) was chosen, for consistency with vertical reactions evaluated on the basis of ASCE 7-05. Hence,

$$V_{14\,ft,sub} = \sqrt{0.7}(130\ mph) = 108.8\ mph \tag{4-3}$$

$$q_z = 0.00256\,(108.8\ mph)^2 = 30.29\ psf \tag{4-4}$$

Pressure Taps and Influence Functions

The roof of the prototype house was divided into tributary areas of the pressure taps with the assumption that pressure coefficient measured by a tap was uniform within its geometric tributary area. Pressure taps were identified for the influence function grid points which fell within the tributary of the pressure taps. Consequently, two or more influence coefficients were

assigned to a pressure tap and load calculations were based on the tributary area of the influence function grid point.

Reaction Loads

Reaction time histories at eight roof-to-wall (gable end connection removed) and eleven wall-to-foundation connections were elevated by "UFDAD" using the wind-tunnel pressure coefficient time histories and the structural influence functions. The structural loads were determined by:

$$R_j(t) = q_z \sum_{i=1} \left[(N_i)_j C_{p,i}(t) A_i \right] \tag{4-5}$$

where $R_j(t)$ is structural load estimated at *jth* load cell at time, t; q_z *is* the velocity pressure evaluated at the mean roof height; $C_{pi}(t)$ is pressure coefficient for *ith* grid point at time t; $(N_i)_j$ is the influence coefficient at the *ith* grid point for *jth* load cell; and A_i is the tributary area of i^{th} grid point.

DAD Results and Analysis

Observed Statistical Values of Structural Reactions

Again, forty files were generated in this analysis each containing structural reaction time histories of the 17 load cells. These times histories are useful in determining peak loads and other statistical values of interests. They can furthermore be used effectively in probabilistic and structural reliability studies. Figures 4-6, 4-7 and 4-8 show the time-histories of the vertical reaction at connections 5, 10 and 15 for wind directions 0^o and 45^o. The sample mean RMS and extreme reactions were measured from the time histories for the forty samples of data. The measured statistical values of reactions for sample 1 are provided in Table 4-1.The statistical values for the other samples are provided in Appendix B.

Average values of RMS and mean reactions were calculated for each wind direction from the eight sample mean and RMS reactions. These quantities are not directly used in structural design but are useful for reliability analysis. Tables 4.2 shows computed RMS and mean reactions. The mean reactions are also shown in Figures 4-7 to 4-11.

Extreme Value Analysis of Vertical Loads

The peak or extreme uplift reactions are important statistical values that are used in structural design. Generally, Lieblein-fitted peak values are more statistically stable quantities than the measured peaks (Ho et al. 2005a). The measured peak reactions from the eight samples for each wind direction were fitted to Extreme Value Type 1 distributions. The location and scale parameters of these distributions were estimated using Best Linear Unbiased Estimators (BLUE) as proposed by Lieblein (1974). The same procedure explained in Chapter 3 of this report was followed.

The location parameter, μ and the scale parameter, β which were estimated for the uplift reactions are provided in Table 4-3. These parameters were used to obtain the probability density functions (PDF) and the cumulative density functions (CPF) of the peak reactions from which the mean peak reactions were estimated..

The "best" expected (mean) peak reaction load and corresponding standard deviation at the *jth* connection, in a given wind direction, were respectively determined as follows:

$$\hat{R}_j = \mu_j + 0.5772\beta_j \qquad s = \beta\pi/\sqrt{6} \tag{4-6}$$

The estimated peak reactions and standard deviations from the Type I Extreme Value analyses are provided in Table 4-4. Figures 4-7 to 4-11 show the expected peak and mean reactions at the connections for all the wind directions considered in this study.

It is observed from the plots that, a greater percentage of the uplift loads were transferred through the roof-to-wall connections (load cells 15 and 19) at the gable end. The highest uplift reaction (1750 lbs) estimated was transferred through load cell 15 for wind directions 0^o and 45^o. It is worth nothing that, the influence coefficients for this connection are higher at the gable edge and the ridge corners, where high suctions were observed. Again its influence surface was wide spread than in the case of the other roof-to-wall connections.

Again, though the connections between the gable end roof and wall were discontinued except at the end connections, reasonable uplift loads are transferred through foundation load cells 11, 12 and 13 for the directions. This is explained by the widespread of their influence surfaces as a result of the diaphragm action in the wall (similar to deep beam action). However, very small loads are transferred through load cell 14.

Relatively higher uplift loads were estimated at all connections for wind direction 0^o than the other azimuths. The loads generally decreased as the direction of the incident increased. Higher positive reactions were transferred through the load cells for wind azimuth 90^o because peak positive pressures enveloped the building for that wind direction.

Vertical Reaction Based on ASCE 7-05 Standard

ASCE 7-05 provides separate provisions for wind design using loads for either the main wind force resisting system (MWFRS) or for components and cladding (C&C) members. Major members of a building, which work together with other members in an assemblage to provide support and stability for the overall building, are designed using wind loads provided for MWFRS. Other members, which are directly loaded, are designed for localized wind load effects on relatively small areas using provisions for C&C.

Roof-to-wall connections (truss reactions) which serve as media for transfer of wind loading on the roof system to walls have in the past (Datin and Prevatt 2007) been designed as

part of the building's MWFRS. However, roof-to-wall connection failures may be likely due to localized wind effects acting on the roof which necessitate estimating wind load reactions at these connections based on C&C pressures. Moreover, ASCE 7-05 lists roof trusses under both C&C and MWFRS, which complicates the interpretation of the code for estimating reactions. For this reason, two separate analyses were done using both wind load provisions.

Velocity Pressure

Vertical reactions loads at roof-to-wall connections of the building were obtained using the Analytical Procedure (Method 2) for low-rise buildings (ASCE/SEI. 2005) with the design wind speed of $V_{33ft,open,3sec}=130\ mph$ (figure 6-1 of ASCE 7-05) and a suburban terrain. A velocity pressure exposure coefficient of $K_z=0.7$ (obtained from table 6-3 of ASCE 7-05) to modify the design wind speed to account for the suburban terrain condition and a mean roof height of 14.3 ft. This is very consistent with the wind speed used in the DAD estimations. A reduction factor, $K_d = 0.85$ to account for wind directionality effect was used in the ASCE 7-05 calculations even though no reduction factor was used in the DAD analysis. The importance factor I and the topographic effect factor K_{zt} were assumed to be unity. The velocity pressure, q_z for ASCE 7-05 calculation is as follows:

$$q_z = 0.00256 K_z K_{zt} K_d V^2_{33\,ft,open,3\,sec} I \tag{4-7}$$

$$q_z = 0.00256(0.7)(1.0)(0.85)(130mph)^2(1.0) = 25.74lb/ft^2 \tag{4-8}$$

ASCE 7-based Design Loads

Wind pressures on the building were determined as the just product of computed velocity pressure and external pressure coefficients because internal coefficients were not considered in the studies. In both MWFRS and C&C analysis, the study external pressure coefficients were determined based on the dimension, $a = 3ft$ (10% of the smallest horizontal dimension).

For ASCE 7-05 MWFRS, external pressure coefficients are defined with respect to roof angles and building surfaces. The building has a roof angle of 18.4^{o} and therefore linear interpolations were used to determine external pressure coefficients. Partitioning of the roof surface into four building surfaces as defined in Figure 6-10 of ASCE 7-05 is shown in Figure 4-12. Partitions were used to determine the pressures on the individual trusses. Table 4-5 shows MWFRS based wind pressures for the different building surface based on the velocity pressure.

In the case of C&C, external pressure coefficients were obtained from Figure 6-11C of the ASCE 7-05. Selection of the coefficients was based on an effective wind area of 300 ft^2, which is a product of 30 ft span length and one-third the span length. The building roof surface again, was partitioned into pressures zones as defined in ASCE 7 (see Figure 4-13). Wind Pressures based on C&C provisions for the zones including the roof overhang as given in Table 4-6.

Wind load intensity on each truss was calculated by multiplying pressure on the truss tributary area by its tributary width. Each truss was loaded with its pressure intensity and analyzed separately in "Visual Analysis 4.0" to determine the structural reaction at its support, for both MWFRS and C&C cases. For MWFRS case, the procedure was repeated for all the eight load patterns defined in Figure 6-10 in ASCE 7 to obtain the maximum uplift reaction.

Comparing Uplifts Reactions Predicted Based on DAD vs. ASCE 7-05

For comparison, the DAD-based reactions results were multiplied by 0.85 to account for the reduced probability of maximum winds coming from any direction, as it was in the case of the ASCE 7-based estimations. The worst uplift loads estimated at each of the roof to wall connections were selected and compared to the peak estimates based on the ASCE 7 Standard for MWFRS and Components and Cladding (C&C).

The comparison of the results based on ASCE 7-05 and DAD methodology are presented in Table 4-7. The results are graphically presented in Figure 4-13.

It is observed that the DAD-based reactions are generally higher than reactions based on ASCE 7-05 MWFRS provisions. At the gable end supports, ASCE 7 MWFRS underestimate the reaction at that support by as much as 28 % as compared to the DAD estimates. Underestimations of reactions by ASCE 7 MWFRS provisions are high at truss supports closer to the gable end of the house. Very close results are however observed between the results at truss supports which are far away from the gable end.

Significantly high reactions (by 6% to 62%) are observed for reactions based on ASCE 7-C&C than in the case of the DAD. Using discrepancies observed in the two comparisons above, the DAD results have a better agreement with ASCE 7 MWFRS estimates than C&C based estimates.

Table 4-1. Measured peak, mean and RMS reactions (lbs) for sample 1

Azimuth	0°				45°				90°				135°				180°			
Load Cells	Neg. Peak	Mean	Pos. Peak	RMS	Neg. Peak	Mean	Pos. Peak	RMS	Neg. Peak	Mean	Pos. Peak	RMS	Neg. Peak	Mean	Pos. Peak	RMS	Neg. Peak	Mean	Pos. Peak	RMS
1	-828	-171	86	199	-408	-96	180	115	-460	-61	287	90	-378	-88	235	106	-245	-23	139	48
2	-939	-201	70	229	-434	-116	137	134	-445	-61	276	87	-346	-83	223	99	-242	-24	132	47
3	-1067	-256	63	287	-749	-140	142	161	-414	-77	327	102	-364	-98	173	113	-259	-30	127	53
4	-1187	-294	67	328	-988	-141	184	167	-410	-82	403	110	-386	-104	139	120	-262	-33	134	56
5	-1099	-278	40	307	-987	-177	93	204	-442	-94	230	112	-327	-103	50	115	-212	-29	115	48
6	-400	-96	22	107	-245	-62	55	70	-178	-35	102	44	-143	-44	49	50	-109	-12	55	22
7	-218	-51	13	57	-123	-33	33	37	-103	-19	57	24	-81	-24	29	28	-61	-7	31	12
8	-335	-82	18	90	-222	-50	43	57	-131	-27	89	34	-112	-34	38	38	-82	-10	41	17
9	-766	-190	37	210	-559	-116	90	135	-275	-63	198	78	-242	-76	75	85	-179	-22	89	38
10	-1149	-291	47	320	-887	-191	110	218	-440	-102	259	122	-354	-117	93	131	-260	-33	132	56
11	-1562	-396	63	436	-1210	-260	146	298	-602	-142	344	168	-483	-161	127	180	-352	-45	181	77
12	-1391	-353	57	389	-1080	-230	134	264	-536	-125	310	150	-432	-142	115	159	-312	-40	161	68
13	-404	-103	16	114	-316	-69	37	79	-159	-38	86	44	-127	-42	32	47	-90	-12	47	20
14	-52	-14	2	15	-42	-10	4	11	-21	-5	11	6	-18	-6	4	6	-11	-2	6	3
15	-1668	-446	67	494	-1754	-308	158	373	-757	-157	308	184	-509	-164	74	182	-345	-49	182	77
19	-1388	-315	50	354	-1340	-328	9	359	-660	-169	50	185	-453	-139	86	153	-215	-36	111	55
20	-1343	-291	55	322	-1067	-310	10	339	-629	-171	60	187	-474	-143	101	157	-234	-32	133	54

Table 4-2. Averaged mean and RMS reactions (lbs)

Load Cells	0°		45°		90°		135°		180°	
	Mean	RMS	Mean	RMS	Mean	RMS	Mean	RMS	Mean	RMS
1	-168	196	-103	121	-63	93	-89	107	-32	53
2	-197	226	-123	140	-62	89	-84	100	-32	52
3	-250	282	-149	168	-78	103	-99	114	-39	58
4	-288	321	-150	174	-83	111	-105	121	-43	62
5	-272	302	-187	212	-95	113	-105	116	-38	54
6	-94	105	-66	73	-36	45	-45	50	-16	24
7	-50	56	-35	39	-19	24	-24	28	-9	13
8	-80	89	-53	60	-28	35	-34	39	-13	19
9	-186	206	-123	140	-64	79	-77	86	-29	42
10	-285	315	-201	227	-103	124	-118	132	-44	63
11	-388	429	-275	310	-143	171	-163	181	-60	86
12	-346	382	-243	275	-127	151	-144	161	-53	77
13	-101	112	-73	82	-38	45	-43	47	-15	22
14	-13	15	-10	12	-5	6	-6	6	-2	3
15	-437	486	-324	385	-159	186	-167	184	-64	88
19	-309	349	-344	372	-169	184	-139	154	-48	63
20	-286	318	-326	352	-171	186	-143	158	-45	63

Table 4-3. Parameters (lbs) for Type I Extreme Value Distribution of peak negative reactions

Load Cells	0°		45°		90°		135°		180°	
	μ	β	μ	β	μ	β	μ	β	μ	β
1	758	61	441	101	380	29	379	28	249	23
2	856	50	463	91	355	35	352	26	241	22
3	1037	40	608	68	391	33	374	21	259	22
4	1168	112	791	82	412	34	399	23	268	22
5	1053	98	875	55	380	38	344	27	225	24
6	369	14	232	21	160	14	148	12	106	7
7	199	11	120	14	88	9	84	6	60	4
8	304	16	206	15	125	9	116	7	82	5
9	698	49	510	32	278	20	256	18	179	11
10	1061	78	824	47	428	30	380	33	261	18
11	1446	105	1123	64	587	42	522	47	355	26
12	1289	96	1000	58	522	38	465	40	315	24
13	377	29	295	17	154	11	137	12	91	7
14	50	4	40	2	21	1	19	1	12	1
15	1608	171	1665	75	630	84	538	46	354	27
19	1257	106	1136	96	598	70	491	39	235	25
20	1125	86	1022	95	563	64	496	27	239	23

Table 4-4. Expected peak negative (uplift) reactions (lbs) and standard deviation (lbs) estimated from BLUE fitted probability distribution

Load Cells	0°		45°		90°		135°		180°	
	Mean	Std	Mean	Std	Mean	Std	Mean	Std	Mean	Std
1	-793	78	-500	129	-397	37	-394	35	-262	29
2	-885	65	-516	117	-375	45	-366	33	-254	28
3	-1061	52	-647	88	-410	42	-386	27	-271	28
4	-1232	144	-838	105	-432	43	-413	30	-281	29
5	-1110	126	-907	70	-402	49	-360	35	-239	31
6	-377	18	-244	28	-168	17	-155	15	-110	9
7	-206	14	-128	18	-93	11	-87	8	-62	5
8	-314	21	-215	20	-130	12	-121	10	-84	6
9	-726	63	-528	41	-289	26	-267	23	-185	14
10	-1106	100	-851	60	-446	39	-399	42	-271	23
11	-1506	134	-1160	82	-611	54	-549	60	-370	34
12	-1344	123	-1033	74	-543	48	-489	52	-329	31
13	-393	37	-304	22	-160	14	-144	16	-96	9
14	-52	5	-42	3	-22	2	-20	2	-13	1
15	-1707	219	-1708	96	-679	108	-564	59	-369	35
19	-1318	135	-1192	123	-638	89	-513	50	-249	31
20	-1175	110	-1077	121	-599	81	-511	35	-252	30

Table 4-5. Pressures based on MWFRS for different building surface

Building Surface	2	3	2E	3E
GC_{pf}	-0.69	-0.47	-1.07	-0.67
Pressure (lb/ft^2)	-17.76	-12.10	-27.54	-17.25

Table 4-6. Pressures based on C&C for different zones

	Roof			Overhang	
Zones	1	2	3	2	3
GC_p	-0.8	-1.2	-2	-2.2	-2.5
Pressure (lb/ft^2)	-20.6	-30.9	-51.5	-56.6	-64.4

Table 4-7. Comparison of uplift reaction estimates based on DAD and ASCE 7-05

Connection Number		1	2	3	4	5	15	19	20
DAD		-674	-752	-902	-1047	-944	-1452	-1120	-999
ASCE 7-05	MWFRS	-763	-763	-763	-830	-830	-1043	-840	-659
	C&C	-956	-956	-956	-956	-1435	-1794	-1794	-1435

Figure 4-1. 1/3 Scale house model for determining influence functions

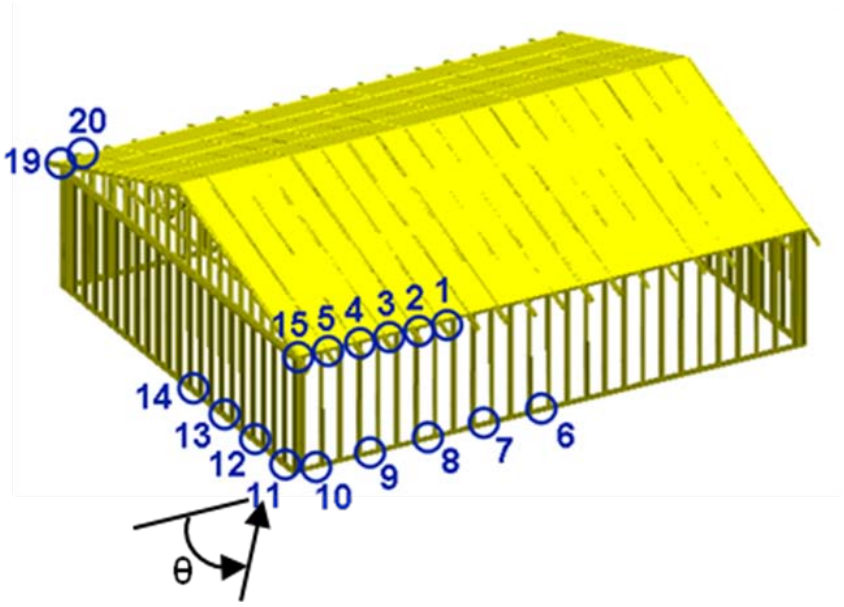

Figure 4-2. Locations of load cells and wind direction

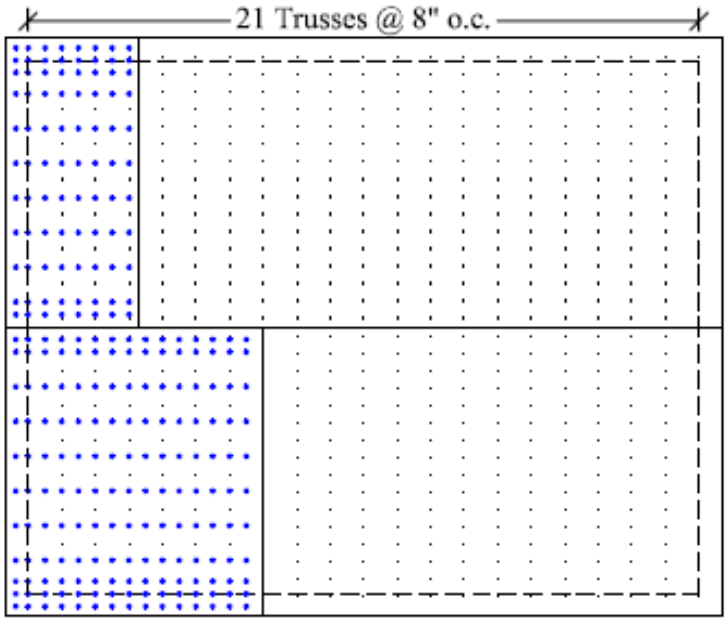

Figure 4-3. Grid points for experimental determination of influence coefficients

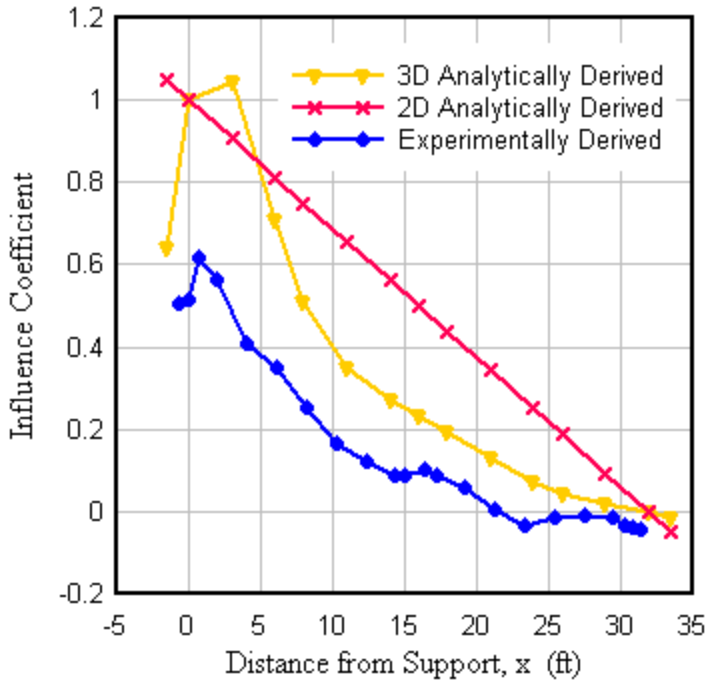

Figure 4-4. Influence lines for vertical reactions at a support (roof-to-wall connection) of an internal truss

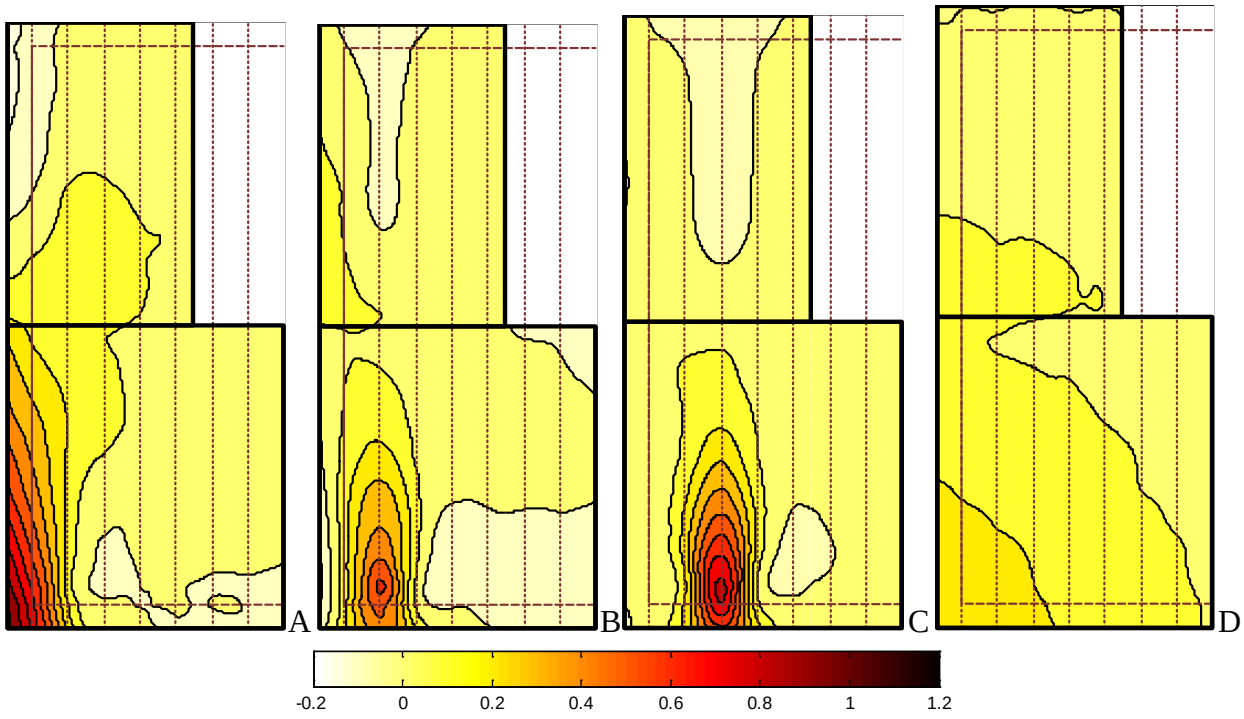

Figure 4-5. Typical influence surfaces for vertical reaction determined on 1/3-scale house model A) load cell 15 B) load cell 5 C) load cell 4 D) load cell 11

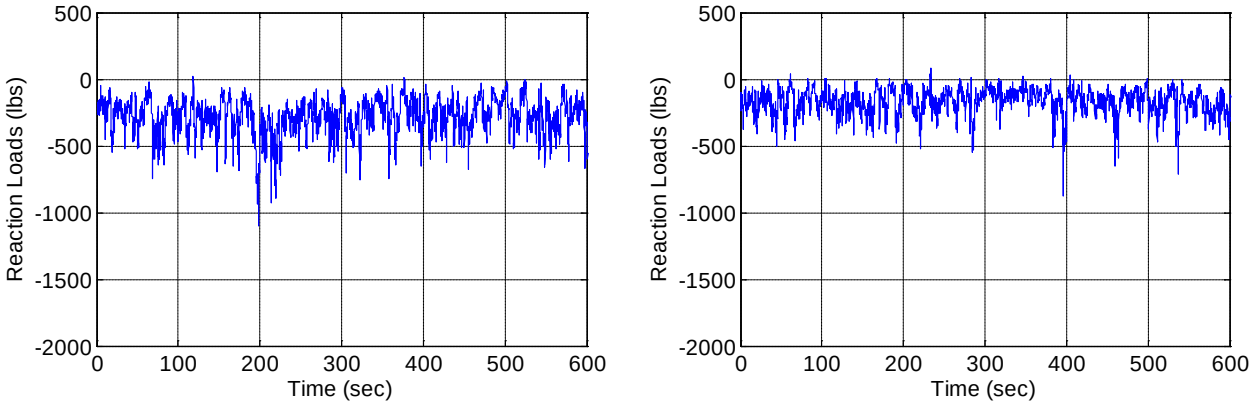

Figure 4-6. First 10 minutes load time Series at roof-to-wall load cell 5 A) wind azimuth 0° B) wind azimuth 45°

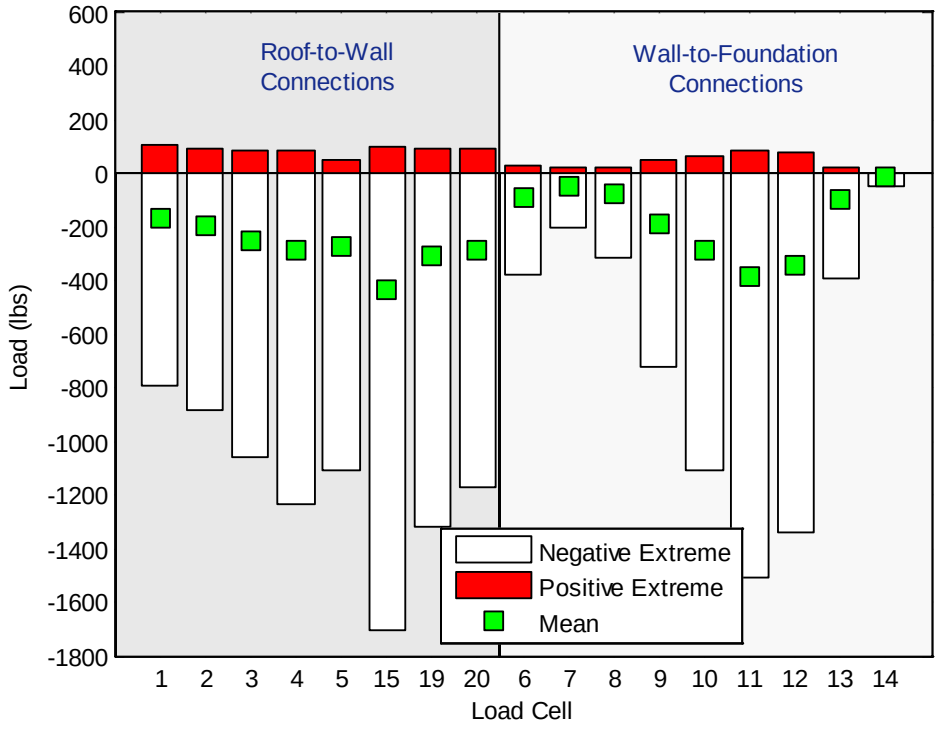

Figure 4-7. Estimated mean and peak vertical reactions at load cells for wind azimuth 000°

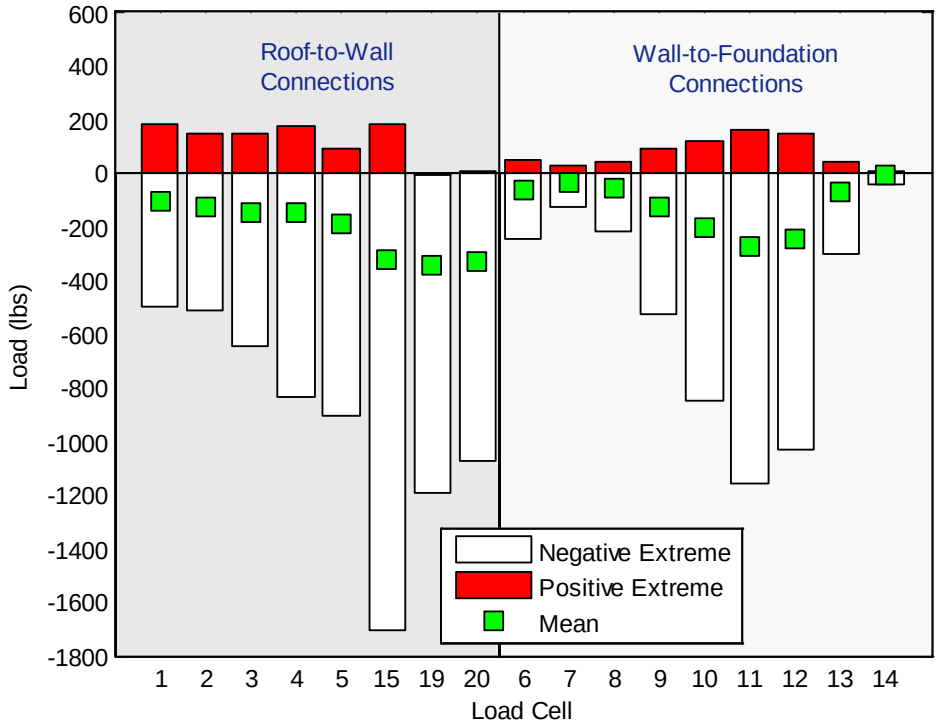

Figure 4-8. Estimated mean and peak vertical reactions at load cells for wind azimuth 045°

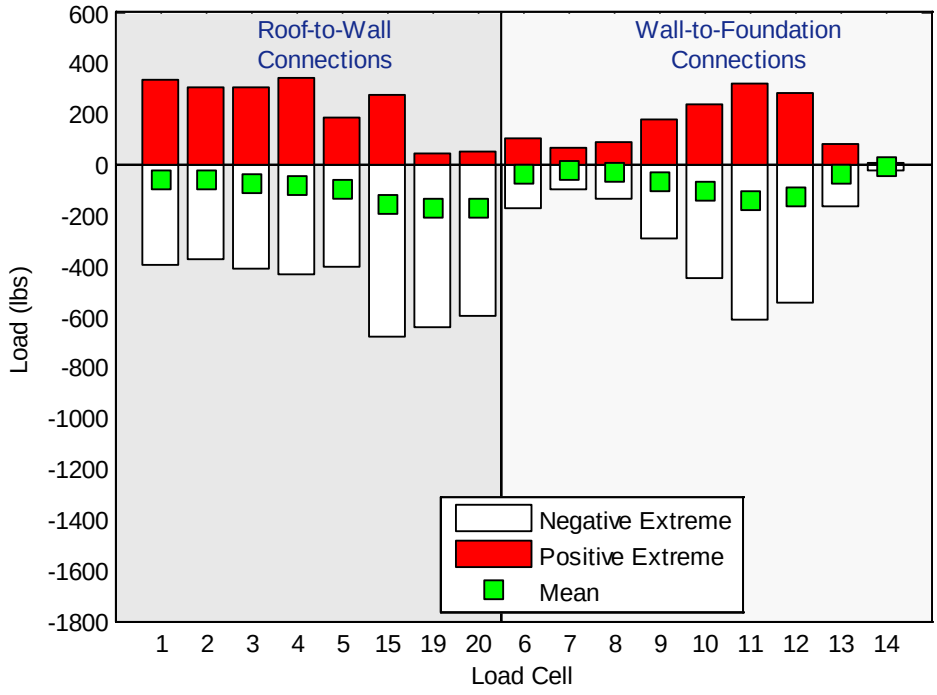

Figure 4-9. Estimated mean and peak vertical reactions at load cells for wind azimuth 090°

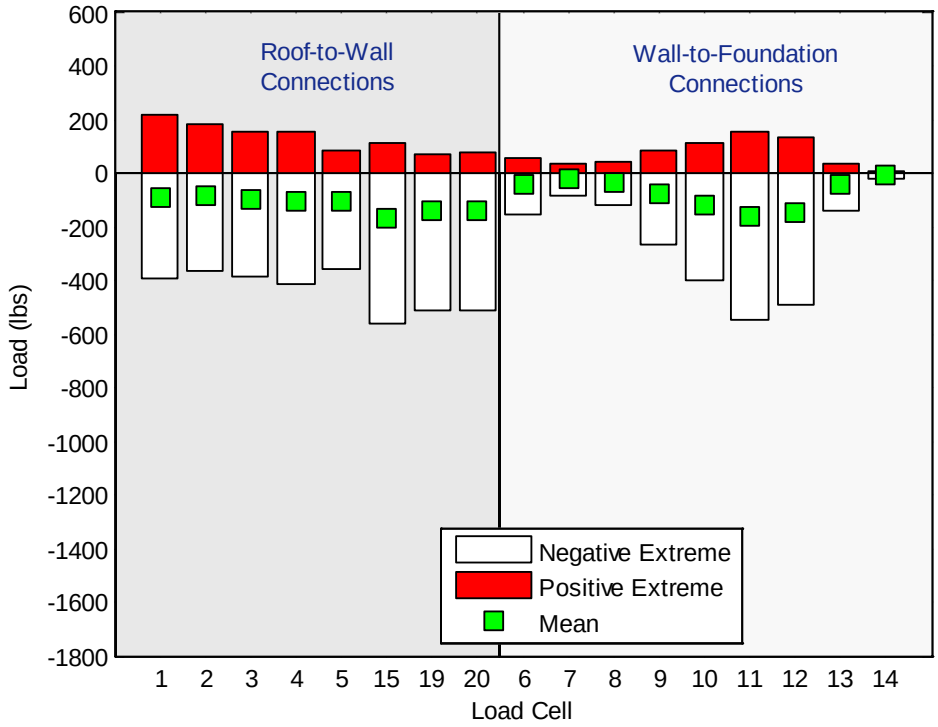

Figure 4-10. Estimated mean and peak vertical reactions at load cells for wind azimuth 135°

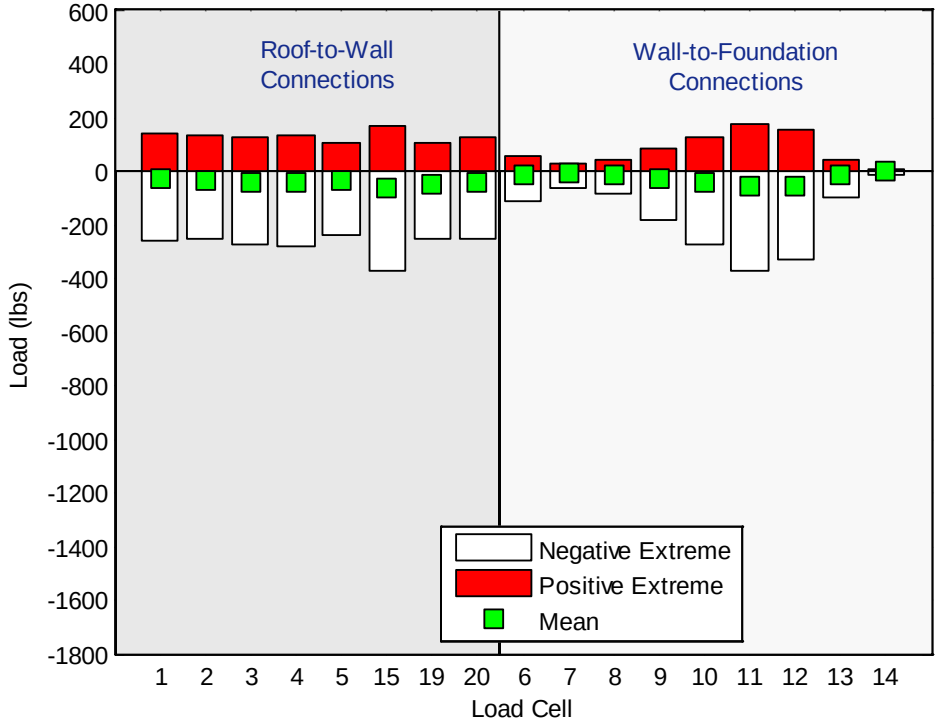

Figure 4-11. Estimated mean and peak vertical reactions at load cells for wind azimuth 180°

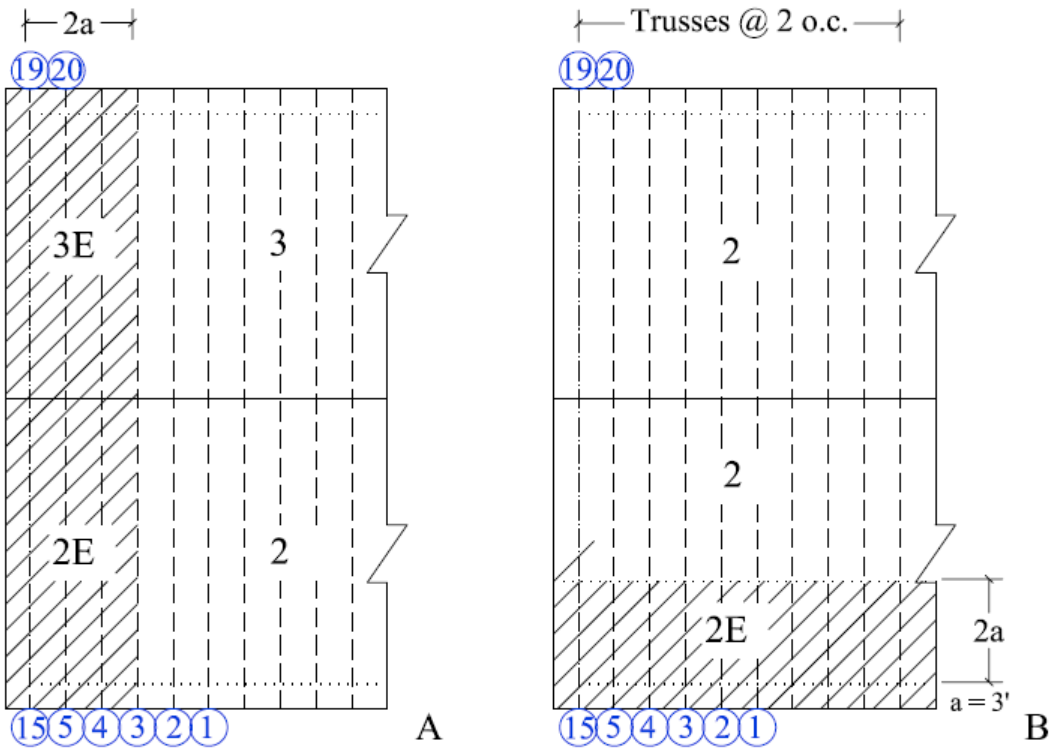

Figure 4-12. Building surfaces for determining wind pressure for each truss based on ASCE 7 provisions for MWFRS A) Transverse direction B) Longitudinal direction

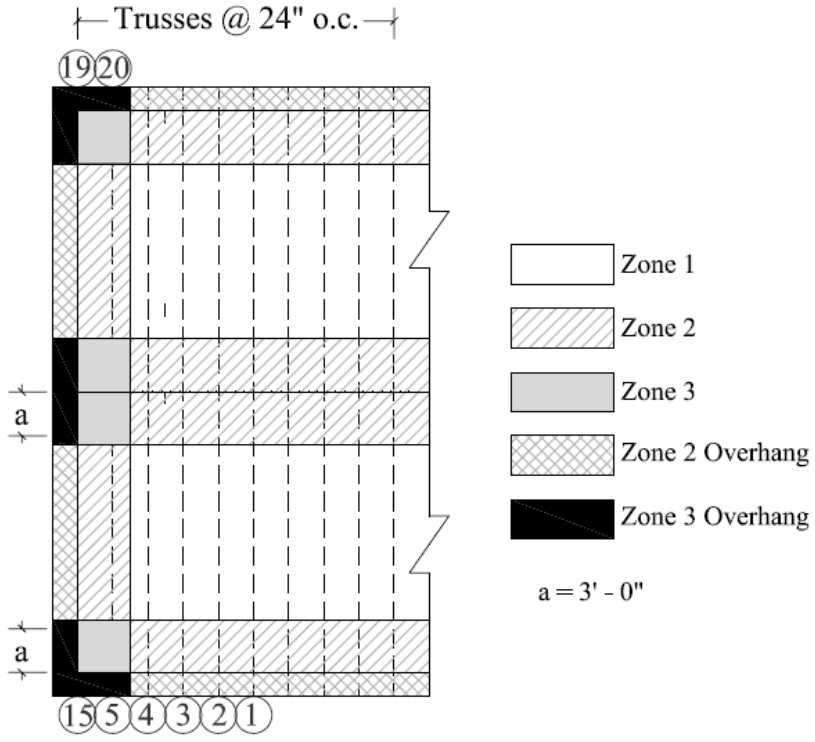

Figure 4-13. Zones for determining wind pressure for each truss based on ASCE 7 provisions for components and cladding

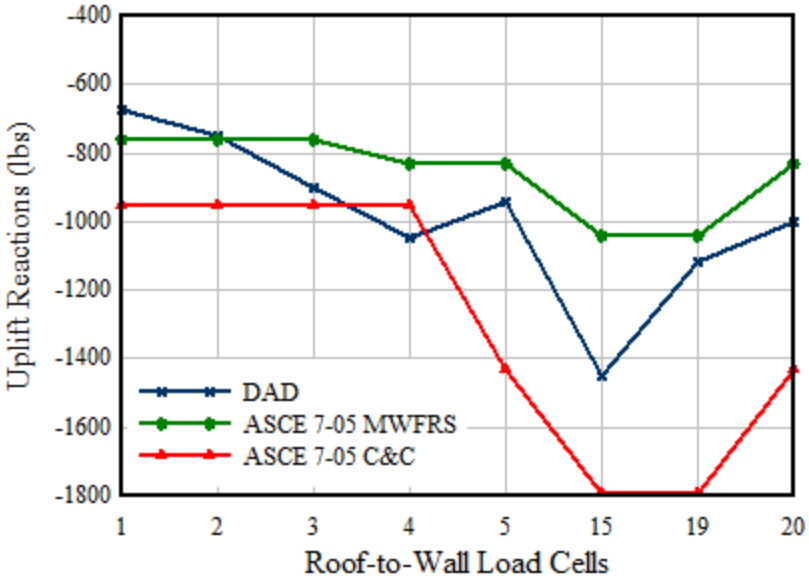

Figure 4-14. Uplift reactions at roof-to-wall load cells based on DAD approach and ASCE 7-05 provisions

CHAPTER 5
WIND FLOW CHARACTERIZATION USING TFI COBRA PROBE

The flow characteristics of wind largely influence the intensity and fluctuation of wind forces on structures. The experimental component of the study includes a scale house model immersed within a wind flow generated by a UF Wind Generator. A multi-hole pressure probe called the Cobra Probe was used to map the wind flow characteristics to provide the necessary information for analyzing the data.

This chapter discusses the Cobra Probe, its principle of operation and pilot flow measurements conducted prior to using it in the main experimental study. Flow characterization of the wind field produced for the experiment is also presented in this chapter.

The Cobra Probe

The Cobra Probe (shown in Figure 5-1A) is a robust and compact multi-hole pressure probe designed by Turbulent Flow Instrumentation (TFI), Australia, for measuring turbulent wind flows. The Cobra probe was first proposed by Shepherd (1981) for mean flow measurements and further developed by Hooper and Musgrove (1997) for resolving turbulence structure. The device has the following advantages:

1. It resolves highly turbulent wind flows into three orthogonal components at high frequency (up to 10000 Hz).
2. It is a robust self contained device.
3. It can withstand significant levels of instrument vibration and maintain accuracy (Watkins et al. 2004).

The high sampling frequency of the probe allows for continuous data streaming, with virtually unlimited data to be recorded while avoiding aliasing and reducing measurement of noise. The Probe has a truncated triangular pyramid-shaped head with four faces ground flat to 45^{o} (Chen et al. 2000). Each face has a 0.5 mm diameter pressure tap located at its center that is

connected to piezo-resistive bridge pressure transducers, and a preamplifier system located within the body of the probe. This arrangement was necessary to minimize the length of tubing so as to achieve a high frequency response as well as mechanically protecting the transducers. The probe has an overall length of 160 mm and a body diameter of 14 mm. The design of the probe is shown in Figure 5-1B.

The principle of operation of the probe is to relate the pressure field detected by four pressure transducers to the magnitude of the instantaneous local velocity vector, yaw and pitch angles and the instantaneous static pressure. Pressure signals measured are corrected for transmission effects, using a predetermined transfer function (frequency response function) of pressure tubing (Chen et al. 2000).

A Series 100 Cobra Probe (Serial ID 193) was used in the study. It has a velocity range of 3 m/s to 60 m/s and an accuracy of 0.5± m/s and was supplied with an interface unit housing an integrated data acquisition and device control software.

Preliminary Experiments Using the Cobra Probe

Pilot experiments were conducted using the Cobra Probe aimed at (1) comparing flow measurements by the probe and hotwire anemometer (b) understanding the use and principle of the probe and (3) evaluating methods in modeling flow field conditions for the study's main experiment.

In all the preliminary experiments, flow measurements were usually sampled by the probe at 5000 Hz and down sampled at a rate of 2500 Hz for 120 seconds per each test run. Before each test, the probe was zeroed to remove offset voltages from its pressure transducers.

Comparing Wind Flow Measurements by the Cobra Probe and Hotwire Anemometer

Flow measurements were simultaneously taken by the cobra probe and a hot-wire anemometer in a generated wind field. Table 5-1 compares the mean axial velocities, U, and

turbulence intensities, I_{uu}, measured by the Cobra Probe and the hot-wire anemometer. Good agreement is observed for the mean velocities. However, significant differences are observed for the turbulence intensities, which may in part be due to errors as a result of relative positions of the instruments.

Wind Tunnel Model

Several tests were done in a small wind tunnel (shown in Figure 5-3) to understand the principle and usage of the probe. The wind tunnel consists of a 10 ft long test section, a contraction area, and a plenum and flow straighter section. It is powered by a 2 ft diameter axial fan. The test section is 24 in wide and 8 in high.

Results from one test where flow measurements were taken at points (shown in Figure 5-4) within a 2D surface at 0.5 in downstream of the wind tunnel exit are presented. Profiles for all the orthogonal mean velocities measured are shown in Figure 5-5. Corresponding turbulence intensity distributions for longitudinal (I_{uu}), transverse (I_{vv}) and vertical (I_{ww}) directions of flow are also displayed in Figure 5-5B. It is seen from the plots that very low transverse and vertical wind velocities are recorded away from the walls as compared to the high axial velocities. Relatively low axial velocities with corresponding high turbulent intensities are observed near the wall surfaces of the test section. This is due to a high frictional effect near the wall surfaces. Figures 5-6 to 5-8 show the 2D variation of the mean velocities and turbulent intensities across the test section. The spectral contents of wind speeds at the exit of the wind tunnel are displayed in Figure 5-9.

Mapping of Wind Field Generated by UF Wind Generator

Velocity and turbulent intensity measurements of the wind flow generated by the UF wind generator were taken prior to this study's experimental work. The main purpose was to investigate if the wind field was uniform within the test area.

The probe was mounted on a computer-controlled traverse to control the horizontal position. Vertical adjustments of the probe were done manually. The traverse frame was set up in two locations laterally to map the wind flow across the section. Figure 5-10 shows the traverse frame within the test area.

The Cobra Probe was used to measure flow characteristics at 90 locations (shown in Figure 5-11) within a cross-section at 16 ft downstream of the wind generator. Each measurement was taken for 60 seconds at a sampling frequency of 10000 Hz and output to file at 5000 Hz. A mean wind velocity of 50 mph (22 m/s) was used for all the tests.

Contour plots of longitudinal, transverse and vertical wind fields are shown in Figures 5-12 and 5-13. Relatively low longitudinal wind speeds at locations outside the jet field were observed. Longitudinal wind speed was generally uniform across the cross-section but decrease near the wall.

Table 5-1. Comparison of flow measurements by Cobra Probe and hot-wire anemometer

Height (in)	Cobra Probe		Hot-wire		%Difference	
	U (m/s)	Iuu (%)	U (m/s)	Iuu (%)	U	Iuu
2	5.47	14.33	5.13	13.38	6.2%	6.6%
6	6.26	13.83	6.36	10.68	1.6%	22.8%
10	5.83	10.15	6.28	11.38	7.7%	12.1%

Figure 5-1. Cobra Probe

Figure 5-2. Cobra Probe and Hot-wire anemometer setup for simultaneous measurements

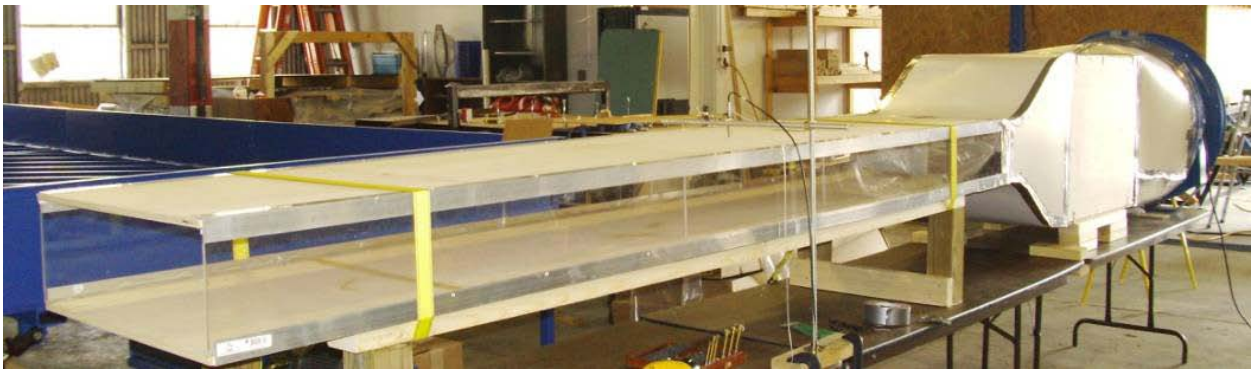

Figure 5-3. Wind tunnel model used in pilot studies

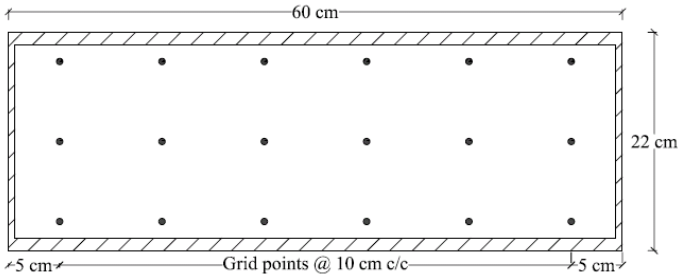

Figure 5-4. Measuring points for mapping flow measurements at of the wind tunnel

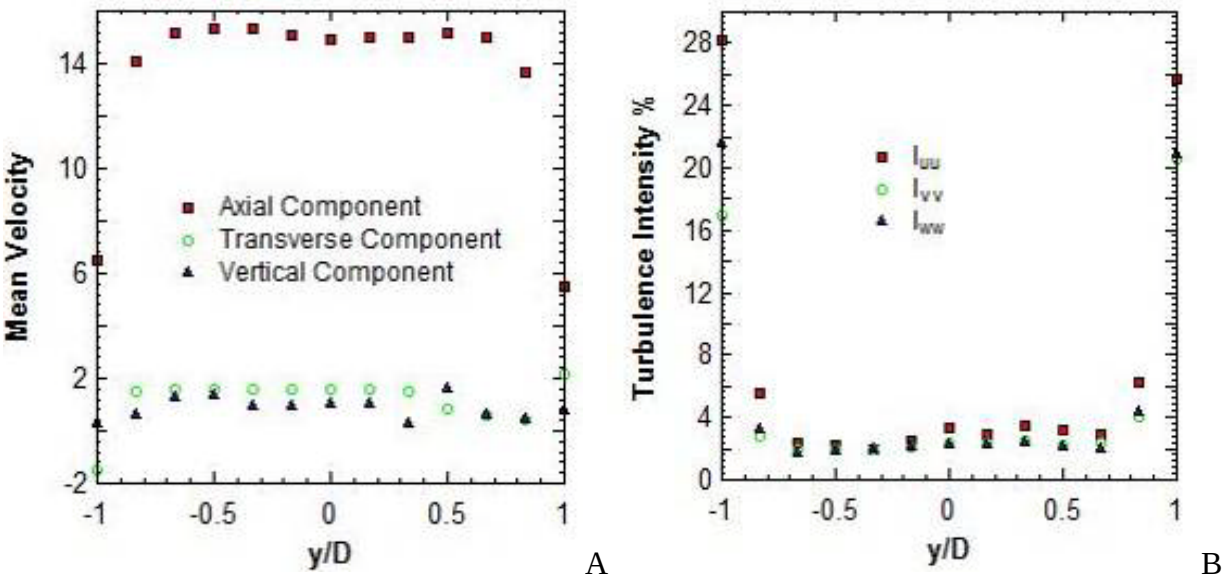

Figure 5-5. Flow measurements at exit of wind tunnel model A) Mean velocity (m/s) distributions. B) Turbulence intensity distributions *(y is distance of grid point relative to the midpoint of test section; D is half the width of test section)*

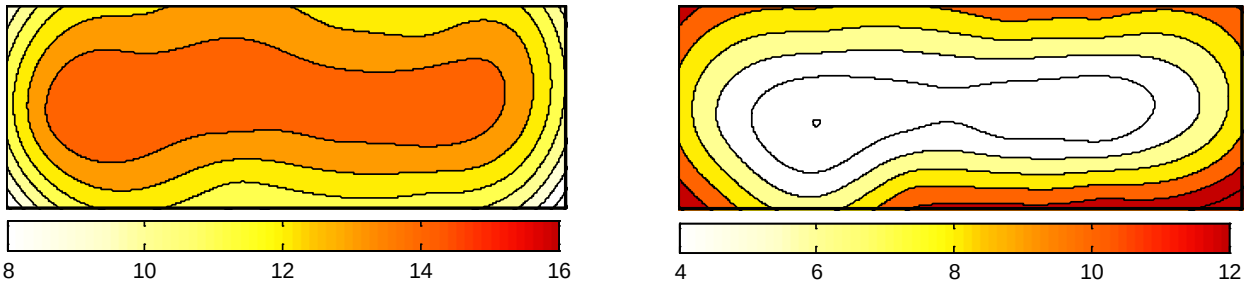

Figure 5-6. Spatial variations of longitudinal velocity (m/s) and turbulence intensity (%) across exit section of wind tunnel model

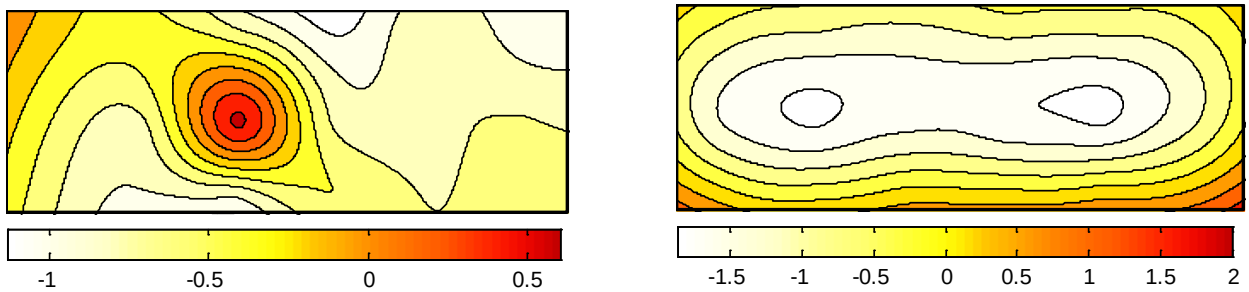

Figure 5-7. Spatial variations of lateral velocity (m/s) and turbulence intensity (%) across exit section of wind tunnel model

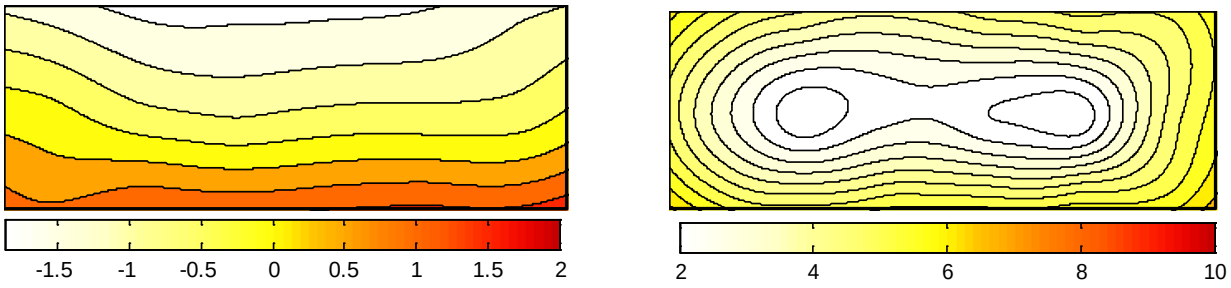

Figure 5-8. Spatial variations of lateral velocity (m/s) and turbulence intensity (%) across exit section of wind tunnel model

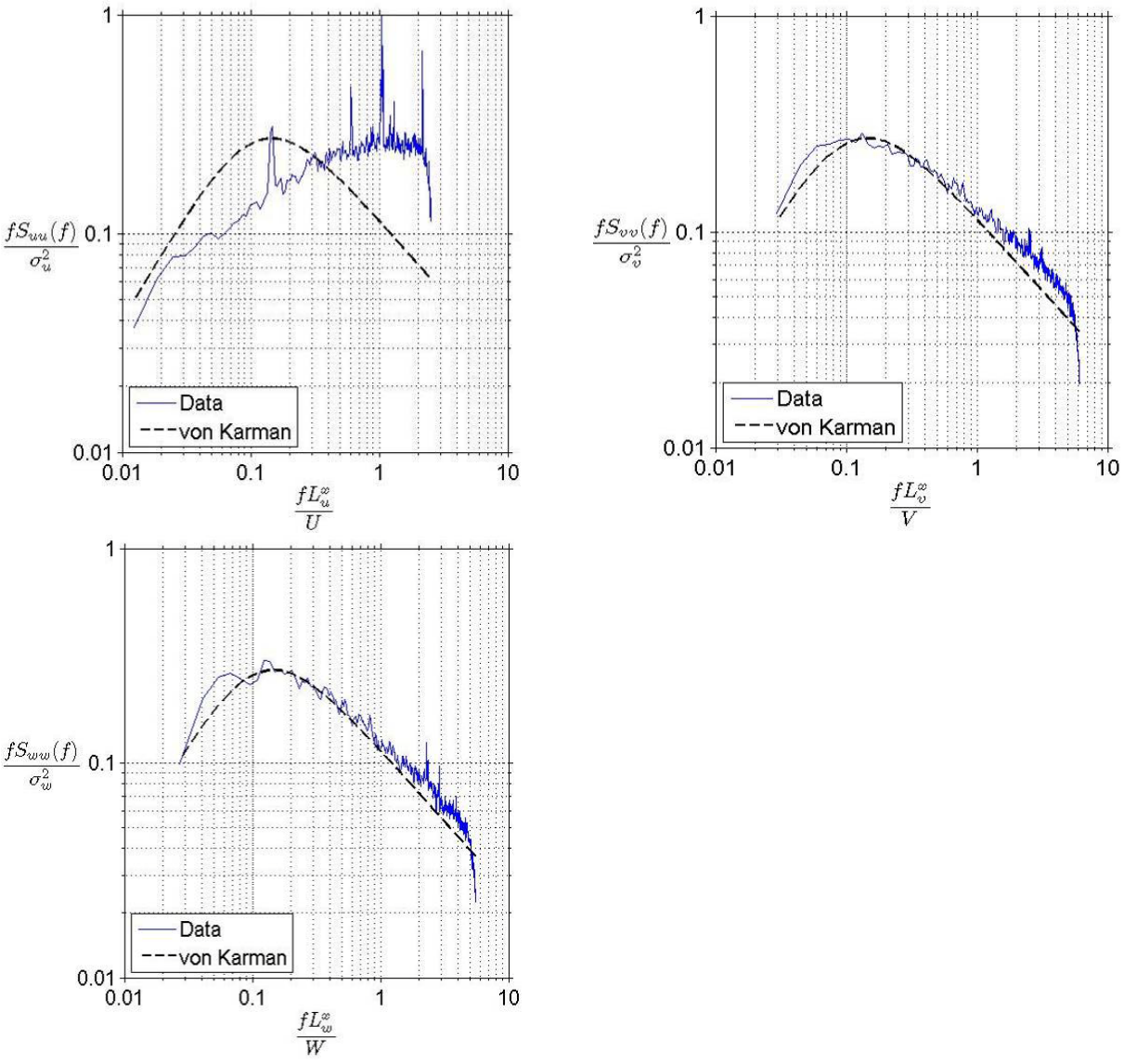

Figure 5-9. Longitudinal, transverse and vertical spectral contents of wind speed at 0.5 in. downstream of the exit of the wind tunnel

Figure 5-10. Position of traverse frame in test section

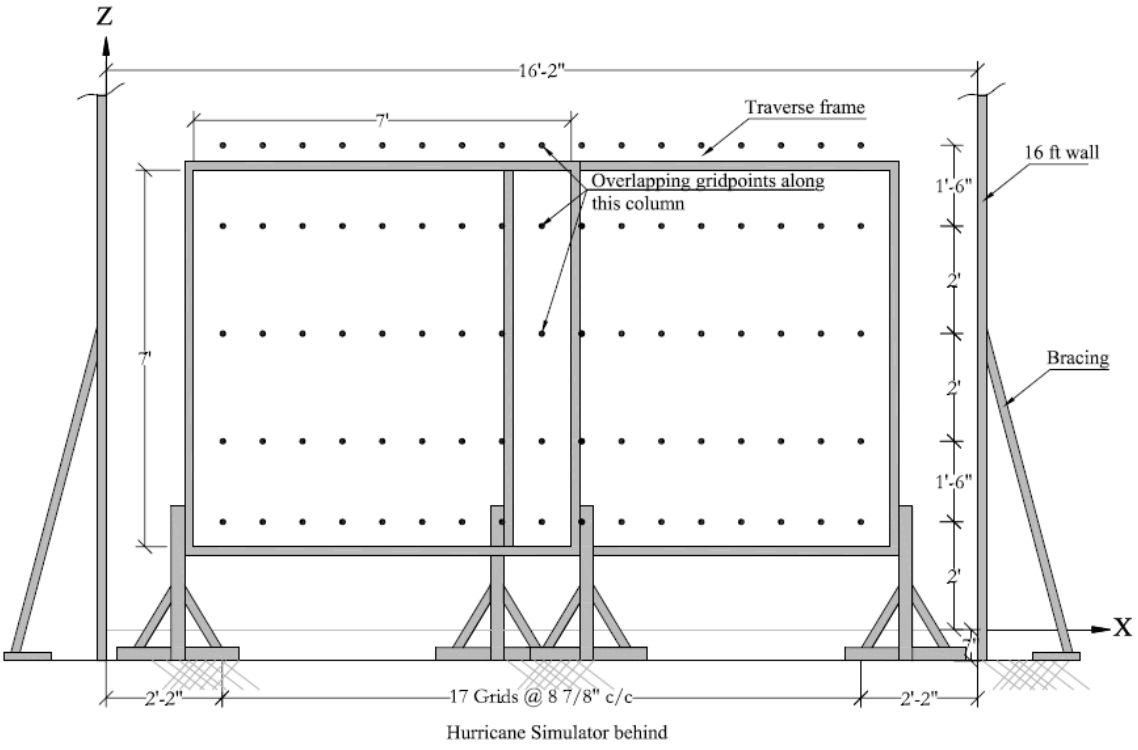

Figure 5-11. Location of measurements points for flow mapping

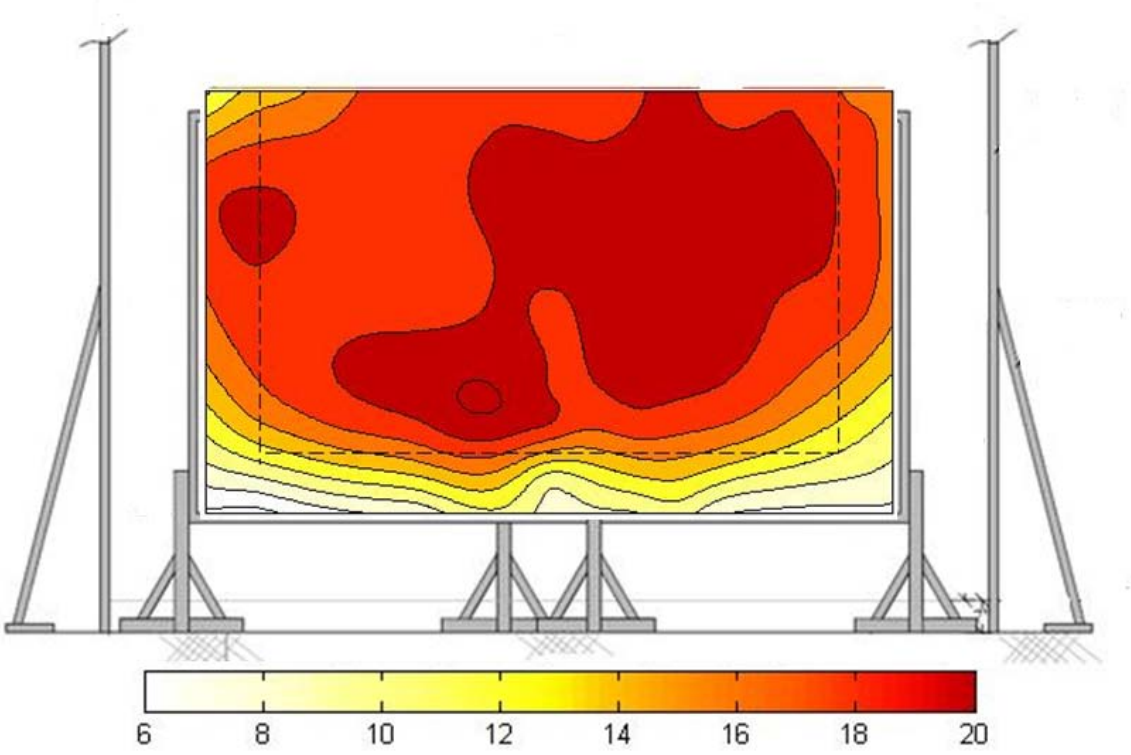

Figure 5-12. Variation of longitudinal wind speed across 2D measurement surface

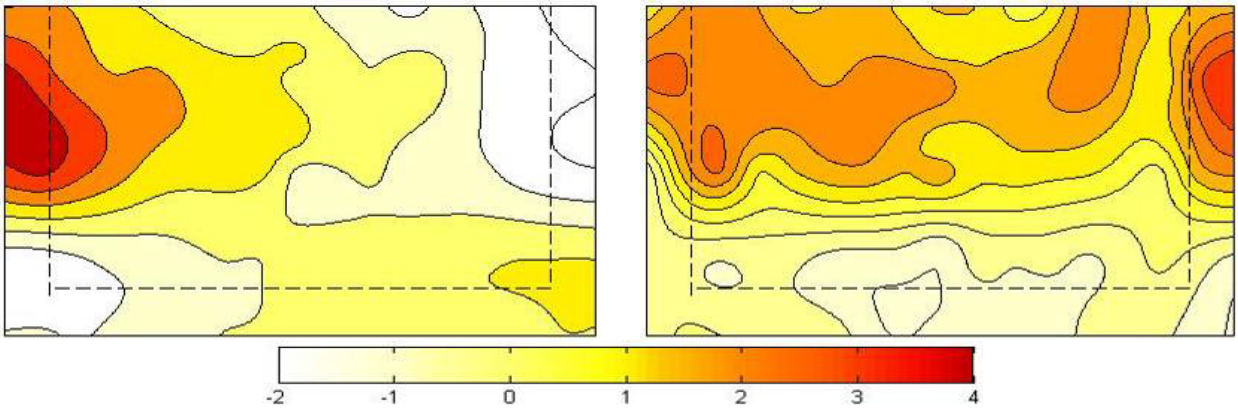

Figure 5-13. Variation of lateral and vertical wind speed across 2D measurement surface

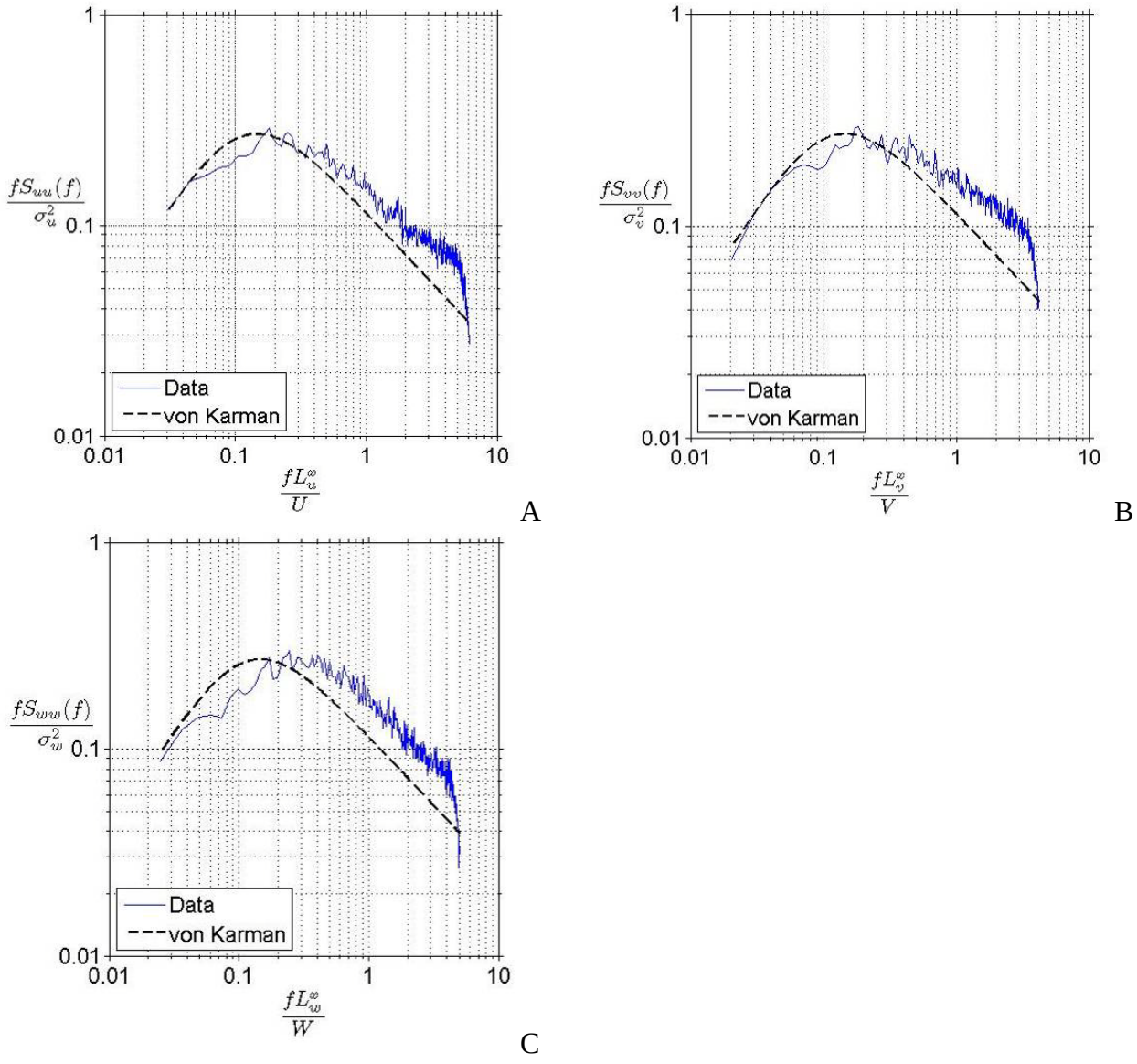

Figure 5-14. Spectral contents of wind speed A) longitudinal B) Transverse C) Vertical

CHAPTER 6
WIND INDUCED PRESSURE AND STRUCTURAL LOAD MEASUREMENTS

The objective of the experimental component of the research is to evaluate the validity of using the DAD methodology to predict wind-induced structural loads as discussed in Chapter 5. This chapter presents the experimental study, results and analysis performed to validate the DAD approach.

Materials and Methods

Scale House Model

The 1/3 scale house (shown in Figure 6-9) was modeled and constructed by Datin et al. (2009) based on non-dimensional geometrical scaling laws. The building model has a rectangular floor plan which is 10 ft wide by 13 ft 4 in. long (30 ft by 40 ft at full scale) and a mean roof height of 4 ft 1 in. (12 ft 3 in at full scale) with a 6 in. (1 ft 6 in at full scale) overhang around the perimeter. It has a gable roof sloping at 18^{o}, with Fink style wood trusses installed at 8 in. spacing (24 in o.c. at full scale). The building model is mounted on a 3 ft high steel frame clad with oriented standard boards (OSB) sheets. To be representative of typical residential constructions, the gable end trusses were connected only at the truss reaction points and not through bottom chords with the end wall.

Pressure and Load Sensors on the Building

Figure 6-1 shows the layout of pressure taps and load cells. Twenty-nine pressure taps were installed on the building model, 25 on the roof and 4 on the walls (See Figure 2 for the distribution of the taps on the roof). The nearest pressure taps to the gable end edge of the roof are installed 3.5 in. from the edge. Each pressure tap was made using 3 in. long, 0.124 in inside diameter (ID) brass tube soldered to a thin metal disc as shown in Figure 6-2A. Figure 6-2B shows the distribution of pressure taps over the house roof. 27 Omega PX 138 pressure

transducers and 2 Setra model 265 transducers were used to capture pressure distributions on the roof and walls of the house. The high port of each transducer was connected to the taps via a 6 in. long 3/16 in. ID vinyl clear tube. The internal pressure was measured using a Dwyer 616-20B transducer. The low ports of the transducers were connected to a single manifold and held at ambient pressure (see Figure 6-3). The specifications of these transducers are given in Table 6-1. Pictures of the three different transducers used are shown in Figure 6-4.

Structural reactions on the building were monitored using twenty-one 300 single axes compression/tension load cells (Futek model LRF 350). Twelve load cells were installed at roof to wall connections and 9 at the wall-to-foundation connections (see Figure 6-5). The building was isolated at the instrumented end to capture the total load reactions through this load cell array.

All these pressure transducers were factory-calibrated. However, a Fluke - 718 1G - pressure calibrator with serial number of 9916005(shown in Figure 6-6) was used to confirm the calibration charts. The data acquisition system consisted of a National Instruments (NI) CompacDAQ chassis (NI cDAQ – 9172) with modules NI 9205 and NI 9219. This data acquisition system was controlled by Measurement and Automation Explorer and LabView software version 8.5. Prior to the experiment, the instruments were left overnight to measure room condition signals to check for possible drift effects in their performances.

Test Arrangement

Two 16 ft tall by 34 long wood framed walls were constructed at the exit the UF wind generator to enclose the test building. The windward face of the 1/3 scale model was placed at approximately18 ft away from the exit to provide a flow development length of at least four times the fan diameter (4.5 ft). The house was oriented in three separate directions (0^o, 45^o and 90^o) to the wind flow. Figure 6-8 shows a layout for the experimental set-up. Figures 5-9 shows

the different orientations of the house in the experimental setup. The house was anchored to the ground to resist all horizontal and vertical movements as well as overturning during the test.

The Cobra Probe was positioned centrally within the test section 6 ft downstream of the contraction of the wind generator to record wind speeds. It was installed at 8 ft above ground to match the mean roof height of the house. A pitot tube, connected to a Dwyer pressure transducer (shown in Figure 6-7), was installed 2 ft above the roof ridge.

Wind Generation

The UF wind generator (shown in Figure 6-10) situated at the Powel Family Structures Lab was developed for testing window and door panels. It generates wind forces by using an 8-fan array of 4.5 ft diameter fans hydraulically powered by four marine diesel engines with a combined 2800 hp. The generator can produce fluctuating winds at speeds up to 120 mph. Further description of its development and operation can be found in Masters et al.(2008).

A mean wind velocity of 50 mph (22 mph) was used for all the tests. The wind speed was chosen based on scaling considerations for equivalent 130 mph full scale mean speed. To produce this speed, the wind generator engines were run at 1000 rpm turning the eight fans at 700 rpm. The wind generator produced approximately 6 % turbulence intensity, measured at the mean roof height, for the experiment.

Experimental Procedure and Measurements

Tests were conducted with the building in three orientations to incident wind flow: 0^o, 90^o and 45^o. Zero degree was taken as wind flowing normal to the gable end wall of the building. Three repeats were done at each house orientation. Data was sampled at 200 Hz lasting 10 minutes for each test. The LabView program synchronized measurements by all the pressure and load sensors and saved them into test file output for each test. The Cobra Probe, which was

controlled by TFI device software, was timed using a digital trigger connected to the LabView program. Sampling by all the measuring instruments started at the same time for all the tests.

Prior to each test, the Cobra Probe was zeroed and initial readings from the transducers and load cells were taken for 120 seconds. These initial records were subtracted from pressure and load measurements before data analysis remove any initial offset of the instruments. The pressure and structural load measurements were low-passed filtered at 100 Hz and their statistical values were measured using a MATLAB-based program.

Experimental Results, Analysis and Discussion

Wind Pressure Measurements

Positive peak pressures (7 – 11 psf) were recorded on the windward walls whereas suctions were recorded on the leeward walls for 0^o and 90^o azimuths. For 45^o degrees, both the instrumented gable end wall and the side wall experienced positive pressures. The internal pressure recorded during all the experiments was zero psf. The wind distribution over the roof of the building was generally characterized by peak suctions especially for the 0^o and 45^o azimuths. Wind suctions were highest along the second interior truss (with load cells 4 and 16) for the 0^o azimuth. High suctions were recorded along the gable edge of the roof while relatively low suctions were measured at the interior roof areas of the roof for the 45^o azimuth. For the 90^o azimuth however, relatively low suctions enveloped the roof of the house except at the eave end area. The wind pressure distributions observed in all these experiments were in good agreements with what is reported in literature and observed from the wind tunnel data.

Wind pressures measured were normalized into pressure coefficients by the velocity pressure at the mean roof height of the building. The pressure coefficients were evaluated using Equation 5-1.

$$C_{p,mrh,i}(t) = \frac{P_i(t)}{1/2\rho\overline{U}_{mrh}^2} \tag{5-1}$$

where $C_{p,mrh,i}(t)$ pressure coefficient at pressure tap i at time t, referenced to the mean wind speed measured at the mean roof height of the building; P_i is the measured wind pressure at tap i; ρ is the air density; U_{mrh} is mean wind speed (mph) recorded at mean roof height by the Cobra Probe.

Pressure coefficients obtained for the nine test repeats are given in Appendix C. Table 6-2 shows the mean, peak and root mean square (RMS) pressure coefficients averaged from results of the three datasets for each wind direction. The peak negative and mean pressure coefficients contour plot results are also shown in Figure 6-11.

Wind-Induced Structural Loads

Measured statistical values of structural loads obtained from each test of the experimental study are provided in Appendix D. The three sample data obtained for each direction were augmented. Each augmented time history was then divided into six segments to obtain six 10-minute (full scale) samples. Mean, peak and RMS reactions were measured from these segments and an extreme value analysis (discussed in Chapter 3 and Chapter 4) was used to estimate the expected positive and negative peak reactions. The Lieblein-BLUE estimators (Lieblein 1974) used in the analysis of the six samples in each direction are provided in Table 5-3. The mean, RMS and expected peak values of structural loads measured by the twenty-one load cells are provided in Table 5-4. These statistical values are average loads from the three datasets for each wind azimuth. The locations of the load cells on a 3D drawing of the house are shown in Figure 6-13. Figures 5-14 to 5-16 show the mean, extreme positive and negative structural reactions. The plots are such that the gable end load cells (15 & 19) are at the center of the roof-to-wall zone. Load cells on the same truss are mirrored about load cells 15 and 19 on the plots for easy comparison of measurements.

Even though there was no connection between the gable end truss and the gable end wall except at end supports of the truss, there was considerable load transferred from the gable end wall to the foundation.

At the 90^o azimuth, significantly high reactions were recorded at the gable end wall-to-foundation load cells than the other load cells. Another unusual observation made for this direction was that load cell 20 recorded high positive reactions whereas adjacent load cells (19 and 16) recorded relatively high negative reactions. Perhaps, these observations could be explained by fact that the portion of the building where these load cells were located was not completely immersed in the wind flow jet (as shown in Figure 5-8) and therefore subjected to unrealistic wind loads.

For incident 0^o azimuth, it is observed that fairly symmetrical loads were recorded at the roof-to-wall connections on side walls. Also, load cells 4 and 16 recorded highest uplift load (26 psf & 22 psf respectively) on either sidewall suggesting that high suctions experienced along the second interior truss were mainly transferred through its support. Load cells located at the gable end measured equally high uplifts as observed in the DAD-based loads of wind tunnel data.

Generally, the structural loads measured at the roof-to-wall connections are highest at the 0^o azimuth and lowest at the 90^o azimuth. This observation was also made in the case of loads computed based on wind tunnel data where the highest loads were estimated for the 0^o azimuth and decreased with wind direction increment of 15^o.

Structural Load Comparison

The envelope pressures over the house were used to estimate the structural loads being transferred through roof-to-wall load cell numbers 4, 5 and 15, and foundation load cell number 11. Predictions were made based on the DAD methodology using the experimentally derived influence coefficients (described in Chapter 4). For comparison with the directly measured

structural loads, actual pressure time histories (not pressure coefficients) based on the wind flow characteristics of the various tests were utilized in the DAD approach as follows:

$$R_j(t) = \sum_{i=1} [(N_i)_j \times A_i \times P_i(t))] \quad (5\text{-}2)$$

where $R_j(t)$ is load reaction in pounds at the *jth* connection at time t; $(N_i)_j$ is influence coefficient at the *ith* grid point for the *jth* connection; A_i is tributary area of *i th* grid point; and $P_i(t)$ is pressure measured at the *ith* grid point at time *t*.

Figures 6-17 to 6-19 show 1 minute records of measured and evaluated reactions. High correlations are observed between the reaction time histories of the two records. The highest correlation coefficient of 0.9 was measured between the records of load cells 15 for the 0^o wind azimuth. Measured correlation coefficients for the records are given in Table 6-5. Even though the estimated and measured reactions are not in excellent agreement as far as magnitude is concerned for some the load cells considered, their records show good trends. It is observed that in almost all the comparisons, the peaks of time histories of the two records seem to be occurring at the same time. Furthermore, significantly more fluctuating signals were obtained using the roof pressures relative to the directly measured load cell signals. It is worth noting that a similar observation was made by Zisis & Stathopoulos (2009) in a parallel study. Zisis & Stathopoulos (2009) attributed this phenomenon to the attenuation effect due to structural and material damping of the building components thereby lowering the fluctuations in the measured signal.

Peak and mean uplift structural loads measured and estimated for the four load cells are provided in Table 6-6. Good agreements are observed comparing the mean and peak reaction in almost all cases. Small discrepancies (lowest is 2%) are seen between the statistical values for load cell 15 as compared to the others. Generally, the DAD methodology underestimated structural loads expected to be transferred through the other load cells considered. This may be

due to the fact that the effective influence surfaces of these load cells were not completely covered with pressure taps. Hence, pressure loads which were transferred through these load cells were not fully captured.

In summary, the DAD methodology adequately predicted the expected loads at roof-to-wall and wall-to-foundation connections based on realistic wind load paths. The ability to estimate structural loads on light framed wood structures using the DAD approach has been demonstrated in this experimental study.

Table 6-1. Manufactures and specifications of pressure sensors

Transducer Model	Manufacturer	Number Used	Range	Output	Response Frequency
PX 138-001 D5V	Omega Engineering	27	± 1 psi (144 psf)	1 to 6 VDC	1000 Hz
265	Setra Systems, Inc.	2	±10 in. H2O (52 psf)	0 to 5 VDC	50 Hz
616 -20B	Dwyer Instruments, Inc.	1	±10 in. H2O (52 psf)	4 to 20 mA	2.5 Hz

Table 6-2. Statistical values of measured pressure coefficients

	0°				45°				90°			
Press. taps	Neg. Peak	Mean	Pos. Peak	RMS	Neg. Peak	Mean	Pos. Peak	RMS	Neg. Peak	Mean	Pos. Peak	RMS
						Roof pressure taps						
1	-1.59	-0.56	-0.06	0.60	-0.15	0.04	0.21	0.06	-0.93	-0.14	0.47	0.24
2	-2.70	-0.51	1.08	0.56	-1.97	-0.05	1.56	0.31	-2.98	-0.33	1.79	0.48
3	-2.74	-0.48	1.77	0.52	-2.70	-0.80	1.24	0.88	-3.01	-0.45	1.94	0.54
4	-2.73	-0.45	1.35	0.50	-2.31	-0.56	0.98	0.60	-2.90	-0.51	1.66	0.58
5	-2.26	-0.52	0.13	0.56	-1.64	0.06	1.38	0.20	-1.75	0.01	1.46	0.20
6	-1.91	-0.53	0.25	0.57	-0.05	0.11	0.27	0.11	-1.68	0.07	1.56	0.24
7	-2.95	-0.47	0.80	0.50	-0.18	0.12	0.41	0.12	-1.71	0.02	1.51	0.24
8	-2.41	-0.42	1.26	0.45	-0.69	0.10	0.77	0.13	-1.81	-0.02	2.00	0.23
9	-1.16	-0.42	0.05	0.44	-3.14	-0.56	1.94	0.67	-0.86	0.10	1.03	0.16
10	-1.30	-0.44	0.05	0.46	-0.41	0.01	0.40	0.06	-0.80	0.10	0.70	0.13
11	-2.23	-0.47	0.16	0.49	-0.17	0.04	0.27	0.06	-0.57	0.15	0.70	0.16
12	-1.86	-0.47	0.54	0.49	-0.18	0.02	0.22	0.05	-0.86	0.38	1.26	0.60
13	-0.89	-0.34	0.09	0.35	-3.16	-0.80	1.41	0.87	-1.02	-0.10	0.51	0.14
14	-1.02	-0.39	-0.06	0.40	-1.25	-0.07	1.03	0.17	-0.53	0.10	0.55	0.11
15	-1.36	-0.42	0.05	0.44	-0.53	-0.10	0.22	0.11	-0.44	0.06	0.39	0.08
16	-1.60	-0.47	0.27	0.49	-0.33	-0.10	0.12	0.11	-0.46	0.08	0.56	0.09
17	-0.85	-0.34	0.07	0.35	-3.28	-1.08	0.82	1.13	-0.47	-0.01	0.64	0.07
18	-1.05	-0.36	-0.07	0.37	-2.30	-0.42	1.30	0.49	-0.40	0.04	0.43	0.07
19	-2.08	-0.45	0.18	0.47	-0.76	-0.39	0.10	0.40	-0.39	0.04	0.33	0.07
20	-1.68	-0.40	0.33	0.41	-1.15	-0.35	0.39	0.36	-0.37	0.05	0.41	0.07
21	-0.88	-0.34	-0.01	0.35	-6.34	-1.72	2.53	1.87	-1.09	-0.05	0.46	0.09
22	-1.02	-0.36	-0.04	0.37	-3.48	-0.64	1.68	0.77	-1.14	-0.03	0.29	0.07
23	-1.56	-0.40	-0.04	0.41	-2.55	-0.54	1.07	0.59	-0.86	-0.02	0.20	0.07
24	-1.31	-0.34	0.03	0.35	-3.21	-0.92	1.37	0.96	-0.91	-0.04	0.30	0.09
25	-1.59	-0.41	0.10	0.43	-1.63	-0.23	1.26	0.30	-0.89	-0.05	0.18	0.09
						Wall pressure taps						
26	-0.63	-0.19	0.15	0.20	0.60	0.79	1.04	0.79	-0.43	0.45	1.64	0.46
27	-1.21	-0.31	0.19	0.32	0.39	0.53	0.72	0.54	0.33	0.92	1.36	0.92
28	0.45	0.77	1.01	0.78	0.55	0.73	0.90	0.73	-1.02	-0.41	-0.07	0.42
29	0.86	1.07	1.25	1.07	0.12	0.35	0.56	0.35	-0.61	0.05	0.65	0.12
						Internal pressure						
30	-0.01	0.00	0.01	0.00	-0.01	0.00	0.01	0.00	-0.03	0.00	0.02	0.01

Table 6-3. Coefficients of BLUE for Type 1 Extreme-Value Distribution (Lieblein 1974)

i	1	2	3	4	5	6
a_i	0.355	0.225	0.166	0.121	0.083	0.048
b_i	-0.459	-0.036	0.073	0.127	0.150	0.146

Table 6-4. Mean, RMS and BLUE estimated peak values of measured structural loads (lbs)

Load Cells	0°				45°				90°			
	Neg. Peak	Mean	Pos. Peak	RMS	Neg. Peak	Mean	Pos. Peak	RMS	Neg. Peak	Mean	Pos. Peak	RMS
Roof-to-wall load cells												
1	-14.3	-8.0	-0.7	8.3	-6.9	-3.9	-1.1	4.0	0.1	3.7	6.5	3.8
2	-10.1	-7.1	-3.1	7.1	-8.6	-5.9	-3.1	5.9	-3.9	0.1	3.8	1.3
3	-13.0	-8.1	-4.6	8.2	-7.5	-5.1	-2.7	5.2	-2.0	1.3	4.4	1.5
4	-25.6	-18.6	-11.8	18.7	-16.1	-12.5	-8.9	12.6	-2.4	1.4	5.0	1.7
5	-19.7	-15.7	-11.5	15.8	-13.0	-9.9	-7.5	9.9	-16.2	-9.0	-4.9	9.1
15	-22.9	-15.3	-9.1	15.5	-17.5	-12.1	-6.8	12.2	-3.4	1.9	6.9	2.5
16	-20.7	-16.3	-12.3	16.3	-20.3	-15.8	-11.5	15.9	-7.2	-3.0	-0.5	3.1
17	-9.7	-5.6	-2.7	5.6	-5.7	-2.3	-1.5	2.4	-3.4	-1.1	0.1	1.3
18	-10.7	-7.1	-4.3	7.2	-13.5	-9.2	-5.2	9.3	-6.4	-1.0	1.9	1.6
19	-20.1	-13.9	-8.8	14.0	-19.0	-13.0	-7.2	13.1	-16.3	-8.5	-2.5	8.8
20	-19.9	-14.2	-9.9	14.3	-19.8	-14.2	-7.7	14.3	5.0	9.3	13.2	9.3
21	-11.0	-6.5	-2.7	6.6	-7.3	-3.7	-1.1	3.9	-6.0	-0.7	1.6	1.3
Wall-to-foundation load cells												
6	-7.6	-3.4	0.2	3.6	-14.3	-9.9	-5.8	10.0	-6.7	-0.3	6.3	2.3
7	-17.5	-11.8	-5.7	11.9	-5.1	-1.1	3.2	1.8	6.4	12.7	19.4	12.9
8	-23.3	-17.7	-11.1	17.8	-4.8	-0.5	3.8	1.5	7.3	14.7	21.4	14.9
9	-22.3	-18.1	-13.3	18.1	-10.7	-7.3	-3.9	7.4	-5.3	2.3	8.8	3.2
10	-21.8	-18.1	-13.7	18.1	-16.7	-13.7	-10.8	13.7	-26.9	-17.4	-10.5	17.5
11	-18.5	-13.7	-8.8	13.8	-19.4	-14.5	-10.2	14.6	-32.3	-21.0	-11.8	21.2
12	-18.8	-14.6	-10.4	14.7	-17.6	-13.5	-9.5	13.6	-44.7	-29.8	-19.0	30.1
13	-10.7	-8.1	-5.5	8.2	-9.7	-7.4	-4.9	7.4	-18.2	-11.7	-6.7	11.8
14	2.7	4.7	6.3	4.7	-2.0	-0.2	1.8	0.7	-5.7	-1.8	1.5	2.1

Table 6-5. Correlation coefficients measured between time histories of measured and estimated reactions

Azimuth	0°				45°				90°			
Load Cell	4	5	11	15	4	5	11	15	4	5	11	15
Coefficient	0.83	0.85	0.56	0.90	0.48	0.30	0.30	0.41	0.47	0.43	0.43	0.45

Table 6-6. Comparison of directly measured and DAD-based estimated reactions

Wind Direction	Load Cell	Peak Uplift (lbs)				Mean (lbs)			
		4	5	11	15	4	5	11	15
0°	DAD	-19.6	-14.7	-16.4	-22.0	-9.7	-8.0	-9.6	-12.3
	Measured	-25.9	-19.7	-18.5	-22.9	-18.6	-15.7	-13.7	-15.3
`45°	DAD	-11.3	-11.4	-11.4	-25.3	-5.0	-5.6	-7.2	-10.3
	Measured	-15.9	-13.0	-19.4	-17.5	-12.5	-9.9	-14.5	-12.1
90°	DAD	-7.8	-5.7	-5.3	-8.8	0.5	0.2	0.5	0.4
	Measured	-3.3	-16.0	-32.3	-3.36	1.4	-9.0	-21.0	1.9

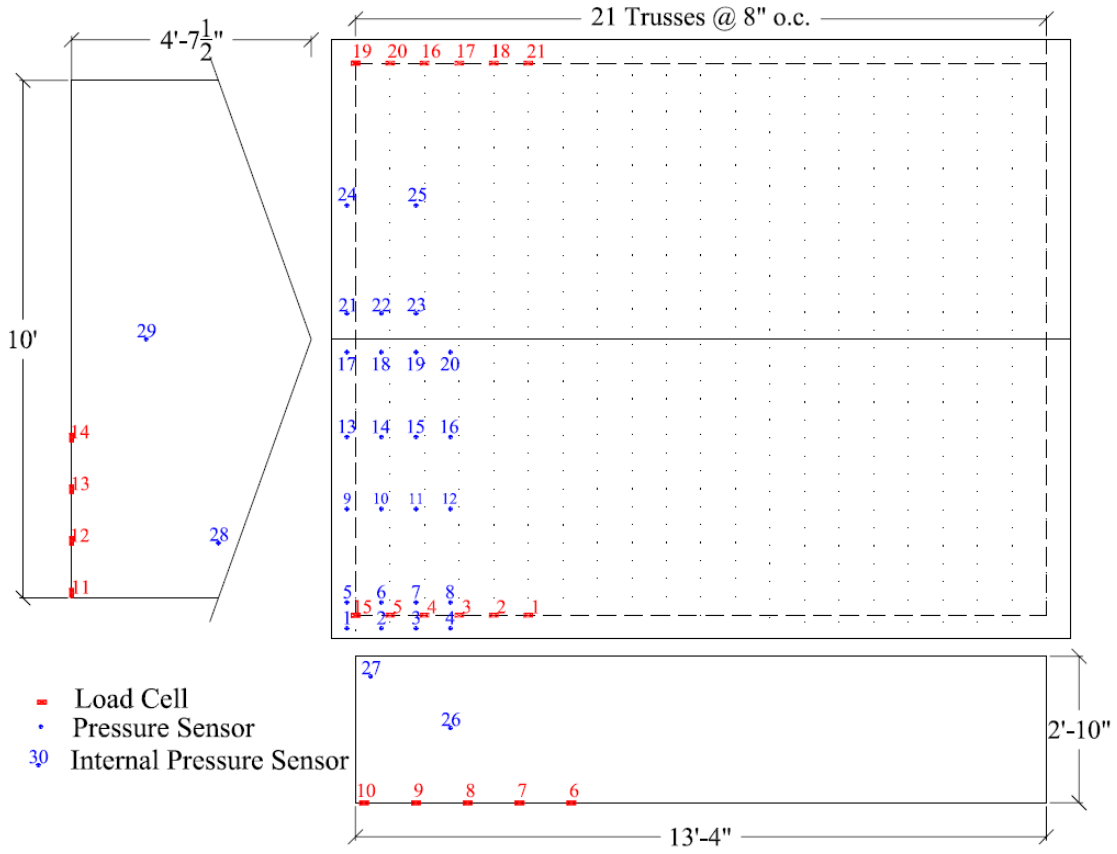

Figure 6-1. Locations of pressure taps and load cells on the scale house model.


A

B

Figure 6-2. A) A pressure tap sample B) Layout of pressure tap over the building roof

Figure 6-3. Interior of the house model


A


B


C

Figure 6-4. Pressure Sensors A) Omega PX 138 B) Setra 265 C) Dwyer 616


A

B

Figure 6-5. Futek load cells A) Roof-to-wall connection B) Wall-to-foundation connection

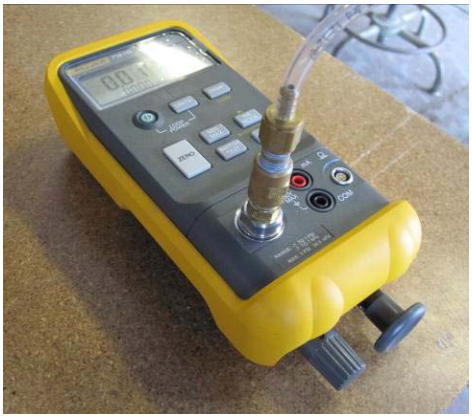

Figure 6-6. Fluke pressure calibrator

Figure 6-7. Dwyer Transducer and pitot-tube for wind velocity measurements

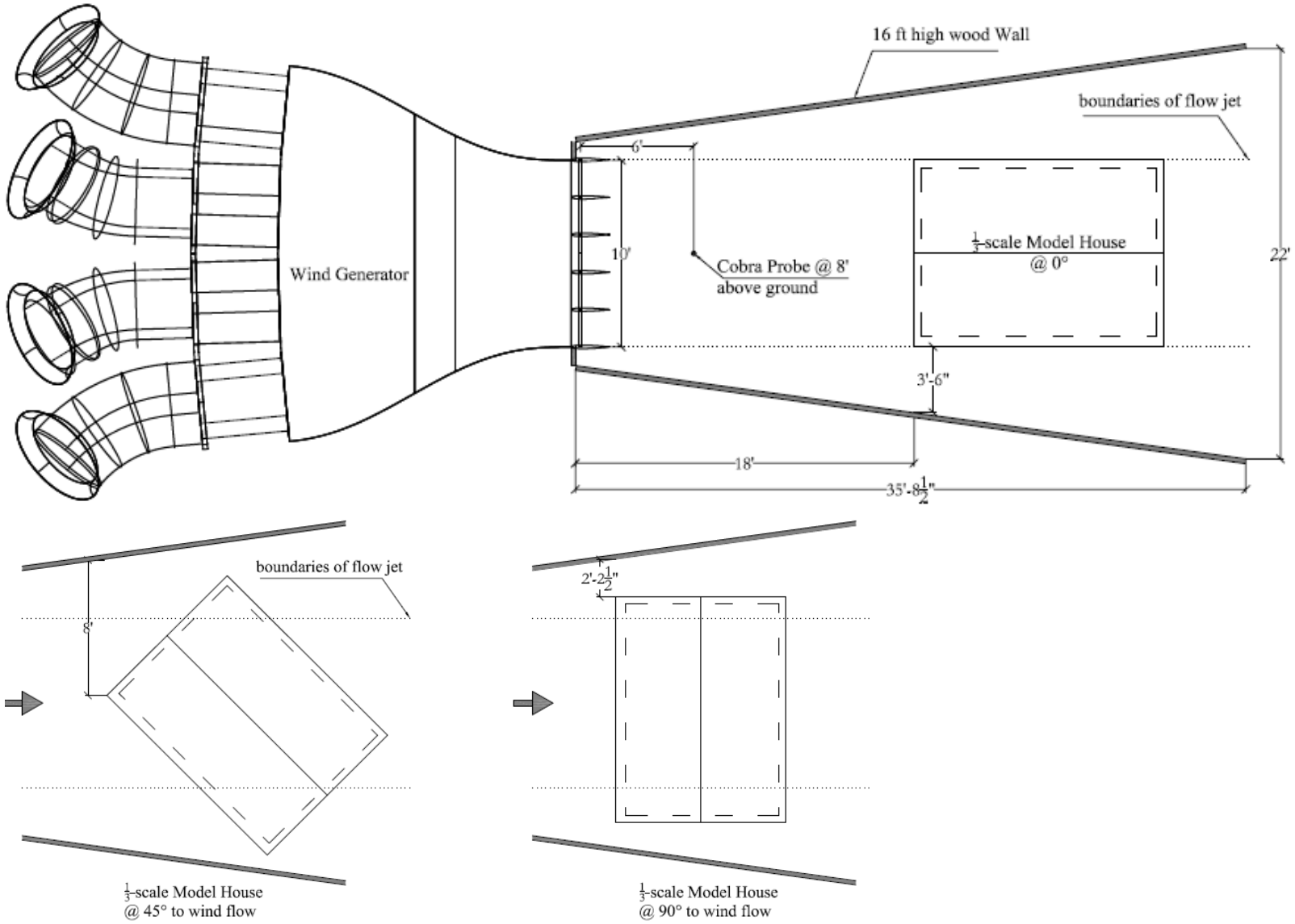

Figure 6-8. Layout of experimental set-up


A


B


C


D

Figure6-9. A) Completed setup B) House at 0^{o} orientation C) House at 45^{o} orientation D) House at 90^{o} orientation

Figure 6-10. UF Wind Generator

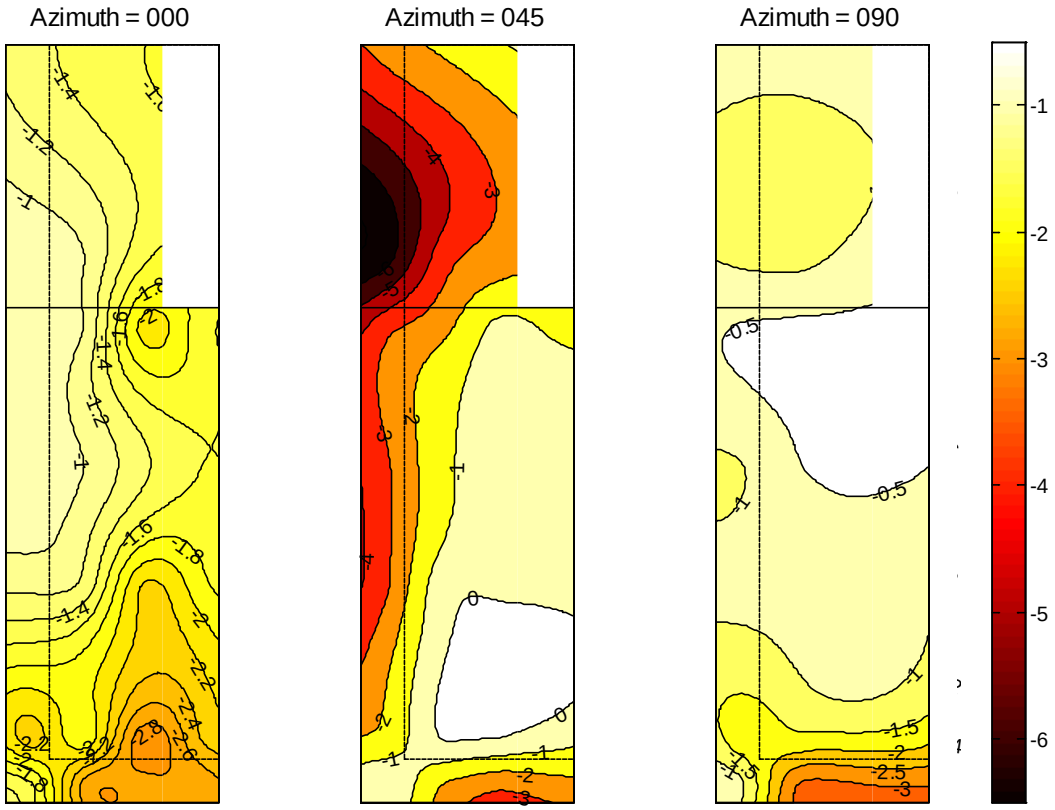

Figure 6-11. Spatial distributions of peak pressure coefficient

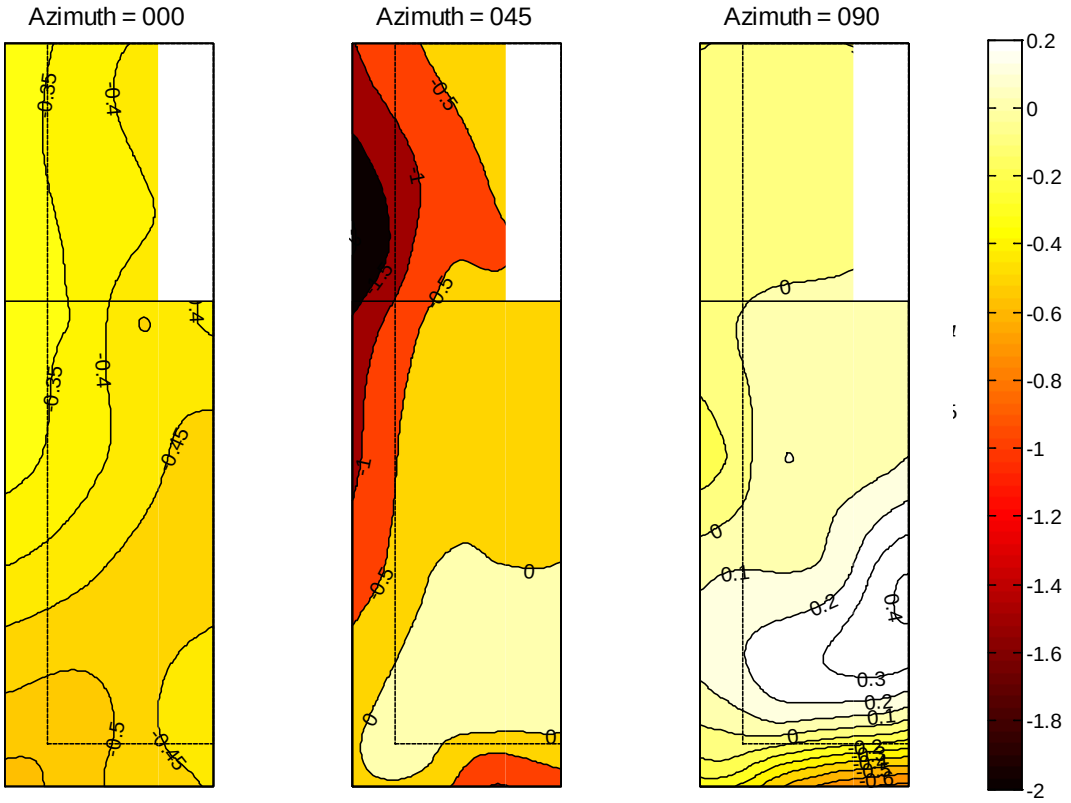

Figure 6-12. Spatial distributions of mean pressure coefficient

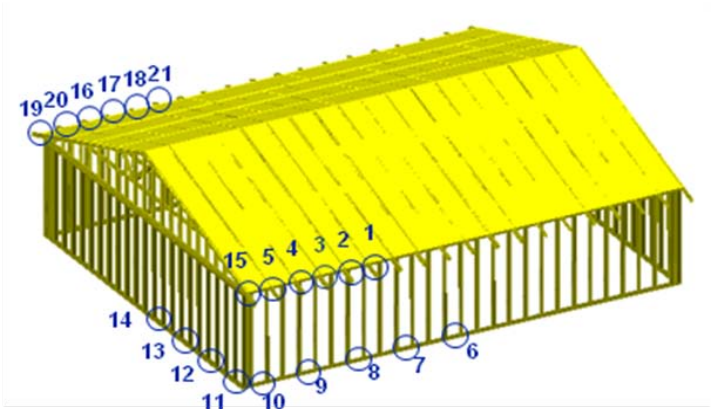

Figure 6-13. Location of load cells on the house

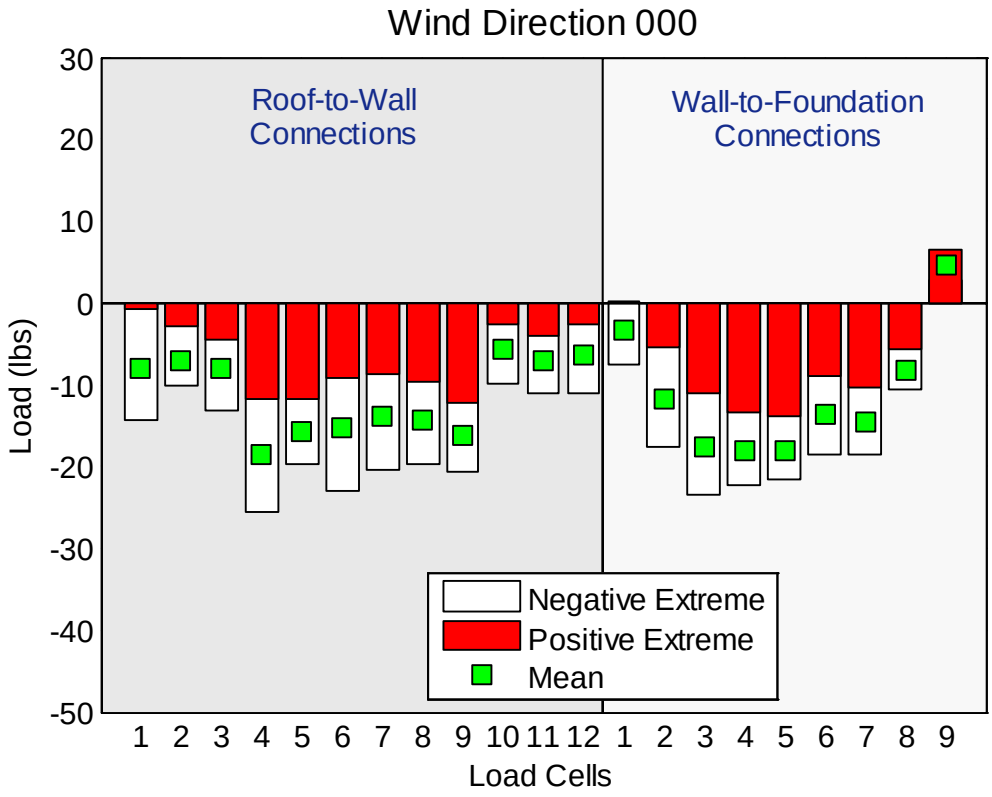

Figure 6-14. Mean and expected peak values of measured structural loads for wind direction 0°

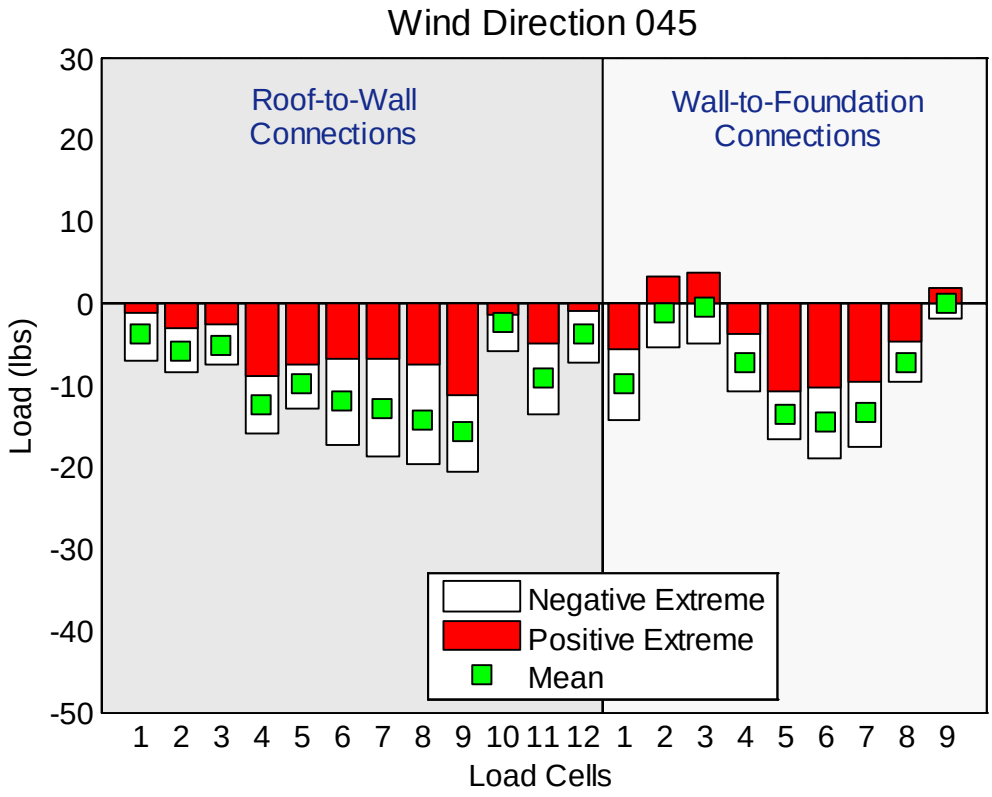

Figure 6-15. Mean and expected peak values of measured structural loads for wind direction 45°

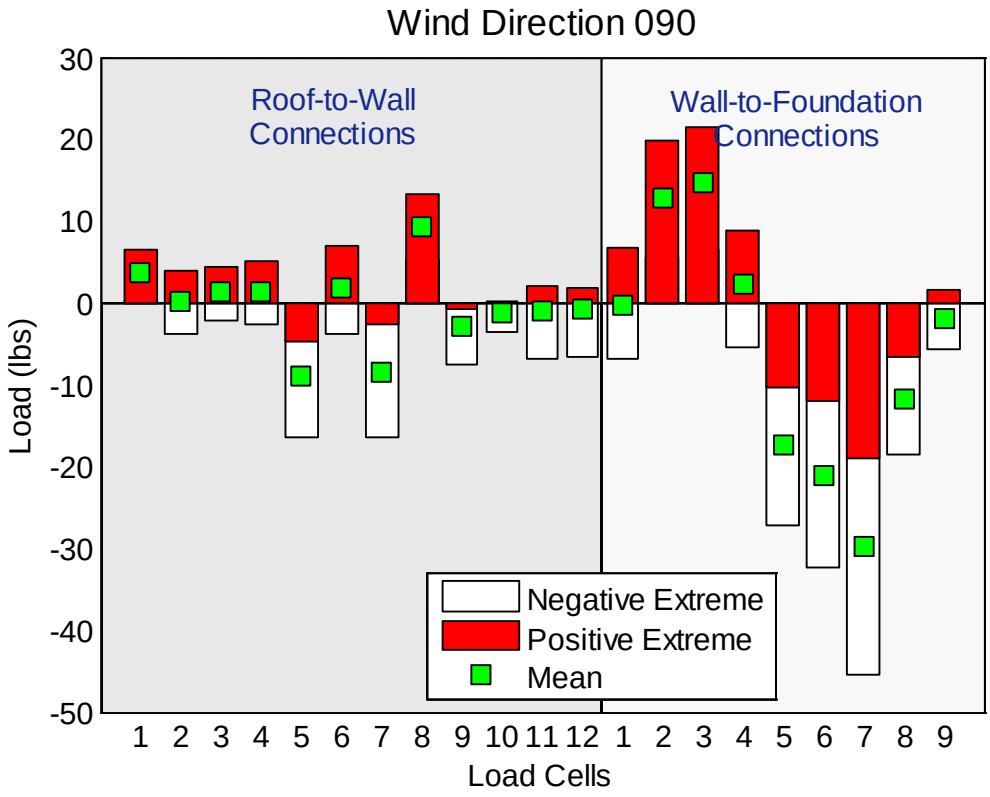

Figure 6-16. Mean and expected peak values of measured structural loads for wind direction 90°

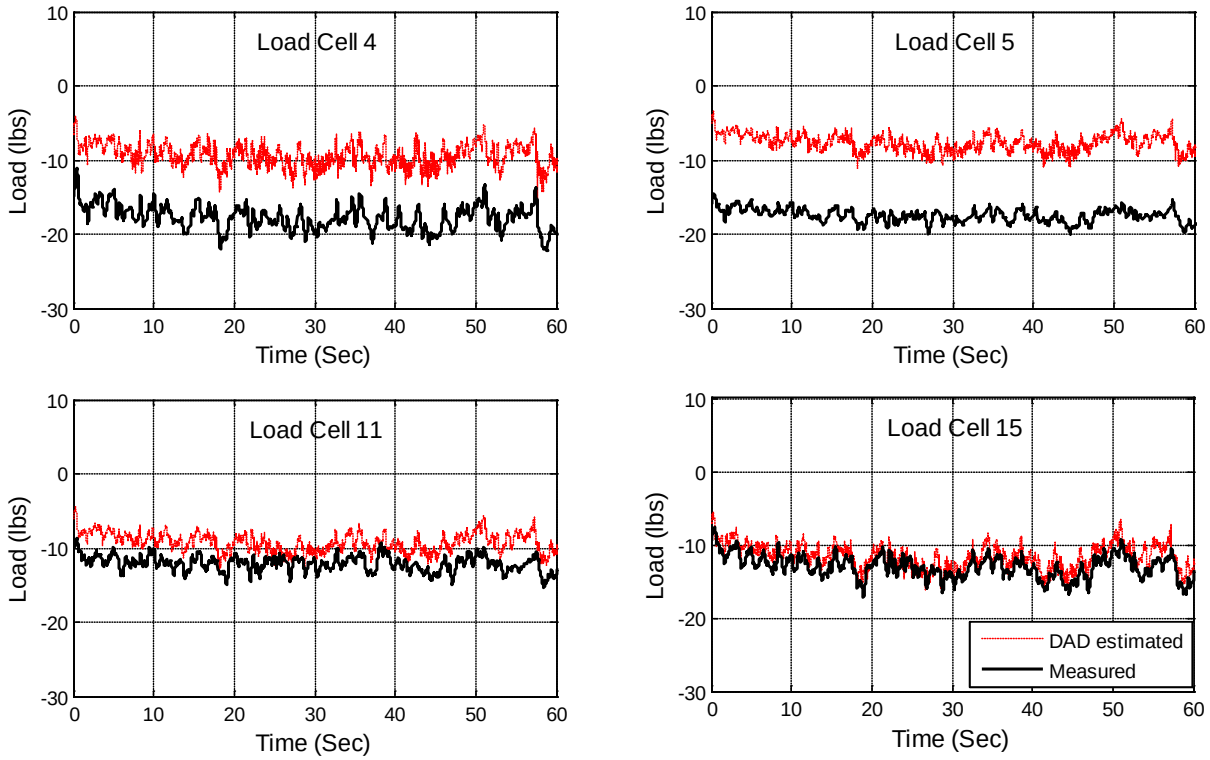

Figure 6-17. Comparison of measured and estimated reactions for wind direction 0°

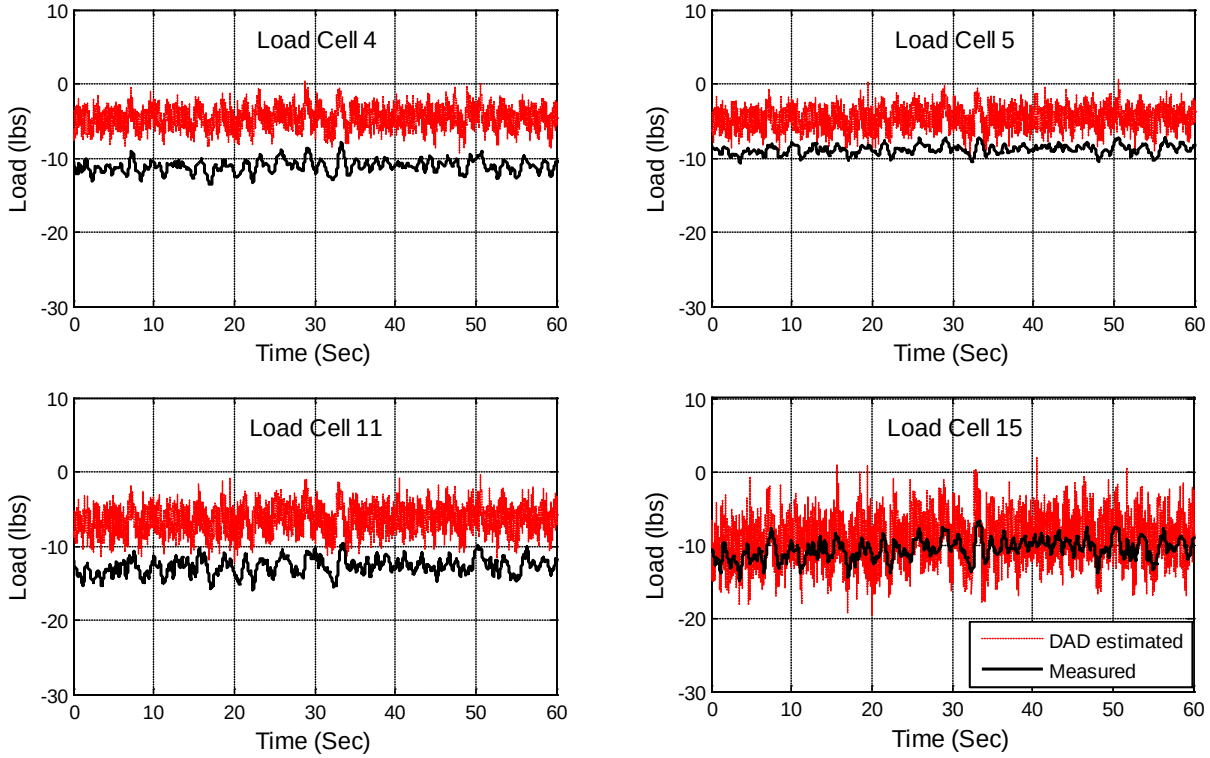

Figure 6-18. Comparison of measured and estimated reactions for wind direction 45°

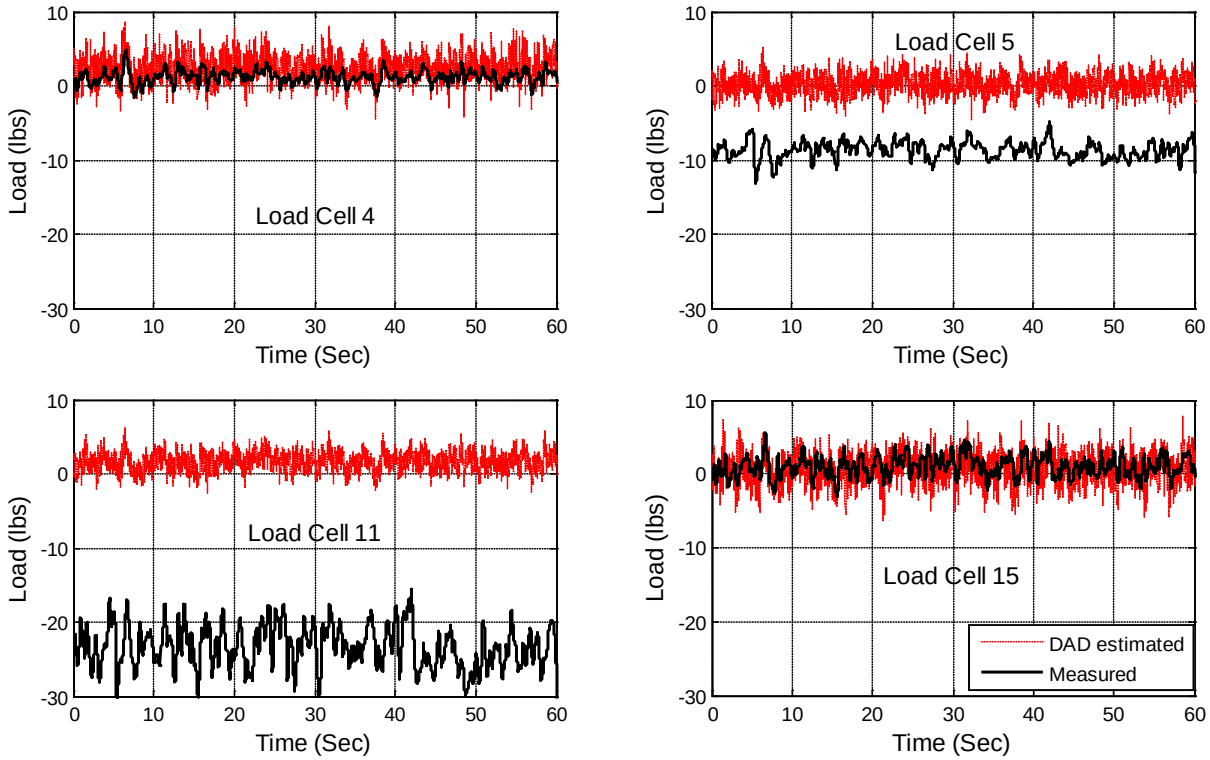

Figure 6-19. Comparison of measured and estimated reactions for wind direction 90°

CHAPTER 7
CONCLUSION AND RECOMMENDATIONS

This chapter provides a summary of work undertaken and key findings made. Significant conclusions which can be drawn from the study as well as recommendations for future research in this study area are discussed.

Summary

Light framed wood structures (LFWS) are by far the largest contributor to monetary losses associated hurricane damages. Inadequate load transfer mechanism provided in wood constructions account significantly to structural failures of such buildings. The need for studies to provide better understanding of wind load paths on LFWS buildings cannot be overemphasize.

This research was aimed at estimating wind-induced structural loads transferred through roof-to-wall and wall-to-foundation connections on LFWS. The estimations were based on Database-Assisted Design (DAD) methodology, developed by the National Institute of Standards and Technology (NIST). This methodology, which utilizes large databases of aerodynamic pressures and climatological information, has been used by other researchers to predict structural responses due to wind forces on steel portal frame buildings. This current study, apart from extending the application of the DAD approach to LFWS, also demonstrates the validity of this methodology to adequately evaluate structural reactions on LFWS.

The project was accomplished in two phases: a hybridized analytical approach and an experimental approach. In the former, spatially distributed pressure coefficients were derived from wind tunnel data for a 1/50 scale model house. These pressure coefficients (time histories) were combined with structural influence coefficients (developed on a 1/3 scale model wood house) through computer-based analysis to generate structural reactions. Peak uplift reactions were estimated from a Lieblein BLUE-fitted distribution of the measured peak reactions. These

were then compared to wind design loads based on ASCE-7 provisions for both Main Wind Force Resisting Systems (MWFRS) and Components and Cladding (C&C). It was realized that using MWFRS pressures underestimated the reactions by up to 32% while C&C provisions resulted in highly conservative estimates (up to 60% overestimation).

In the experimental study, the 1/3-scale wood house model was instrumented with pressure and load sensors. The house was subjected to wind forces while load and pressure measurements were simultaneously taken. Based on the DAD approach, structural reactions were estimated using measured roof pressures and results were compared to directly-measured structural loads. Even though significantly fluctuating reaction records were obtained using the DAD in comparison to the directly measured reaction records, the two quantities were highly correlated. Again, good agreements were found comparing mean and peak values of the estimated and measured reactions.

Conclusions

The conclusions of this study can be summarized as follows:

1. Local peak pressure coefficients derived from wind tunnel analysis are considerably higher, in most cases, than ASCE 7-05 component and cladding external pressure coefficients. However, an excellent agreement is observed between the wind tunnel area-averaged pressure coefficients and the ASCE 7 standard provisions.

2. ASCE 7-05 MWFRS provisions produced lower peak reactions (average of 21% lower) than predictions based on DAD methodology while predictions based on ASCE 7-05 components and cladding were generally higher.(average of 33 % higher) than DAD-based reactions.

3. Despite limited match of the wind generated in the experiment to realistic wind flows, overall the roof pressure distributions on the 1/3-scale house were reasonably matched to the wind tunnel pressure spatial distributions in the literature.

4. The structural reaction time history obtained using the DAD method had greater dynamic content than the time history of directly measured structural reactions. Despite this fact there was still good a greement between the peak values and the mean values of DAD results and the measured reactions.

5. DAD-based reactions were highly correlated with directly measured structural reactions.

6. Both the analytical and experimental components of this study confirmed that maximum uplifts loads are transferred through the gable end supports.

7. Lastly, a wider spread of load sharing through wall-to-foundation connection was observed in both analytical and experimental studies. This may be due to diaphragm (deep beam) actions of the building walls.

Finally, the study has not just extended the application of DAD methodology to LFWS but has evaluated its validity to adequately evaluate structural reactions on LFWS through an experimental study.

Recommendation

Notwithstanding the significant findings reported in this study and its possible influence on design practices for LFWS, further research is needed in order to fully comprehend wind load paths in LFWS. Recommendations for future research in this discipline are discussed below.

1. The study house is a simple rectangular gable roof structure. Most typical residential structures have complex shapes which may result in different pressure distributions on houses and subsequently different wind load paths. It is recommended that studies are done on LFWS with complex building shapes and different configurations.

2. In future experimental studies, load cells should be installed around the whole perimeter of the 1/3-scale building at roof-to-wall and wall-to-foundation interfaces. This will ensure that wind load paths are not unduly affected by the stiffness of the load cells.

3. Also, the entire roof of the house should be equipped with pressure sensors so that the DAD methodology could be validated at all critical connections.

4. A better boundary layer condition should be created for future experiments so that comparison can be made between field and wind tunnel measurements.

5. Reliability studies should be carried out to quantify the uncertainty parameters for load estimations on LFWS based on DAD approach.

APPENDIX A
MEAN, RMS AND EXTREME VALUES OF WIND TUNNEL PRESSURE COEFFICIENTS

Table A-1. Peak, mean and RMS pressure coefficients of selected pressure taps

	0°				45°				90°			
Press. Taps	Neg. Peak	Mean	Pos. Peak	RMS	Neg. Peak	Mean	Pos. Peak	RMS	Neg. Peak	Mean	Pos. Peak	RMS
1	-2.74	-0.37	0.16	0.43	-4.14	-0.81	0.17	0.92	-1.74	-0.25	0.12	0.28
2	-2.43	-0.37	0.21	0.43	-4.13	-0.83	0.15	0.94	-1.67	-0.22	0.11	0.25
3	-2.22	-0.37	0.35	0.43	-4.39	-0.78	0.22	0.90	-1.60	-0.23	0.10	0.26
4	-2.16	-0.36	0.34	0.42	-3.80	-0.79	0.19	0.89	-2.02	-0.22	0.21	0.25
5	-2.10	-0.32	0.43	0.39	-3.56	-0.71	0.23	0.80	-1.19	-0.20	0.12	0.23
6	-1.84	-0.22	0.49	0.28	-2.65	-0.60	0.23	0.67	-1.02	-0.20	0.10	0.23
7	-1.79	-0.15	0.48	0.21	-2.17	-0.52	0.16	0.58	-0.88	-0.20	0.09	0.22
8	-1.42	-0.13	0.46	0.18	-1.86	-0.49	0.06	0.53	-0.93	-0.22	0.06	0.24
9	-1.20	-0.18	0.33	0.21	-1.72	-0.50	-0.03	0.54	-1.06	-0.30	0.00	0.31
10	-1.13	-0.11	0.39	0.15	-1.60	-0.45	0.01	0.48	-1.01	-0.23	0.04	0.25
11	-0.86	-0.09	0.28	0.13	-1.46	-0.42	0.01	0.44	-1.11	-0.25	0.03	0.27
12	-0.86	-0.07	0.29	0.11	-1.40	-0.33	0.09	0.36	-0.96	-0.20	0.08	0.22
13	-0.72	-0.08	0.31	0.11	-1.27	-0.31	0.08	0.34	-0.94	-0.21	0.08	0.23
14	-0.70	-0.08	0.24	0.11	-1.19	-0.28	0.09	0.31	-0.94	-0.21	0.06	0.23
15	-0.65	-0.06	0.27	0.09	-1.22	-0.24	0.09	0.27	-0.97	-0.20	0.08	0.22
16	-0.60	-0.05	0.25	0.09	-1.16	-0.22	0.10	0.25	-1.04	-0.20	0.09	0.22
17	-0.55	-0.05	0.24	0.08	-1.20	-0.18	0.16	0.21	-1.09	-0.20	0.10	0.23
18	-0.56	-0.08	0.21	0.10	-1.12	-0.22	0.14	0.24	-1.19	-0.23	0.08	0.25
19	-0.58	-0.08	0.20	0.10	-1.22	-0.21	0.12	0.23	-1.35	-0.23	0.09	0.25
20	-0.56	-0.09	0.18	0.11	-1.36	-0.21	0.12	0.24	-1.41	-0.24	0.08	0.26
21	-0.53	-0.07	0.19	0.09	-1.50	-0.20	0.14	0.24	-1.43	-0.23	0.10	0.26
22	-0.78	0.84	2.34	1.04	-1.22	0.51	2.06	0.65	-1.06	0.62	2.10	0.76
262	-0.40	-0.10	0.13	0.11	-0.52	-0.13	0.12	0.14	-0.74	-0.15	0.36	0.18
263	-0.44	-0.09	0.16	0.11	-0.50	-0.11	0.21	0.13	-0.64	-0.11	0.43	0.14
264	-0.45	-0.07	0.18	0.09	-0.46	-0.10	0.23	0.12	-0.57	-0.08	0.45	0.12
265	-0.44	-0.07	0.20	0.09	-0.48	-0.10	0.24	0.12	-0.55	-0.08	0.44	0.12
266	-0.45	-0.07	0.22	0.09	-0.48	-0.08	0.27	0.10	-0.45	-0.05	0.44	0.10
267	-0.50	-0.06	0.23	0.08	-0.42	-0.08	0.29	0.10	-0.43	-0.04	0.46	0.09
268	-0.57	-0.05	0.25	0.08	-0.48	-0.08	0.28	0.11	-0.46	-0.05	0.47	0.10
269	-0.63	-0.06	0.26	0.09	-0.45	-0.09	0.29	0.11	-0.46	-0.06	0.45	0.10

Table A-1. (Cont'd)

	0°				45°				90°			
Press. Taps	Neg. Peak	Mean	Pos. Peak	RMS	Neg. Peak	Mean	Pos. Peak	RMS	Neg. Peak	Mean	Pos. Peak	RMS
270	-0.56	-0.07	0.24	0.09	-0.45	-0.08	0.29	0.11	-0.43	-0.05	0.46	0.10
273	-0.77	-0.08	0.33	0.11	-0.47	-0.09	0.28	0.11	-0.48	-0.07	0.47	0.11
274	-0.86	-0.13	0.34	0.16	-0.52	-0.13	0.26	0.15	-0.53	-0.12	0.41	0.14
275	-1.02	-0.14	0.33	0.17	-0.50	-0.12	0.27	0.14	-0.49	-0.10	0.43	0.13
276	-1.09	-0.12	0.44	0.17	-1.15	-0.05	0.47	0.08	-0.39	-0.01	0.50	0.08
277	-1.30	-0.20	0.46	0.25	-1.34	-0.04	0.50	0.08	-0.40	-0.02	0.52	0.09
278	-2.15	-0.32	0.36	0.38	-1.90	-0.07	0.40	0.12	-0.58	-0.05	0.47	0.10
279	-2.15	-0.37	0.40	0.42	-2.28	-0.09	0.53	0.23	-0.48	-0.04	0.53	0.10
280	-2.29	-0.37	0.28	0.43	-2.29	-0.16	0.58	0.33	-0.54	-0.04	0.56	0.10
281	-2.22	-0.36	0.26	0.42	-2.08	-0.20	0.66	0.35	-0.64	-0.06	0.54	0.12
282	-2.13	-0.37	0.21	0.42	-1.90	-0.21	0.73	0.34	-0.81	-0.12	0.51	0.17
367	-0.57	-0.09	0.21	0.11	-1.26	-0.16	0.28	0.20	-1.59	-0.25	0.60	0.31
368	-0.63	-0.08	0.20	0.10	-1.28	-0.17	0.33	0.20	-1.61	-0.22	0.67	0.29
369	-0.63	-0.07	0.20	0.10	-1.18	-0.16	0.38	0.20	-1.58	-0.20	0.69	0.28
370	-0.63	-0.07	0.21	0.09	-1.31	-0.16	0.44	0.21	-1.59	-0.20	0.76	0.28
371	-0.69	-0.07	0.23	0.09	-1.37	-0.17	0.43	0.21	-1.50	-0.20	0.80	0.27
372	-0.66	-0.07	0.25	0.09	-1.31	-0.17	0.41	0.22	-1.37	-0.20	0.73	0.27
373	-0.65	-0.07	0.24	0.10	-1.47	-0.17	0.47	0.22	-1.51	-0.20	0.75	0.27
374	-0.69	-0.06	0.26	0.09	-1.43	-0.17	0.47	0.22	-1.43	-0.20	0.78	0.27
375	-0.83	-0.07	0.32	0.10	-1.35	-0.18	0.46	0.23	-1.43	-0.21	0.72	0.27
376	-0.92	-0.07	0.34	0.10	-1.52	-0.18	0.50	0.23	-1.48	-0.20	0.73	0.27
377	-0.97	-0.15	0.26	0.17	-1.40	-0.21	0.46	0.26	-1.56	-0.31	0.67	0.36
378	-0.96	-0.12	0.30	0.15	-1.50	-0.21	0.45	0.25	-1.58	-0.25	0.71	0.30
379	-1.02	-0.18	0.24	0.21	-1.43	-0.25	0.37	0.29	-1.60	-0.31	0.71	0.35
380	-1.17	-0.12	0.41	0.17	-1.29	-0.14	0.50	0.20	-1.32	-0.18	0.86	0.25
381	-1.26	-0.15	0.39	0.20	-1.38	-0.13	0.53	0.19	-1.45	-0.18	0.86	0.25
382	-1.45	-0.18	0.36	0.24	-1.32	-0.11	0.56	0.18	-1.38	-0.16	0.90	0.25
383	-1.60	-0.24	0.41	0.29	-1.20	-0.11	0.63	0.19	-1.44	-0.18	0.91	0.26
384	-2.01	-0.28	0.42	0.34	-1.23	-0.11	0.70	0.20	-1.47	-0.19	0.85	0.27
385	-2.25	-0.32	0.43	0.39	-1.73	-0.08	0.83	0.21	-1.62	-0.18	0.90	0.27
386	-2.52	-0.39	0.44	0.47	-1.86	-0.02	0.85	0.19	-1.75	-0.18	0.85	0.27
387	-3.71	-0.47	0.39	0.59	-3.91	-0.04	0.89	0.33	-1.45	-0.18	0.73	0.26

APPENDIX B
MEASURED STATISTICAL VALUES OF VERTICAL REACTIONS DERIVED FROM WIND TUNNEL DATA

Table B-1. Measured peak, mean and RMS reactions (lbs) for sample 2

Azimuth	0°				45°				90°				135°				180°			
Load Cells	Neg. Peak	Mean	Pos. Peak	RMS	Neg. Peak	Mean	Pos. Peak	RMS	Neg. Peak	Mean	Pos. Peak	RMS	Neg. Peak	Mean	Pos. Peak	RMS	Neg. Peak	Mean	Pos. Peak	RMS
1	-812	-178	101	204	-375	-99	170	117	-411	-69	352	99	-439	-107	151	124	-272	-28	177	51
2	-878	-207	72	234	-400	-119	120	136	-376	-69	318	95	-403	-100	140	116	-254	-28	159	49
3	-1031	-262	58	292	-577	-146	99	164	-408	-87	300	112	-440	-117	145	131	-256	-35	134	56
4	-1220	-301	50	333	-730	-146	155	170	-423	-95	310	121	-468	-124	157	139	-266	-38	134	59
5	-1008	-285	19	313	-869	-183	47	207	-382	-106	176	122	-365	-123	104	134	-225	-35	104	51
6	-374	-99	25	109	-212	-64	31	71	-163	-40	115	48	-176	-53	50	58	-111	-14	56	23
7	-204	-52	16	58	-107	-34	20	38	-92	-21	68	26	-100	-29	29	32	-62	-8	33	13
8	-300	-84	15	92	-192	-51	25	58	-120	-31	91	38	-137	-40	39	44	-85	-11	39	18
9	-688	-195	24	214	-484	-120	50	136	-268	-71	187	85	-296	-90	86	99	-185	-26	87	40
10	-1044	-299	30	327	-785	-197	60	221	-414	-115	245	134	-433	-139	121	152	-273	-39	127	60
11	-1423	-407	41	446	-1071	-268	80	302	-570	-159	331	185	-596	-191	165	209	-374	-54	173	82
12	-1270	-363	36	397	-952	-238	72	268	-508	-141	298	164	-531	-170	147	186	-332	-48	154	73
13	-372	-106	10	116	-280	-71	19	80	-151	-42	84	49	-155	-50	42	55	-97	-14	44	21
14	-49	-14	2	15	-38	-10	2	11	-21	-6	12	7	-20	-7	5	7	-13	-2	6	3
15	-1476	-458	61	504	-1644	-315	119	374	-669	-175	220	201	-558	-195	127	212	-343	-58	162	83
19	-1286	-323	98	360	-1024	-344	-58	369	-698	-183	14	198	-507	-163	64	176	-243	-44	102	60
20	-1303	-300	100	331	-910	-325	-31	348	-647	-186	19	200	-507	-168	74	182	-229	-40	129	59

Table B-2. Measured peak, mean and RMS reactions (lbs) for sample 3

Azimuth	0°				45°						90°						135°				180°			
Load Cells	Neg. Peak	Mean	Pos. Peak	RMS	Neg. Peak	load cells	Neg. Peak	Mean	Pos. Peak	RMS	Neg. Peak	load cells	Neg. Peak	Mean	Pos. Peak	RMS	Neg. Peak	load cells	Neg. Peak	Mean
1	-771	-179	104	205	-399	-100	184	119	-384	-72	495	101	-356	-77	184	95	-317	-33	153	55
2	-858	-206	96	233	-494	-123	164	140	-405	-72	440	97	-342	-73	163	89	-287	-33	147	53
3	-1061	-259	85	289	-601	-151	156	171	-478	-90	437	114	-357	-86	148	101	-315	-41	142	60
4	-1327	-297	54	328	-779	-153	170	179	-519	-98	477	123	-385	-91	157	107	-320	-44	144	64
5	-1227	-281	19	308	-1041	-192	95	219	-454	-109	243	125	-336	-91	66	103	-262	-40	135	56
6	-361	-98	26	109	-249	-66	51	74	-180	-41	159	49	-146	-39	51	45	-133	-17	64	25
7	-200	-52	17	58	-128	-35	31	39	-98	-22	95	27	-82	-21	31	25	-75	-9	35	14
8	-293	-83	17	91	-219	-53	44	61	-144	-32	121	38	-114	-30	40	34	-100	-13	49	19
9	-696	-193	27	212	-553	-125	100	143	-328	-73	244	87	-249	-67	79	76	-216	-30	107	44
10	-1087	-295	20	324	-903	-205	134	233	-498	-118	313	136	-371	-103	101	117	-320	-45	159	65
11	-1479	-402	22	441	-1237	-280	178	318	-681	-164	421	188	-511	-142	138	160	-438	-62	218	89
12	-1321	-358	20	393	-1104	-248	161	282	-606	-145	378	167	-457	-125	125	142	-390	-55	193	79
13	-389	-105	4	115	-324	-75	44	84	-177	-43	106	50	-135	-37	35	42	-114	-16	56	23
14	-53	-14	1	15	-43	-11	5	12	-24	-6	14	7	-19	-5	5	6	-15	-2	7	3
15	-1723	-450	31	497	-1980	-334	231	402	-720	-180	349	204	-507	-145	79	163	-408	-66	214	90
19	-1400	-321	49	359	-1139	-352	-19	379	-667	-186	34	200	-542	-122	36	136	-275	-49	113	65
20	-1160	-299	97	330	-1104	-335	-9	361	-657	-189	42	203	-505	-125	44	139	-278	-46	140	64

Table B-3. Measured peak, mean and RMS reactions (lbs) for sample 4

Azimuth	0°				45°				90°				135°				180°			
Load Cells	Neg. Peak	Mean	Pos. Peak	RMS	Neg. Peak	Mean	Pos. Peak	RMS	Neg. Peak	Mean	Pos. Peak	RMS	Neg. Peak	Mean	Pos. Peak	RMS	Neg. Peak	Mean	Pos. Peak	RMS
1	-787	-174	86	201	-873	-98	257	117	-353	-74	349	101	-358	-86	200	103	-291	-34	120	53
2	-912	-202	73	229	-979	-120	228	137	-324	-73	307	97	-331	-81	168	97	-289	-34	108	52
3	-1162	-256	68	287	-718	-147	237	167	-361	-90	309	113	-390	-95	143	110	-295	-41	112	59
4	-1471	-295	67	328	-926	-150	264	174	-418	-97	324	122	-431	-101	139	116	-317	-45	122	63
5	-1291	-279	47	308	-874	-186	148	211	-365	-107	151	123	-333	-101	98	112	-317	-41	91	55
6	-409	-97	21	107	-267	-64	85	72	-148	-41	115	49	-138	-43	52	49	-117	-17	45	24
7	-212	-51	13	57	-142	-34	48	38	-81	-22	69	27	-78	-23	33	27	-66	-9	26	13
8	-354	-82	15	91	-220	-52	70	59	-117	-32	89	38	-112	-33	39	37	-90	-13	34	19
9	-837	-191	35	211	-518	-121	154	138	-264	-73	179	87	-249	-74	74	83	-198	-31	73	43
10	-1266	-293	48	322	-847	-199	203	224	-408	-117	226	135	-367	-114	107	127	-292	-46	107	64
11	-1720	-399	61	438	-1159	-271	273	306	-557	-162	304	187	-501	-157	145	175	-399	-63	146	87
12	-1536	-355	54	391	-1028	-240	245	271	-496	-144	273	166	-449	-139	128	155	-354	-56	130	78
13	-448	-104	14	114	-305	-72	67	81	-146	-43	76	49	-131	-41	37	46	-103	-16	38	23
14	-59	-14	2	15	-44	-10	7	12	-20	-6	10	7	-19	-6	5	6	-14	-2	5	3
15	-2008	-449	94	497	-1757	-322	293	382	-616	-177	205	201	-535	-161	134	178	-458	-67	135	89
19	-1378	-318	100	357	-1132	-340	5	366	-590	-181	11	194	-463	-135	80	149	-309	-51	75	65
20	-1073	-295	71	326	-1012	-323	21	348	-560	-185	10	198	-470	-138	91	153	-301	-49	89	64

Table B-4. Measured peak, mean and RMS reactions (lbs) for sample 5

Azimuth	0°				45°				90°				135°				180°			
Load Cells	Neg. Peak	Mean	Pos. Peak	RMS	Neg. Peak	Mean	Pos. Peak	RMS	Neg. Peak	Mean	Pos. Peak	RMS	Neg. Peak	Mean	Pos. Peak	RMS	Neg. Peak	Mean	Pos. Peak	RMS
1	-745	-158	121	185	-499	-101	151	120	-396	-45	335	80	-383	-88	213	106	-242	-33	142	54
2	-851	-188	102	216	-516	-124	134	141	-373	-44	286	76	-345	-84	171	99	-241	-33	128	53
3	-1016	-240	97	270	-628	-152	156	171	-429	-56	239	86	-372	-98	136	113	-271	-41	132	59
4	-1100	-276	102	310	-802	-153	176	177	-449	-59	255	92	-400	-105	118	120	-270	-44	136	63
5	-970	-261	65	291	-850	-190	117	215	-380	-73	147	93	-327	-104	51	116	-220	-40	118	55
6	-360	-89	34	100	-266	-66	62	74	-175	-27	95	37	-151	-44	53	50	-102	-17	59	25
7	-199	-47	20	53	-139	-35	35	39	-97	-14	59	21	-86	-24	34	27	-57	-9	34	14
8	-298	-76	27	85	-226	-53	49	60	-134	-21	69	29	-117	-34	38	38	-80	-13	44	19
9	-665	-178	59	198	-542	-125	109	141	-292	-48	132	65	-254	-76	66	85	-173	-30	97	43
10	-1006	-273	78	302	-877	-204	152	229	-441	-79	168	102	-370	-117	76	131	-253	-46	142	64
11	-1373	-371	103	412	-1191	-279	205	313	-605	-109	228	141	-510	-161	105	180	-346	-62	195	88
12	-1227	-331	92	367	-1057	-247	183	277	-537	-97	204	125	-453	-143	94	160	-308	-55	173	78
13	-360	-97	26	107	-314	-74	51	83	-159	-29	58	37	-133	-42	26	47	-90	-16	50	23
14	-48	-13	4	14	-44	-11	6	12	-22	-4	8	5	-19	-6	4	6	-12	-2	6	3
15	-1489	-420	111	470	-1607	-327	220	386	-611	-125	259	154	-526	-165	74	183	-349	-66	182	89
19	-1255	-296	82	335	-1298	-354	12	382	-597	-141	61	158	-549	-138	51	153	-255	-50	105	65
20	-1053	-272	71	304	-1213	-335	38	361	-545	-141	67	158	-558	-141	56	157	-249	-47	140	64

Table B-5. Measured peak, mean and RMS reactions (lbs) for sample 6

Azimuth	0°				45°				90°				135°				180°			
Load Cells	Neg. Peak	Mean	Pos. Peak	RMS	Neg. Peak	Mean	Pos. Peak	RMS	Neg. Peak	Mean	Pos. Peak	RMS	Neg. Peak	Mean	Pos. Peak	RMS	Neg. Peak	Mean	Pos. Peak	RMS
1	-683	-159	95	189	-639	-106	168	124	-366	-56	281	89	-427	-88	294	107	-237	-34	127	54
2	-795	-189	88	220	-479	-125	146	142	-345	-55	285	85	-405	-84	265	100	-223	-35	127	53
3	-1055	-242	81	275	-715	-148	140	168	-379	-68	311	96	-382	-98	233	114	-239	-42	120	60
4	-1301	-279	90	315	-928	-147	173	172	-376	-72	348	102	-390	-104	214	121	-255	-46	114	64
5	-1180	-264	73	295	-962	-185	71	210	-343	-85	209	102	-387	-105	90	117	-213	-42	88	56
6	-362	-90	36	102	-263	-66	49	74	-156	-32	103	42	-156	-44	88	51	-101	-17	50	25
7	-186	-48	20	54	-152	-35	29	39	-87	-17	59	23	-88	-24	54	28	-57	-9	29	14
8	-316	-77	26	87	-236	-53	39	60	-120	-25	86	32	-122	-34	65	39	-79	-14	36	19
9	-753	-180	56	201	-576	-123	82	140	-265	-57	184	73	-274	-76	128	86	-174	-31	77	44
10	-1169	-275	80	307	-906	-201	105	227	-406	-92	244	113	-423	-118	159	132	-255	-47	111	65
11	-1596	-375	111	418	-1229	-275	140	310	-555	-128	330	156	-582	-163	216	182	-347	-65	153	89
12	-1424	-334	96	373	-1099	-243	127	274	-493	-113	297	139	-516	-144	194	161	-309	-58	135	79
13	-419	-98	27	109	-322	-73	34	82	-146	-34	84	41	-153	-43	54	48	-89	-17	39	23
14	-56	-13	4	14	-43	-10	3	12	-20	-5	11	6	-21	-6	6	6	-11	-2	5	3
15	-1883	-425	119	475	-1649	-325	160	385	-547	-142	310	169	-590	-168	133	186	-335	-69	136	91
19	-1124	-300	139	342	-1192	-342	1	370	-531	-157	44	172	-536	-140	61	155	-226	-52	82	66
20	-1162	-276	133	310	-1072	-325	-4	351	-494	-157	58	172	-531	-144	72	160	-220	-49	105	65

Table B-6. Measured peak, mean and RMS reactions (lbs) for sample 7

Azimuth	0°				45°				90°				135°				180°			
Load Cells	Neg. Peak	Mean	Pos. Peak	RMS	Neg. Peak	Mean	Pos. Peak	RMS	Neg. Peak	Mean	Pos. Peak	RMS	Neg. Peak	Mean	Pos. Peak	RMS	Neg. Peak	Mean	Pos. Peak	RMS
1	-826	-159	142	190	-453	-108	176	125	-416	-62	285	92	-416	-91	221	109	-232	-33	136	54
2	-899	-188	147	219	-481	-127	142	144	-395	-61	217	88	-416	-86	164	102	-229	-34	125	52
3	-1003	-240	152	273	-544	-151	122	170	-434	-76	222	102	-373	-100	118	116	-251	-41	132	59
4	-1068	-276	172	312	-729	-150	139	174	-446	-80	266	109	-393	-107	125	122	-251	-44	134	63
5	-1020	-261	95	292	-835	-187	77	212	-409	-93	186	111	-380	-106	57	117	-214	-40	106	55
6	-369	-90	54	102	-219	-67	44	75	-187	-35	79	44	-154	-45	48	51	-108	-17	55	25
7	-205	-47	31	54	-122	-36	27	40	-104	-19	47	24	-86	-25	31	28	-60	-9	31	14
8	-295	-76	42	86	-193	-54	36	60	-144	-27	62	35	-118	-35	32	39	-79	-13	42	19
9	-659	-178	92	200	-484	-125	75	141	-318	-63	142	78	-265	-78	57	87	-171	-30	90	43
10	-998	-273	121	305	-791	-204	99	229	-482	-102	203	122	-410	-120	75	134	-248	-46	130	64
11	-1361	-371	161	416	-1075	-278	135	312	-664	-141	273	169	-564	-165	101	184	-333	-62	177	88
12	-1208	-331	143	370	-958	-246	122	277	-590	-125	246	150	-500	-146	90	163	-294	-56	157	78
13	-351	-97	40	108	-284	-74	34	83	-174	-37	71	44	-148	-43	25	48	-85	-16	46	23
14	-45	-13	5	14	-40	-11	4	12	-24	-5	10	6	-21	-6	3	6	-12	-2	6	3
15	-1549	-420	141	471	-1672	-327	166	387	-650	-157	290	185	-613	-169	64	186	-351	-67	171	89
19	-1259	-293	73	336	-1199	-343	5	371	-576	-166	72	181	-540	-140	39	155	-252	-50	107	64
20	-1118	-272	114	306	-1033	-326	13	353	-570	-168	69	183	-522	-144	49	159	-276	-47	134	64

Table B-7. Measured peak, mean and RMS reactions (lbs) for sample 8

Azimuth	0°				45°				90°				135°				180°			
Load Cells	Neg. Peak	Mean	Pos. Peak	RMS	Neg. Peak	Mean	Pos. Peak	RMS	Neg. Peak	Mean	Pos. Peak	RMS	Neg. Peak	Mean	Pos. Peak	RMS	Neg. Peak	Mean	Pos. Peak	RMS
1	-846	-165	109	194	-432	-115	164	131	-386	-62	318	93	-398	-88	210	105	-265	-33	137	55
2	-917	-195	100	224	-431	-134	130	149	-339	-61	299	89	-349	-83	176	99	-266	-33	126	54
3	-1096	-248	98	279	-635	-157	131	175	-377	-76	301	103	-413	-98	169	113	-284	-41	121	61
4	-1185	-285	108	318	-832	-156	150	179	-411	-82	337	110	-461	-104	202	120	-309	-45	120	66
5	-1085	-269	61	297	-859	-193	77	216	-433	-95	173	113	-440	-104	162	116	-272	-41	104	57
6	-389	-93	35	104	-225	-70	38	77	-155	-36	97	45	-179	-44	63	50	-105	-17	50	25
7	-214	-49	20	55	-112	-37	24	41	-83	-19	59	24	-98	-24	38	27	-60	-9	29	14
8	-327	-79	29	88	-203	-56	34	62	-132	-28	79	35	-139	-34	50	38	-83	-13	36	20
9	-750	-184	63	204	-504	-130	67	145	-309	-64	164	79	-309	-76	111	85	-188	-31	80	44
10	-1130	-282	83	311	-803	-211	91	234	-483	-103	216	123	-471	-117	162	131	-278	-46	121	66
11	-1538	-384	107	423	-1093	-288	123	320	-656	-142	294	170	-647	-161	222	180	-379	-63	167	91
12	-1371	-342	97	377	-975	-255	111	283	-584	-126	264	151	-576	-143	197	160	-339	-56	148	81
13	-400	-100	27	110	-286	-76	31	84	-172	-38	75	45	-170	-42	57	47	-98	-16	43	23
14	-53	-13	4	14	-39	-11	4	12	-24	-5	10	6	-24	-6	7	6	-13	-2	6	3
15	-1863	-432	114	478	-1647	-336	132	393	-853	-159	240	187	-702	-166	233	184	-383	-68	160	92
19	-1372	-308	115	349	-1172	-351	-16	376	-779	-168	49	184	-497	-138	120	153	-224	-52	117	67
20	-1189	-283	92	314	-1158	-334	5	357	-662	-170	56	186	-514	-142	136	158	-235	-49	144	67

APPENDIX C
PRESSURE COEFFICIENTS MEASURED IN THE 1/3-SCALE HOUSE TEST

Table C-1. Measured peak, mean and RMS pressure coefficients for test repeat 1

	0°				45°				90°			
Press. Taps	Neg. Peak	Mean	Pos. Peak	RMS	Neg. Peak	Mean	Pos. Peak	RMS	Neg. Peak	Mean	Pos. Peak	RMS
Roof Pressure Taps												
1	-1.47	-0.52	-0.03	0.55	-0.15	0.05	0.22	0.07	-0.90	-0.16	0.44	0.26
2	-2.42	-0.50	1.05	0.54	-1.90	-0.06	1.55	0.34	-3.50	-0.36	1.66	0.50
3	-2.90	-0.47	1.85	0.51	-2.77	-0.82	1.29	0.90	-3.26	-0.49	1.61	0.57
4	-2.62	-0.44	0.92	0.49	-1.94	-0.56	1.73	0.60	-3.00	-0.54	1.31	0.60
5	-2.05	-0.49	0.08	0.52	-1.54	0.07	1.24	0.20	-1.86	0.01	1.51	0.21
6	-1.85	-0.50	0.22	0.53	-0.04	0.12	0.26	0.12	-1.63	0.06	1.47	0.25
7	-2.48	-0.45	0.71	0.48	-0.15	0.13	0.53	0.14	-1.92	0.01	1.51	0.25
8	-1.86	-0.41	1.48	0.44	-0.63	0.11	0.81	0.15	-2.05	-0.05	2.17	0.24
9	-0.98	-0.40	-0.01	0.41	-3.30	-0.57	1.91	0.68	-0.81	0.10	1.09	0.16
10	-1.31	-0.42	0.31	0.44	-0.42	0.03	0.39	0.06	-0.76	0.10	0.71	0.12
11	-2.32	-0.45	0.43	0.47	-0.14	0.05	0.24	0.06	-0.59	0.14	0.70	0.16
12	-2.05	-0.46	0.47	0.48	-0.15	0.03	0.24	0.05	-0.08	1.15	1.98	1.15
13	-0.79	-0.33	0.20	0.34	-3.62	-0.82	1.00	0.88	-1.01	-0.11	0.46	0.15
14	-1.02	-0.37	-0.06	0.38	-1.38	-0.06	1.04	0.16	-0.59	0.09	0.47	0.11
15	-1.39	-0.41	0.11	0.42	-0.47	-0.08	0.18	0.10	-0.44	0.05	0.42	0.07
16	-1.52	-0.46	0.21	0.48	-0.32	-0.09	0.11	0.10	-0.56	0.07	0.71	0.09
17	-1.03	-0.32	0.01	0.33	-3.18	-1.12	1.08	1.17	-0.41	-0.01	0.77	0.07
18	-1.27	-0.36	-0.05	0.37	-2.53	-0.43	1.64	0.50	-0.32	0.04	0.47	0.07
19	-2.21	-0.45	0.03	0.47	-0.75	-0.38	0.04	0.39	-0.39	0.04	0.36	0.07
20	-1.54	-0.40	-0.09	0.41	-1.28	-0.34	0.42	0.36	-0.29	0.04	0.40	0.06
21	-0.92	-0.34	0.02	0.35	-6.61	-1.71	2.91	1.86	-0.96	-0.05	0.36	0.08
22	-1.20	-0.36	-0.04	0.37	-3.70	-0.67	1.57	0.80	-0.65	-0.03	0.21	0.06
23	-1.86	-0.40	-0.08	0.42	-2.46	-0.54	1.04	0.59	-0.55	-0.02	0.21	0.05
24	-2.02	-0.34	-0.01	0.36	-3.23	-0.89	2.05	0.93	-0.82	-0.04	0.24	0.08
25	-1.53	-0.43	0.27	0.44	-1.58	-0.26	1.19	0.33	-0.66	-0.05	0.15	0.08
Wall Pressure Taps												
26	-0.58	-0.19	0.17	0.20	0.64	0.83	1.07	0.83	-0.41	0.46	1.73	0.47
27	-1.14	-0.30	0.00	0.32	0.39	0.56	0.73	0.56	0.23	0.92	1.26	0.92
28	0.46	0.76	0.98	0.76	0.54	0.72	0.88	0.72	-0.93	-0.43	-0.14	0.44
29	0.93	1.08	1.26	1.08	0.11	0.36	0.60	0.36	-0.64	0.04	0.57	0.11
Interior Pressure Taps												
30	-0.01	0.00	0.01	0.00	0.00	0.01	0.02	0.01	0.00	0.01	0.02	0.01

Table C-2. Measured peak, mean and RMS pressure coefficients for test repeat 2

	0°				45°				90°			
Press. Taps	Neg. Peak	Mean	Pos. Peak	RMS	Neg. Peak	Mean	Pos. Peak	RMS	Neg. Peak	Mean	Pos. Peak	RMS
Roof Pressure Taps												
1	-1.66	-0.53	-0.06	0.57	-0.16	0.03	0.20	0.05	-0.99	-0.12	0.56	0.23
2	-2.43	-0.49	1.08	0.53	-1.98	-0.05	1.58	0.30	-2.35	-0.29	1.69	0.44
3	-2.92	-0.46	1.82	0.51	-2.64	-0.80	1.11	0.87	-2.55	-0.40	1.96	0.49
4	-2.63	-0.44	1.40	0.48	-2.30	-0.56	0.56	0.60	-2.65	-0.48	1.60	0.55
5	-2.46	-0.50	0.34	0.53	-1.66	0.05	1.56	0.20	-1.51	0.02	1.55	0.18
6	-1.96	-0.50	0.18	0.54	-0.06	0.10	0.26	0.10	-1.54	0.07	1.67	0.22
7	-4.54	-0.45	0.80	0.48	-0.29	0.10	0.35	0.11	-1.35	0.01	1.39	0.23
8	-2.80	-0.41	1.08	0.44	-0.67	0.09	0.81	0.12	-1.85	-0.02	1.85	0.21
9	-1.13	-0.40	-0.02	0.42	-3.27	-0.55	2.02	0.67	-0.75	0.10	0.94	0.15
10	-1.19	-0.43	-0.11	0.45	-0.36	0.01	0.36	0.06	-0.74	0.10	0.81	0.12
11	-1.84	-0.45	-0.05	0.47	-0.20	0.03	0.28	0.05	-0.56	0.14	0.69	0.15
12	-1.51	-0.46	0.34	0.48	-0.20	0.01	0.21	0.04	-1.49	-0.20	0.73	0.47
13	-0.76	-0.34	0.00	0.35	-2.97	-0.80	1.88	0.87	-0.92	-0.10	0.50	0.13
14	-0.98	-0.38	-0.07	0.39	-1.16	-0.08	1.16	0.17	-0.37	0.09	0.62	0.11
15	-1.36	-0.41	0.08	0.43	-0.47	-0.10	0.20	0.12	-0.34	0.06	0.34	0.08
16	-1.52	-0.46	0.38	0.48	-0.33	-0.10	0.13	0.12	-0.43	0.08	0.57	0.09
17	-0.75	-0.35	-0.04	0.36	-3.47	-1.06	0.67	1.11	-0.50	-0.02	0.43	0.07
18	-1.05	-0.35	-0.06	0.36	-2.10	-0.42	1.12	0.49	-0.36	0.03	0.35	0.06
19	-1.97	-0.44	0.42	0.46	-0.75	-0.39	0.19	0.40	-0.35	0.04	0.31	0.06
20	-1.89	-0.39	1.14	0.41	-1.04	-0.35	0.25	0.36	-0.39	0.05	0.49	0.07
21	-0.95	-0.33	-0.04	0.34	-5.94	-1.69	2.75	1.85	-0.73	-0.04	0.23	0.08
22	-0.91	-0.36	-0.03	0.36	-3.67	-0.64	1.71	0.76	-1.54	-0.03	0.36	0.06
23	-1.59	-0.39	0.02	0.41	-2.40	-0.54	1.10	0.59	-0.67	-0.01	0.20	0.06
24	-0.78	-0.33	0.06	0.34	-3.00	-0.91	0.98	0.95	-0.99	-0.05	0.24	0.09
25	-1.60	-0.41	-0.08	0.42	-1.76	-0.23	1.44	0.30	-0.97	-0.04	0.18	0.08
Wall Pressure Taps												
26	-0.53	-0.18	0.18	0.20	0.59	0.77	1.10	0.77	-0.41	0.40	1.89	0.42
27	-1.08	-0.30	0.18	0.32	0.40	0.52	0.74	0.52	0.27	0.89	1.30	0.90
28	0.41	0.74	0.99	0.75	0.55	0.72	0.91	0.72	-1.01	-0.38	0.00	0.39
29	0.71	1.04	1.23	1.05	0.09	0.33	0.56	0.34	-0.53	0.06	0.67	0.12
Interior Pressure Taps												
30	-0.01	0.00	0.01	0.00	-0.01	0.00	0.01	0.00	-0.08	0.00	0.02	0.01

Table C-3. Measured peak, mean and RMS pressure coefficients for test repeat 3

	0°				45°				90°			
Press. Taps	Neg. Peak	Mean	Pos. Peak	RMS	Neg. Peak	Mean	Pos. Peak	RMS	Neg. Peak	Mean	Pos. Peak	RMS
Roof Pressure Taps												
1	-1.63	-0.62	-0.09	0.66	-0.14	0.05	0.21	0.06	-0.90	-0.13	0.40	0.25
2	-3.24	-0.55	1.12	0.60	-2.03	-0.03	1.55	0.28	-3.10	-0.33	2.03	0.51
3	-2.41	-0.49	1.62	0.54	-2.68	-0.78	1.32	0.86	-3.23	-0.46	2.26	0.56
4	-2.95	-0.46	1.74	0.52	-2.70	-0.55	0.65	0.60	-3.06	-0.52	2.07	0.59
5	-2.28	-0.59	-0.03	0.62	-1.73	0.05	1.36	0.20	-1.87	0.02	1.32	0.21
6	-1.93	-0.59	0.36	0.63	-0.05	0.11	0.27	0.11	-1.87	0.09	1.54	0.26
7	-1.84	-0.51	0.89	0.54	-0.10	0.12	0.36	0.12	-1.87	0.05	1.64	0.26
8	-2.58	-0.43	1.24	0.47	-0.78	0.10	0.71	0.13	-1.54	0.00	1.97	0.23
9	-1.35	-0.45	0.18	0.47	-2.86	-0.54	1.91	0.66	-1.01	0.11	1.05	0.17
10	-1.41	-0.48	-0.05	0.50	-0.44	0.01	0.46	0.06	-0.89	0.11	0.59	0.13
11	-2.53	-0.50	0.10	0.52	-0.18	0.04	0.30	0.06	-0.55	0.16	0.70	0.17
12	-2.03	-0.50	0.81	0.52	-0.20	0.01	0.21	0.04	-1.02	0.18	1.08	0.20
13	-1.13	-0.36	0.06	0.38	-2.89	-0.79	1.34	0.86	-1.13	-0.11	0.56	0.15
14	-1.05	-0.41	-0.04	0.42	-1.21	-0.07	0.89	0.17	-0.61	0.10	0.58	0.12
15	-1.33	-0.45	-0.03	0.46	-0.64	-0.10	0.28	0.12	-0.54	0.06	0.42	0.09
16	-1.75	-0.50	0.21	0.52	-0.33	-0.10	0.12	0.11	-0.38	0.08	0.41	0.10
17	-0.77	-0.35	0.24	0.36	-3.18	-1.06	0.71	1.12	-0.50	-0.01	0.72	0.08
18	-0.82	-0.38	-0.11	0.38	-2.28	-0.41	1.14	0.48	-0.53	0.04	0.48	0.08
19	-2.05	-0.47	0.08	0.49	-0.78	-0.39	0.08	0.40	-0.42	0.04	0.33	0.08
20	-1.63	-0.41	-0.04	0.43	-1.15	-0.35	0.50	0.37	-0.42	0.05	0.34	0.08
21	-0.77	-0.35	-0.02	0.36	-6.48	-1.75	1.92	1.90	-1.57	-0.05	0.79	0.11
22	-0.94	-0.37	-0.05	0.38	-3.06	-0.62	1.77	0.74	-1.22	-0.04	0.30	0.10
23	-1.23	-0.41	-0.06	0.42	-2.79	-0.54	1.06	0.60	-1.38	-0.02	0.19	0.09
24	-1.11	-0.34	0.04	0.35	-3.41	-0.95	1.07	0.99	-0.92	-0.05	0.42	0.10
25	-1.65	-0.41	0.10	0.42	-1.57	-0.21	1.17	0.27	-1.04	-0.05	0.21	0.10
Wall Pressure Taps												
26	-0.77	-0.19	0.11	0.20	0.57	0.77	0.96	0.77	-0.48	0.48	1.31	0.50
27	-1.41	-0.31	0.39	0.33	0.38	0.52	0.68	0.52	0.50	0.95	1.52	0.95
28	0.49	0.82	1.06	0.82	0.56	0.74	0.90	0.74	-1.11	-0.42	-0.07	0.43
29	0.93	1.08	1.27	1.08	0.14	0.34	0.53	0.35	-0.64	0.06	0.72	0.13
Interior Pressure Taps												
30	-0.01	0.00	0.01	0.00	-0.01	0.00	0.01	0.00	-0.01	0.00	0.01	0.00

APPENDIX D
STRUCTURAL REACTIONS MEASURED IN THE 1/3-SCALE HOUSE TEST

Table D-1. Measured peak, mean and RMS reactions for test repeat 1

	0°				45°				90°			
Load Cell	Neg. Peak	Mean	Pos. Peak	RMS	Neg. Peak	Mean	Pos. Peak	RMS	Neg. Peak	Mean	Pos. Peak	RMS
Roof-to-wall load cells												
1	-13.5	-7.7	-0.9	7.9	-6.2	-3.7	-1.3	3.8	1.4	5.0	9.1	5.1
2	-10.9	-6.9	-3.1	7.0	-6.6	-4.5	-1.7	4.6	-5.1	-1.0	3.3	1.4
3	-13.5	-8.0	-4.1	8.1	-6.8	-4.8	-2.6	4.8	-2.7	0.8	4.2	1.2
4	-26.4	-19.5	-11.1	19.6	-13.9	-11.1	-7.9	11.1	-2.9	1.1	4.8	1.4
5	-22.3	-18.2	-14.6	18.3	-11.4	-8.7	-6.6	8.7	-17.8	-9.8	-4.5	9.9
15	-20.5	-13.4	-7.4	13.6	-15.3	-10.7	-6.1	10.7	-4.2	0.8	6.6	1.7
16	-22.8	-18.3	-14.5	18.3	-19.4	-15.1	-10.9	15.2	-8.6	-4.6	-2.3	4.7
17	-11.4	-5.8	-2.8	5.9	-5.1	-2.0	-1.5	2.1	-3.6	-1.4	0.0	1.4
18	-11.8	-7.1	-4.1	7.2	-12.2	-8.1	-4.2	8.2	-7.0	-1.4	1.9	1.8
19	-21.2	-13.6	-8.7	13.8	-17.2	-12.0	-5.8	12.1	-16.0	-7.9	-1.0	8.2
20	-20.8	-14.3	-10.1	14.4	-17.4	-13.1	-6.7	13.2	3.9	8.3	13.4	8.4
21	-10.3	-6.3	-2.8	6.4	-5.9	-2.8	-0.7	2.9	-7.4	-1.0	1.7	1.4
Wall-to-foundation load cells												
6	-7.3	-2.6	1.5	2.9	-12.5	-8.0	-4.1	8.1	-9.5	-2.2	5.4	2.8
7	-17.3	-11.7	-5.6	11.8	-4.1	-0.3	3.8	1.2	4.5	12.5	20.9	12.7
8	-23.3	-18.3	-11.9	18.3	-3.8	0.3	4.3	1.2	5.1	14.1	21.6	14.3
9	-24.2	-19.7	-15.1	19.8	-9.6	-6.8	-4.0	6.9	-6.8	1.4	9.1	2.6
10	-24.7	-20.8	-15.2	20.9	-15.1	-12.4	-9.7	12.4	-29.3	-18.6	-10.0	18.8
11	-20.6	-15.1	-8.8	15.3	-16.5	-12.2	-7.6	12.3	-37.3	-24.6	-13.7	24.8
12	-21.7	-16.6	-11.2	16.6	-16.0	-12.6	-8.8	12.7	-50.3	-31.8	-19.1	32.0
13	-11.2	-7.2	-3.7	7.3	-8.3	-6.5	-4.6	6.6	-20.1	-12.6	-7.1	12.7
14	3.1	5.8	8.1	5.8	-1.2	0.4	2.0	0.6	-6.7	-2.6	1.5	2.8

Table D-2. Measured peak, mean and RMS reactions for test repeat 2

	0°				45°				90°			
Load Cell	Neg. Peak	Mean	Pos. Peak	RMS	Neg. Peak	Mean	Pos. Peak	RMS	Neg. Peak	Mean	Pos. Peak	RMS
Roof-to-wall load cells												
1	-15.0	-8.3	1.8	8.6	-7.1	-3.7	-0.4	3.8	-0.4	3.1	6.2	3.2
2	-10.5	-7.3	-2.0	7.4	-9.3	-6.5	-3.1	6.5	-3.3	0.6	4.3	1.1
3	-12.9	-8.1	-4.6	8.2	-7.7	-5.3	-2.1	5.3	-1.5	1.6	4.7	1.8
4	-25.5	-18.4	-10.1	18.6	-17.0	-13.3	-9.3	13.4	-2.3	1.6	6.1	1.9
5	-19.6	-14.9	-9.6	15.0	-14.5	-10.5	-7.5	10.5	-13.5	-8.1	-4.2	8.2
15	-23.2	-14.7	-8.5	15.0	-18.9	-13.1	-7.1	13.2	-4.0	2.5	7.9	2.9
16	-23.3	-16.1	-8.2	16.2	-21.3	-16.2	-10.9	16.3	-6.2	-1.8	0.6	1.9
17	-11.7	-5.7	-2.2	5.8	-6.3	-2.4	-1.4	2.6	-3.6	-0.9	0.4	1.0
18	-11.2	-7.4	-3.5	7.4	-13.9	-9.7	-4.8	9.8	-6.9	-0.6	2.3	1.3
19	-19.6	-13.2	-8.2	13.3	-19.8	-13.6	-6.9	13.7	-15.4	-8.2	-2.6	8.4
20	-21.2	-15.0	-9.0	15.1	-21.9	-15.3	-7.5	15.4	4.2	9.6	14.7	9.7
21	-11.6	-6.4	-1.7	6.5	-8.0	-4.2	-0.8	4.3	-6.7	-0.5	2.0	1.0
Wall-to-foundation load cells												
6	-8.0	-3.5	1.4	3.7	-15.3	-10.7	-5.3	10.7	-5.9	0.7	7.4	2.0
7	-17.8	-11.9	-4.4	12.0	-6.0	-1.3	4.7	2.0	6.0	13.0	20.3	13.1
8	-23.9	-17.7	-9.3	17.8	-5.6	-0.7	4.8	1.6	6.8	14.9	22.7	15.1
9	-22.6	-17.8	-11.4	17.8	-11.8	-7.7	-2.8	7.8	-3.4	2.7	10.4	3.3
10	-21.5	-17.8	-10.8	17.9	-17.9	-14.4	-11.3	14.4	-23.9	-16.0	-9.5	16.1
11	-19.0	-14.0	-7.8	14.1	-20.9	-15.7	-11.0	15.8	-28.7	-18.8	-9.2	19.0
12	-16.6	-12.6	-9.0	12.7	-19.5	-13.8	-9.0	13.9	-43.2	-28.3	-13.9	28.6
13	-10.0	-7.2	-4.9	7.2	-10.2	-7.5	-2.4	7.5	-18.9	-11.2	-4.9	11.4
14	2.8	4.6	6.1	4.7	-2.5	-0.4	3.9	0.8	-6.4	-1.6	2.2	2.0

Table D-3. Measured peak, mean and RMS reactions for test repeat 3

	0°				45°				90°			
Load Cell	Neg. Peak	Mean	Pos. Peak	RMS	Neg. Peak	Mean	Pos. Peak	RMS	Neg. Peak	Mean	Pos. Peak	RMS
Roof-to-wall load cells												
1	-14.6	-8.0	-0.2	8.3	-7.9	-4.2	-1.2	4.3	-2.4	2.9	5.4	3.1
2	-10.0	-7.0	-1.9	7.1	-9.4	-6.6	-3.6	6.6	-5.1	0.7	4.6	1.4
3	-13.9	-8.1	-3.3	8.2	-8.0	-5.3	-2.7	5.4	-2.9	1.4	4.6	1.7
4	-25.8	-17.9	-9.0	18.0	-16.7	-13.2	-9.0	13.2	-4.7	1.4	5.6	1.9
5	-18.6	-14.1	-10.0	14.2	-13.8	-10.4	-7.7	10.5	-22.4	-9.1	-4.6	9.3
15	-26.5	-17.8	-10.9	17.9	-18.2	-12.5	-6.3	12.6	-4.2	2.3	7.3	2.8
16	-18.6	-14.4	-10.1	14.5	-21.2	-16.0	-11.4	16.1	-10.7	-2.6	0.2	2.8
17	-9.3	-5.1	-2.0	5.2	-6.6	-2.4	-1.5	2.5	-4.7	-1.1	0.5	1.3
18	-10.8	-6.9	-4.0	7.0	-15.1	-9.9	-5.4	10.0	-8.5	-1.0	2.6	1.8
19	-21.9	-14.9	-8.2	15.0	-19.6	-13.5	-6.8	13.6	-23.1	-9.5	-3.2	9.8
20	-18.7	-13.4	-8.0	13.5	-20.6	-14.3	-7.0	14.5	6.2	9.9	13.2	9.9
21	-12.1	-6.7	-3.0	6.8	-8.8	-4.2	-1.1	4.3	-9.2	-0.5	2.2	1.5
Wall-to-foundation load cells												
6	-8.4	-4.1	-0.6	4.2	-16.1	-11.1	-6.8	11.2	-8.9	0.7	7.8	2.2
7	-18.3	-11.8	-5.8	11.9	-6.3	-1.8	2.7	2.2	3.5	12.8	19.8	12.9
8	-23.5	-17.1	-10.9	17.2	-6.0	-1.0	3.4	1.7	5.3	15.1	21.8	15.2
9	-20.8	-16.8	-11.8	16.8	-11.4	-7.4	-3.3	7.5	-8.6	2.8	8.9	3.5
10	-19.3	-15.6	-11.4	15.6	-17.4	-14.3	-10.7	14.4	-30.8	-17.6	-10.4	17.7
11	-17.1	-12.0	-7.1	12.1	-20.7	-15.6	-10.3	15.7	-34.2	-19.8	-11.3	20.0
12	-19.0	-14.6	-10.2	14.7	-18.0	-14.1	-10.3	14.2	-52.3	-29.5	-18.1	29.7
13	-12.5	-10.1	-7.7	10.1	-10.7	-8.2	-5.9	8.2	-21.4	-11.3	-6.1	11.4
14	1.3	3.5	5.8	3.6	-2.3	-0.5	1.0	0.7	-6.0	-1.3	2.5	1.8

LIST OF REFERENCES

ASCE/SEI. (2005). "Minimum design loads for buildings and other structures." 7-05, American Society of Civil Engineers, Reston, VA.

Chen, J., Haynes, B. S., and Fletcher, D. F. (2000). "Cobra probe measurements of mean velocities, Reynolds stresses and higher-order velocity correlations in pipe flow." *Experimental Thermal and Fluid Science*, 21(4), 206-217.

Datin, P. L., and Prevatt, D. O. (2007). "Wind Uplift Reactions at Roof-to-Wall Connections of Wood-Framed Gable Roof Assembly." 12th International Conference on Wind Engineering, Australasian Wind Engineering Society, Cairns, Australia.

Datin, P. L., Prevatt, D. O., and Mensah, A. "Performance Based Wind Engineering: Interaction of Hurricanes with Residential Structures." *Engineering Research and Innovation Conference*, Honolulu, Hawaii.

Davenport, A. G., Surry, D., and Stathopoulos, T. (1978). "Wind loads on low-rise buildings." Universtiy of Ontario, London, Ontario, Canada.

Doudak, G., McClure, G., Smith, I., Hu, L., and Stathopoulos, T. (2005). "Monitoring Structural Response of a Wooden Light-Frame Industrial Shed Building to Environmental Loads." *Journal of Structural Engineering*, 131(5), 794-805.

FEMA. (2005). "Mitigation Assessment Team Report: Hurricane Ivan in Alabama and Florida - Observations, Recommendations, and Technical Guidance." FEMA 489, Federal Emergency Management Agency.

Ginger, J. D., and Letchford, C. W. (1993). "Characteristics of large pressures in regions of flow separation." *Journal of Wind Engineering and Industrial Aerodynamics*, 49, 301-310.

Ginger, J. D., Reardon, G. F., and Whitbread, B. J. (2000). "Wind load effects and equivalent pressures on low-rise house roofs." *Engineering Structures*, 22(6), 638-646.

Hibbeler, R. C. (2006). *Structural Analysis*, Pearson Prentice Hall, New Jersey.

Ho, T. C. E., Surry, D., Morrish, D., and Kopp, G. A. (2005a). "The UWO contribution to the NIST aerodynamic database for wind loads on low buildings: Part 1. Archiving format and basic aerodynamic data." *Journal of Wind Engineering and Industrial Aerodynamics*, 93(1), 1-30.

Ho, T. C. E., Surry, D., Morrish, D., and Kopp, G. A. (2005b). "The UWO contribution to the NIST aerodynamic database for wind loads on low buildings: Part 1. Archiving format and basic aerodynamic data." 93(1), 1-30.

Hooper, J. D., and Musgrove, A. R. (1997). "Reynolds stress, mean velocity, and dynamic static pressure measurement by a four-hole pressure probe." *Experimental Thermal and Fluid Science*, 15(4), 375-383.

Jang, S., Lu, L.-W., Sadek, F., and Simiu, E. (2002). "Database-assisted wind load capacity estimates for low-rise steel frames." *Journal of Structural Engineering*, 128(12), 1594-1603.

Kopp, G. A., and Chen, Y. (2006). "Database-assisted design of low-rise buildings: Aerodynamic considerations for a practical interpolation scheme." *Journal of Structural Engineering*, 132(6), 909-917.

Lieblein, J. (1974). "Efficient Methods fo Extreme-Value Methodo logy." National Bureau of Standards, Washington, D.C.

Liu, Z., Prevatt, D. O., Gurley, K. R., Aponte-Bermudez, L., and Reinhold, T. A. (2009). "Field Measurement and Wind Tunnel Simulation of Hurricane Wind Loads on a Single Family Dwelling." *Engineering Structures*, (in press).

Main, J. A., and Fritz, W. P. (2006). "Database-Assisted Design for Wind: Concepts, Software, and Examples for Rigid and Flexible Buildings." National Institute of Science and Technology, Gaithersburg, MD.

Martin, K. G., Gupta, R., Prevatt, D. O., Datin, P. L., and van de Lindt, J. W. (2010). "Evaluation of System Effects and Structural Load Paths in a Wood-Framed Structure." *Journal of Architectural Engineering*, Submitted for review 25 Feb. 2010.

Masters, F., Gurley, K., and Prevatt, D. O. (2008). "Full-Scale Simulation of Turbulent Wind-Driven Rain Effects on Fenestration and Wall Systems." 3rd International Symposium on Wind Effects on Buildings and Urban Environment, Tokyo, Japan.

National Institute of Standards and Technology, N. (2008). "windPressure-DAD software for rigid, gable roof buildings." http://www.itl.nist.gov/div898/winds/wind_pressure/wind_pressure.htm, Date accessed: 12/20/09.

NIST. (2003). "NIST/SEMATECH e-Handbook of Statistical Methods." National Institute of Standards and Technology. Retrieved March 8, 2007, from http://www.itl.nist.gov/div898/handbook/.

Rigato, A., Chang, P., and Simiu, E. (2001). "Database-assisted design, standardization, and wind direction effects." *Journal of Structural Engineering*, 127(8), 855-860.

Rosowsky, D., and Schiff, S. (2003). "What are our expectations, objectives, and performance requirements for wood structures in high wind regions?" *Natural Hazards Review*, 4(3), 144-148.

Rosowsky, D. V., Walsh, T. G., and Crandell, J. H. (2003). "Reliability of residential woodframe construction from 1900 to present." *Forest Products Journal*, 53(4), 19-28.

Sadek, F., Diniz, S., Kasperski, M., Gioffre, M., and Simiu, E. (2004). "Sampling Errors in the Estimation of Peak Wind-Induced Internal Forces in Low-Rise Structures." *Journal of Engineering Mechanics*, 130(2), 235-239.

Sadek, F., and Simiu, E. (2002). "Peak Non-Gaussian Wind Effects for Database-Assisted Low-Rise Building Design." *Journal of Engineering Mechanics*, 128(5), 530-539.

Shepherd, I. C. (1981). "Four-Hole Pressure Probe for Fluid Flow Measurements in Three Dimensions." *Journal of Fluids Engineering, Transactions of the ASME*, 103(4), 590-594.

Simiu, E., and Miyata, T. (2006). *Design of Buildings and Bridges for Wind, A Practical Guide for ASCE-7 Standard Users and Designers of Special Structures*, John Wiley & Sons, Inc., New Jersey.

Simiu, E., Sadek, F., Whalen, T. M., Jang, S., Lu, L.-W., Diniz, S. M. C., Grazini, A., and Riley, M. A. (2003). "Achieving safer and more economical buildings through database-assisted, reliability-based design for wind." *Journal of Wind Engineering and Industrial Aerodynamics*, 91(12-15), 1587-1611.

Simiu, E., and Scanlan, R. H. (1996). *Wind Effects on Structures - Fundamentals and Applications to Design*, John Wiley & Sons, Inc., New York.

Simiu, E., and Stathopoulos, T. (1997). "Codification of wind loads on buildings using bluff body aerodynamics and climatological data bases." *Journal of Wind Engineering and Industrial Aerodynamics*, 69-71, 497-506.

St. Pierre, L. M., Kopp, G. A., Surry, D., and Ho, T. C. E. (2005). "The UWO contribution to the NIST aerodynamic database for wind loads on low buildings: Part 2. Comparison of data with wind load provisions." *Journal of Wind Engineering and Industrial Aerodynamics*, 93(1), 31-59.

Stathopoulos, T. (1979). "Turbulent Wind Action on Low-rise Buildings," Universtiy of Ontario, London, Ontario, London.

Suresh Kumar, K., and Stathopoulos, T. (2000). "Wind loads on low building roofs: a stochastic perspective." *Journal of Structural Engineering*, 126(8), 944-956.

van de Lindt, J. W., Graettinger, A., Gupta, R., Skaggs, T., Pryor, S., and Fridley, K. J. (2007). "Performance of Wood-Frame Structures during Hurricane Katrina." *Journal of Performance of Constructed Facilities*, 21(2), 108-116.

Watkins, S., Mousley, P., and Vino, G. "The Development and Use of Dynamic Pressure Probes With Extended Cones of Acceptance (ECA)." *15th Australasian Fluid Mechanics Conference*, The University of Sydney, Sydney, Australia.

Whalen, T., Simiu, E., Harris, G., Lin, J., and David, S. (1998). "The use of aerodynamic databases for the effective estimation of wind effects in main wind-force resisting

systems:: application to low buildings." *Journal of Wind Engineering and Industrial Aerodynamics*, 77-78, 685-693.

Whalen, T. M., Sadek, F., and Simiu, E. (2002). "Database-assisted design for wind: Basic concepts and software development." *Journal of Wind Engineering and Industrial Aerodynamics*, 90(11), 1349-1368.

Whalen, T. M., Shah, V., and Yang, J.-S. (2000). "A Pilot Project For Computer-Based Design of Low-Rise Buildings for Wind Loads - The WiLDE-LRS User's Manual." Purdue University, West Lafayette, IN.

Zisis, I., and Stathopoulos, T. (2009). "Wind-Induced Cladding and Structural Loads on Low-Wood Building." *Journal of Structural Engineering*, 135(4), 437-447.

BIOGRAPHICAL SKETCH

Akwasi Frimpong Mensah was born and raised in Takoradi, Ghana. He graduated with a Bachelor of Science degree in civil engineering from the Kwame Nkrumah University of Science and Technology in May 2006. He served as a teaching assistant for a year with the same institution after graduating and later on worked as a Civil/ Structural Engineer with Comptran Engineering and Planning Associates, Accra for another year. He joined University of Florida in pursuit of a master degree in August 2008. He anticipates receiving a degree of Master of Science in Civil Engineering in August 2010. The author hopes to practice as an engineer and also lecture in the discipline.